Surface Initiated N-carboxyanhydride Ring Opening Polymerization: Designing Nanohybrids for Biomedical Applications

A thesis submitted for the Degree of Doctor of Philosophy

By

TUSHAR BORASE (MSc)

The research work described in this thesis was carried out under the supervision of

Dr. ANDREAS HEISE

SCHOOL OF CHEMICAL SCIENCES

DUBLIN CITY UNIVERSITY

Sept. 2014

DECLARATION

I hereby certify that this material, which I now submit for assessment on the program of study leading to the award of **PhD** is entirely my own work, and that I have exercised reasonable care to ensure that the work is original, and does not to the best of my knowledge breach any law of copyright, and has not been taken from the work of others save and to the extent that such work has been cited and acknowledged within the text of my work.

Signed: _____ (Candidate) ID No.: 59101636 Date: / /2014

ACKNOWLEDGEMENTS

It's finally time for me to finish my wonderful PhD journey. While I am enthusiastic to finally bring this part of my life to accomplishment, I have to say it has allowed me to get to know some outstanding individuals.

First and foremost I wish to express my sincere gratitude to my supervisor Dr. Andreas Heise for believing in my abilities and offering me an opportunity to work with him. I would like to thank him for always being so encouraging, supportive, patient, kind and for all his excellent ideas. For me he has been much more than a mere supervisor but a person from whom I learnt many things which would help me to be a better person in my life.

I would like to express my sincere gratitude to the people who have travelled along with me on this journey and made it so much better (and much more fun)! Past and present members of the group –Fabrice, Paul, Hui, Jin, Ida, Claudia, Zeliha, Antonis, Mark, Jaco, Saltuk, Timo and Louis, Eugenia; you guys are truly memorable! I would specially like to thank my friend Dr. Jaywant Phopase who always guided and encouraged me to achieve my career goals. I also would like to thank friends I met in Dublin – Rohit, Mukund, Sanjay, Harshad, Chandra, Mayank, Gurmeet, Sushrut, Nilesh, Ian, Ashwini, Shruti, Priyanka, Viji, Monika, Guisy, Lily and Fadwa without whom my social life wouldn't be complete.

Special thanks to my research collaborator Dr. Dermot Brougham from Dublin City University for his valuable guidance and scientific support. I also would like to thank his group members, especially Ninjbadgar and Eoin for their quick and reliable help during the course of the collaboration.

I would like to thank all the technical staff at School of Chemical Sciences at Dublin City University for their kind and generous help during my PhD studies.

I also would like to thank my research supervisor Dr. M. G. Kulkarni and Dr. M. V. Badiger from National Chemical Laboratory, Pune, India, who supported and motivated me during my early research career at NCL.

I wish to thank my parents for their blessings, support, love and motivation which have made possible the achievement of my goals. I am in debt to my beloved parents for being always proud of me and for their everlasting love. I also would like to thank my sisters for their love and joyous support during all the ups and downs of my research carrier. I couldn't find the words to thank my best friends Ali and Manjusha for their love and for always standing by me in every situation of my life since the destiny crossed our lives.

And finally, I would like to thank Science Foundation of Ireland for the financial support for my PhD at School of Chemical Sciences, Dublin City University, Dublin Ireland.

Tushar

Dublin, Ireland.

Table of content

ABSTRACT

Synthetic polypeptides are of great importance in biomedical applications as they are directly modelled on natural proteins and can mimic their functions in biological systems. Thus, synthetic polypeptides display properties such as biocompatibility, biodegradability, bioavailability, bioadhesion and could find applications in drug delivery, tissue engineering, implants, therapeutics. The availability of wide range of functionality of the synthetic polypeptides arising from the vast pool of natural and non-natural amino acids has been used to modify and to impart new functionalities to the synthetic materials such as organic/inorganic nanoparticles, surfaces, synthetic polymeric architectures, films. This new class of hybrid materials with enhanced biocompatibility are advantageous over their constituent components and show promising candidature in advanced biomedical applications.

N-carboxyanhydride Ring Opening Polymerization (NCA-ROP) is a lucrative technique to synthesize polypeptides with controlled molecular weights and narrow polydispersities. Surface intiated N-carboxyanhydride ring opening polymerization (SI-NCA-ROP) by an immobilized intiator has been investigated to teather synthetic polypeptides onto the desired material surfaces. SI-NCA-ROP has been employed from silica nanoparticle surfaces to engineer synthetic polypeptide grafted smart hybrid materials capable of changing microscopic properties according to the changes in pH of the external micro-environment. These silica polypeptide hybrids have shown their applicability in pH responsive cargo release systems. Similarly, surface grafted synthetic polypeptides have been used to modify and improve dispersion properties of iron-oxide magnetic nanoparticles useful in imaging and drug delivery applications. Grafting of highly hydrophilic glycosylated polypeptides have shown improved aqueous dispersion properties of these inorganic nanoparticles useful for MRI imaging and bio-recognition. In an extended study, polypeptides comprising two amino acids have been grafted from iron oxide nanoparticle surfaces to engineer new hybrids with excellent aqueous dispersibility and siRNA vector ability. These co-polypeptide grafted nanoparticle hybrids shown to retain their bio-recognition ability besides improving aqueous dispersibilty and imparting

siRNA vectorability, which highlights their applicability as theranostics. In summary, we have presented novel polypeptide hybrid materials by SI-NCA-ROP and their advanced biomedical applications.

Abbreviations

AMM	Activated monomer mechanism
APTS	3-Aminopropyl trimethoxysilane
ATRP	Atom transfer radical polymerization
BLG	γ-benzyl-L-glutamate
ε-CBZ-PLL	poly(ε-carbobenzyoxy-L-lysine)
CDB	Cumyl dithiobenzoate
CuAAC	Copper catalyzed azide-alkyne click
CT	Computed tomography
DEPN	N-tert-butyl-N-(1-diethylphosphono-2,2-dimethylpropyl) nitroxide
d_{hyd}	Hydrodynamic size
DLS	Dynamic Light Scattering
DMF	Dimethylformamide
DNA	Deoxyribonucleic acid
EDC	1-Ethyl-3-(3-dimethylaminopropyl)carbodiimide
FTIR	Fourier transforms infrared
GFP	Green fluorescent protein
GPC	Gel permeation chromatography
GP-MNP	Glycopeptide-grafted superparamagnetic Fe_3O_4 nanoparticles
GTP	Group transfer polymerization
HF	Hydrofluoric acid
HVT	High vacuum technique
LTT	Low temperature technique
MALDI	Matrix-assisted laser desorption/ionization

MEMA	2-(N-morpholino)ethyl methacrylate
MNP	Magnetic nanoparticles
MRI	Magnetic resonance imaging
NAM	Normal amine mechanism
NCA	N-carboxyanhydride
NCA-ROP	N-carboxyanhydride ring opening polymerization
NMP	Nitroxide mediated polymerization
NMR	Nuclear magnetic resonance
OEGMA	oligo(ethylene glycol) methacrylate
OMS	Ordered mesoporous silica
PAT	Photoaucostic computed tomography
PBLG	poly(benzyl-L-glutamate)
PCBL	poly(ε-carbobenzyloxy-L-lysine)
PDI	polydispersity index
PGA	poly(glutamic acid)
PLL	poly-L-lisine
PMA	poly(acrylamide)
QD	Quantum dots
RAFT	Reversible addition-fragmentation chain transfer polymerization
RNA	Ribonucleic acid
ROP	Ring opening polymerization
SEC	Size exclusion chromatography
SI-NCA-ROP	Surface initiated N-carboxyanhydride ring opening polymerization
siRNA	Small interfering ribonucleic acid
SPINOs	Superparamagnetic iron-oxide nanoparticles

S_{sp}	Surface specific area
TEM	Transverse electron microscope
TGA	Thermogravimetric analysis
THF	Tetrahydrofuran
tBLC	S-(*tert*-butyl) cysteine
ZLL	ε-carbobenzyloxy-L-lysine

Chapter 1

Introduction

1.1 Introduction

In recent years tremendous research activities targeting the development of nanotechnology has revolutionized the diagnosis and treatment of tumour, pain and infectious diseases.[1] These advanced therapeutics harness the opportunities provided by nanoparticles arising from their unique properties to monitor the drug kinetics and to increase the drug efficacy by improving drug solubility, extending half life and by reducing immunogenicity.[2-5] Nanoparticles that have been studied for biomedical applications range from noble metals[6,7] like Ag, Au to semiconductors[8,9] like CdS, ZnS, SiO_2, TiO_2 and magnetic compounds[10,11,12] like Fe_2O_3/Fe_3O_4, $CoFe_2O_3$, etc. These inorganic nanoparticles offer high surface to volume ratios and size dependent unique optical, magnetic, electronic, or catalytic properties.[13] Another class, organic nanoparticles or soft nanoparticles, which include liposome[14], polymeric micelles[15] and nanogels[16] offer features like wide range of functionality for conjugation of targeting ligands and ability of carrying both hydrophobic and hydrophilic payload into respective components of the self assembly structures.[17]

Organic/inorganic hybrid systems are interesting "intermediate" class and often display unique features compared to the constituting component alone. Compared to conventional materials enhanced performance can often be achieved by the systematic tuning of the functionalities of the constituting components of hybrid materials.[18,19] This opens a potential for new advanced applications such as imaging[20], sensors[21], drug delivery[22], etc. Organic components such as polymers have been widely used to form inorganic-polymer hybrids to improve dispersion, biocompatibility and functional properties of inorganic materials.[23] Inorganic-polymer hybrids have been synthesized by coating polymer onto an inorganic nanoparticle surface by physical, chemical, ionic and adsorption methods.[24] Chemically tethered polymer inorganic hybrids are synthesized either by anchoring pre-formed, end functional polymers onto functional inorganic surfaces by using known coupling chemistry (grafting onto)[25,26] or by polymerization of monomers from inorganic surfaces by immobilized initiators (grafting from).[27] In the later case, the grafting density of polymer chains per square unit surface area is higher due to lower sterical hindrance for monomers to reach the growing polymer site (**Fig.: 1.1**).

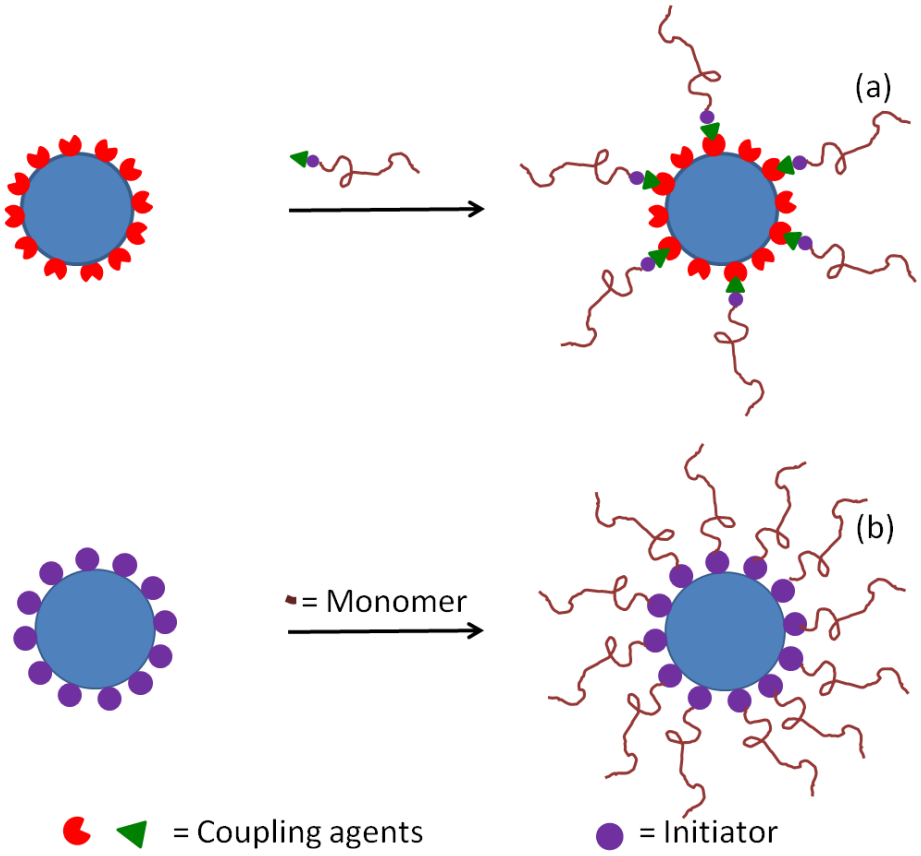

Figure 1.1: Hybrid material synthesis by 'grafting onto' (a) and 'grafting from' (b) approach.

Various polymerization methods have been developed to design inorganic-polymer hybrids by the 'grafting from' approach, in particular conventional controlled radical polymerization methods such as atom transfer radical polymerization (ATRP)[28], reversible addition-fragmentation chain transfer polymerization (RAFT)[29], nitroxide mediated polymerization (NMP)[30,31] and ring opening polymerization (ROP)[32,33]. Excellent control over the polymer thickness and the large choice of readily available monomers with a range of functionalities make controlled radical polymerization techniques of vinyl monomers advantageous over other polymerizations from inorganic surfaces. However the corresponding polymers have a disadvantage of not being biodegradable and in some cases not biocompatible, which is detrimental for their application in some biomedical devices. Hybrid materials constituting biocompatible and biodegradable organic component derived

from renewable resources (e.g. amino acids, carbohydrates, lactons, lactides) can overcome these drawbacks of synthetic vinyl polymers.[34] The use of polypeptides for the functionalization of inorganic nanoparticles offers biocompatibility in conjugation with diverse functionality dependent on the particular amino acid chosen from a pool of natural and non-natural amino acids. Consequently, in recent times increasing attention has been given by research community to investigate synthetic polypeptides as building blocks for functional hybrid materials for advanced biomedical applications. 'Surface grafting' of the synthetic polypeptides using α-amino acid N-carboxyanhydride ring opening polymerization (NCA-ROP) is the most commonly used technique to decorate surfaces with synthetic polypeptide brushes.

1.2 Synthetic Polypeptides

Synthetic peptides or poly(amino acid)s are polymers derived from the 20 natural and many non-natural amino acids. Due to their structural similarities to natural proteins and peptides, these materials can address the challenges of biocompatibility and biodegradability associated with fully synthetic polymers. Moreover, these synthetic polypeptides may adopt stable secondary structures like helices, sheets and random coil through non-covalent interactions leading to novel self-assembled supramolecular structures.[35] Additionally, these polypeptides can reveal a transition in response to the change in local environment like temperature, pH, salt etc. depending on the side chain functionality of constituting amino acids.[36,37,38] All these advantages make polypeptide based materials interesting for the use in various biomedical applications such as sensors, drug delivery, tissue engineering among others.[39] Two synthetic approaches, namely solid phase peptide synthesis (SPPS) and α-amino acid N-carboxyanhydride ring opening polymerization (NCA-ROP) are employed to synthesize synthetic polypeptides. Both synthetic techniques offer advantages and limitations over the other. Polypeptide with well defined and precisely controlled amino acid sequence can be obtained by SPPS method via step-wise coupling of protected amino acid on a solid support.[40] Nowadays, SPPS is a routine and robust method to synthesize sequenced polypeptides with small and medium size (up to 50 amino acids) with

high yield and purities on laboratory scale. However, incomplete coupling steps, side reactions, low yield and increased difficulty in purification are drawbacks in the synthesis of peptides with increasing chain lengths.[41] In comparison, high molecular weight homo and copolypeptides with unspecific sequences can be synthesized by NCA ring opening polymerization. Over a century after the first report of amino acid anhydride synthesis by Leuches in 1906, many advances has been made in the NCA-ROP technique leading to precise control over the structure, molecular weight, narrow polydispersities, and ease of synthesis.[42,43,44,45]

1.3 N-carboxyanhydride Ring Opening Polymerization

Herman Leuches in early 1906, reported the first synthesis of an amino acid NCA and its ring opening polymerization.[46] In the publications reported in 1906 and 1907, he called the polymerization products of NCA's 'anhydride form of amino acid'. From its amorphous character and lack of sharp melting point, later in 1908 he concluded the products being polymeric modifications of α-lactum. After 1921, a definite role of NCA as a monomer to synthesize high molar mass polypeptides by ring opening polymerization using water, alcohol and primary amine as initiators was demonstrated by Curtius[47], Wessely[48] and their co-workers. NCAs of α-amino acids can also be synthesized by an alternative method by treatment of amino acids or their derivatives with phosgene. (Fuchs-Fartig method, **Scheme: 1.1**).[49] Handling of harmful phosgene could be avoided by use of alternatives like triphosgene, diphosgene, di-tert-butyltricarbonate, i.e. reagents capable of in situ generation of phosgene in an anhydride ring closing reaction.[50]

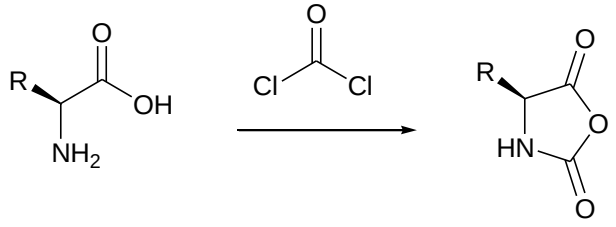

Scheme1.1: N-carboxyanhydride synthesis by Fuchs-Farthing method.[49]

1.3.1 Mechanistic insight into NCA-ROP

Before reports of living ring opening polymerization of NCA by Deming[42], most researchers agreed on two possible pathways for NCA ring opening polymerization, i.e Normal Amine Mechanism (NAM) and Activated Monomer Mechanism (AMM). A variety of nucleophiles such as primary amines and bases such as metal alkoxides, tertiary amines can be used for initiating ROP of NCA. The NAM is attributed to strong nucleophiles whereas AMM is attributed to strong bases. For secondary amine as NCA-ROP initiating moiety, coexistence of both mechanisms is proposed.

1.3.1.1 Normal Amine Mechanism (NAM)

Non-ionic initiators bearing at least one free hydrogen atom such as primary amines, secondary amines, alcohols and water are proposed to initiate NCA-ROP by NAM. Initiation occurs by nucleophilic attack of the base on the C5 carbonyl of the NCA to give an intermediate unstable carbamic acid further decarboxylating to produce a new free amino group, which sequentially attacks a new NCA monomer (**Scheme 1.2**). The higher nucleophilicity of the primary amines over those of the polymer amino groups results in a faster initiation than propagation rate leading to polypeptides with low polydispersities. Carbamic acid-CO_2 equilibrium, solvent and presence of water and other impurities may cause deviation from the living nature of polymerization. An intermediate carbamic acid can form a salt with the amino group of the propagating chains, which influences the reaction kinetics resulting in higher than first order reaction kinetics.

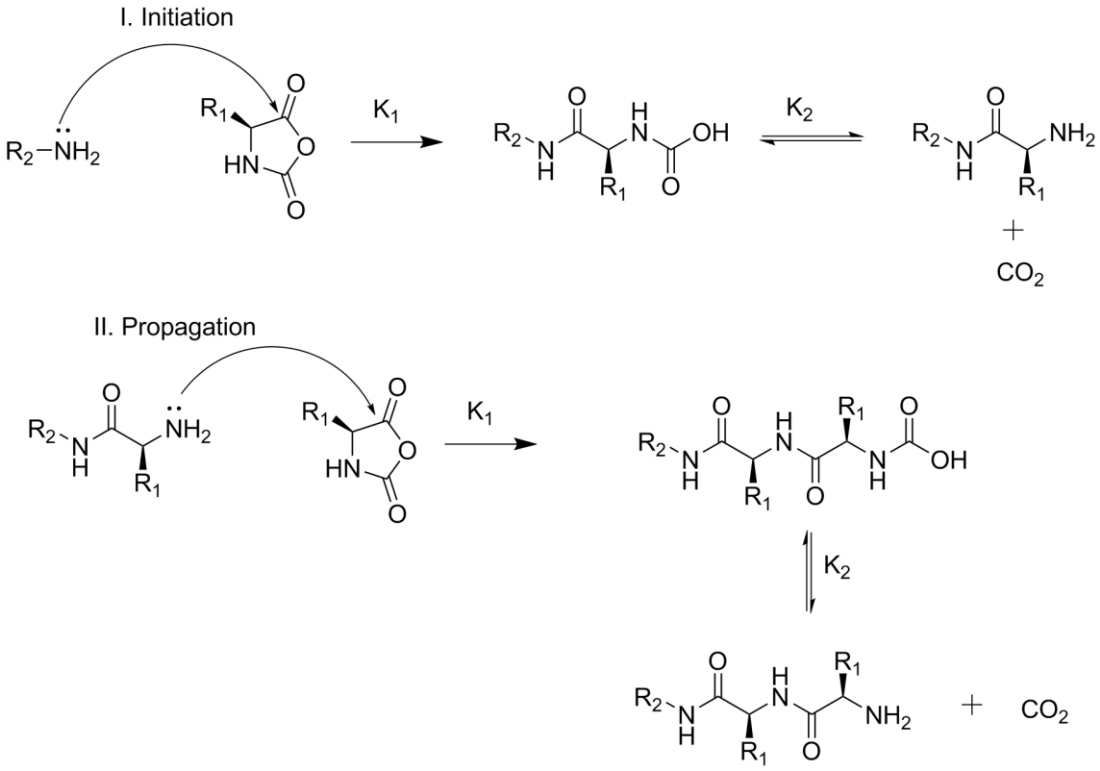

Scheme 1.2: Normal Amine Mechanism for NCA Polymerization.

1.3.1.2 Activated Amine Mechanism (AMM)

Ballard and co-workers[51] first proposed this mechanism to explain tertiary amine initiated NCA-ROP of DL-phenylalanine, which was further used by Szwarc[52] to illustrate basic salt initiated NCA-ROP (**Scheme 1.3**). In this mechanism, the initiator acts as a base rather than a nucleophile abstracting a proton from the 3-N of the NCA resulting in the corresponding anion, which attacks the 5-CO of another NCA followed by simultaneous release of CO_2, creating a new anion. Monomer and solvent impurities play an important role in AMM, which can affect the reaction kinetics. Since the AMM proceeds via anions, propagation is faster than in NAM resulting in the formation of higher molecular weights polypeptides, whereas slower initiation than propagation in AMM leads to high polydispersities.

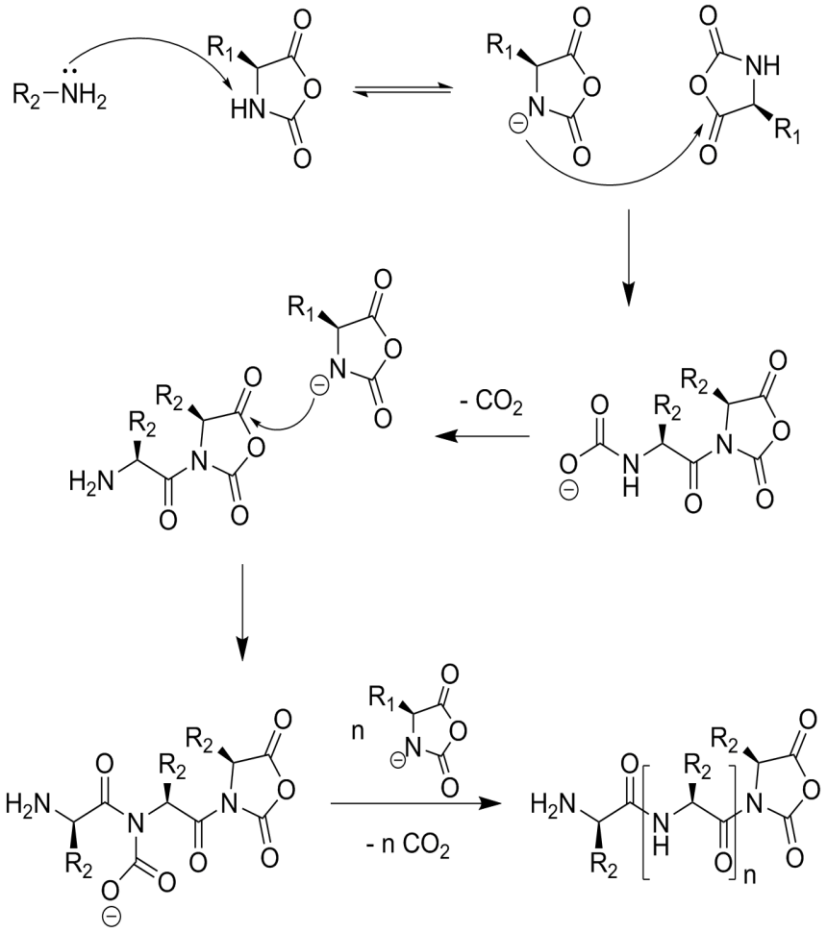

Scheme 1.3: Activated monomer mechanism (AMM) for NCA polymerization.

1.3.1.3 'Living/Controlled' Polymerization of NCA

The term 'living polymers' was first introduced by M. Swarc in connection with an anionic polymerization of vinyl monomers.[53] The definition 'Living' combines two characteristics: first, the reactive end-groups of propagating chains should remain unchanged (alive) after 100 % conversion of the monomer and second, the molecular weight distributions should be narrow, (PDI bellow 1.2). In 1997, Deming explored a new class of NCA-initiators, transition metal analogues of strong bases, to achieve first known 'Living' NCA polymerization.[42] Since strongly basic initiators build up high molecular weight

polypeptides, it was hypothesized that fast chain-propagation can relatively minimize chain-transfer reactions. Various transition metal complexes such as amido, alkoxy, alkyl and carbamate complexes were screened for NCA polymerization activity and control of the polymerization. Zerovalent nickel and cobalt initiators [i.e., bpyNi(COD)[49] and $(PMe_3)_4Co$[54], COD = 1,5-cyclooctadiene] showed high efficiency and good control, reflected in synthesis of homo- and block-co-polypeptides with predictable molecular weights and low PDI. Both these metals react identically with NCA monomers by oxidative addition across anhydride bonds of NCA to from metallacyclic complexes which is general requirement for living NCA polymerization by transition metal initiators (**Scheme 1.4**). The presence of a metal in the final polypeptide and non-reactivity towards N-substituted NCA such as proline, are the major drawbacks of this technique.[55] Recently, a transition metal platinum complex namely [bis(diphenylphosphino)-ethane][N-((1S,2R)-2-amido-1,2-diphenylethyl)-4 methylbenzenesulfonamidato] platinum, has been shown to work as an efficient initiator for NCA-ROP.[56] Primary amine hydrochlorides are also capable of NCA-ROP provided the polymerization should be conducted at elevated temperatures.[57] Schlaad envisioned that the AMM pathway would be avoided at elevated temperatures as the concentration of the free amine species increases with the increase in rate of exchange of free amine and amine hydrochloride. Primary amine hydrochloride end-capped polystyrene was used as a macro-initiator to polymerize Z-L-lysine-NCA at temperatures between 40-80 °C, yielding block copolymers with narrow polydispersities (PDI < 1.1) in 64-84% yield. However, this technique is not useful for the synthesis of multi-block co-polypeptides owing to incomplete polymerization due to low reactivity of the active species, making separation of the unreacted monomer from polymer difficult. In 2004, the first neat NCA polymerization initiated by primary amines was reported by Hadjichristidis and co-workers.[58] Drawbacks concluded from previously reported NAM techniques led this group to use highly purified monomers and the application of high vacuum techniques (HVT) for polymerization. Using this methodology a wide variety of NCA's could be polymerized to produce homo and block co-polypeptides. Various complex macromolecular architectures such as multi-block linear, star and star-block co-peptide have been synthesized by using this technique.[59]

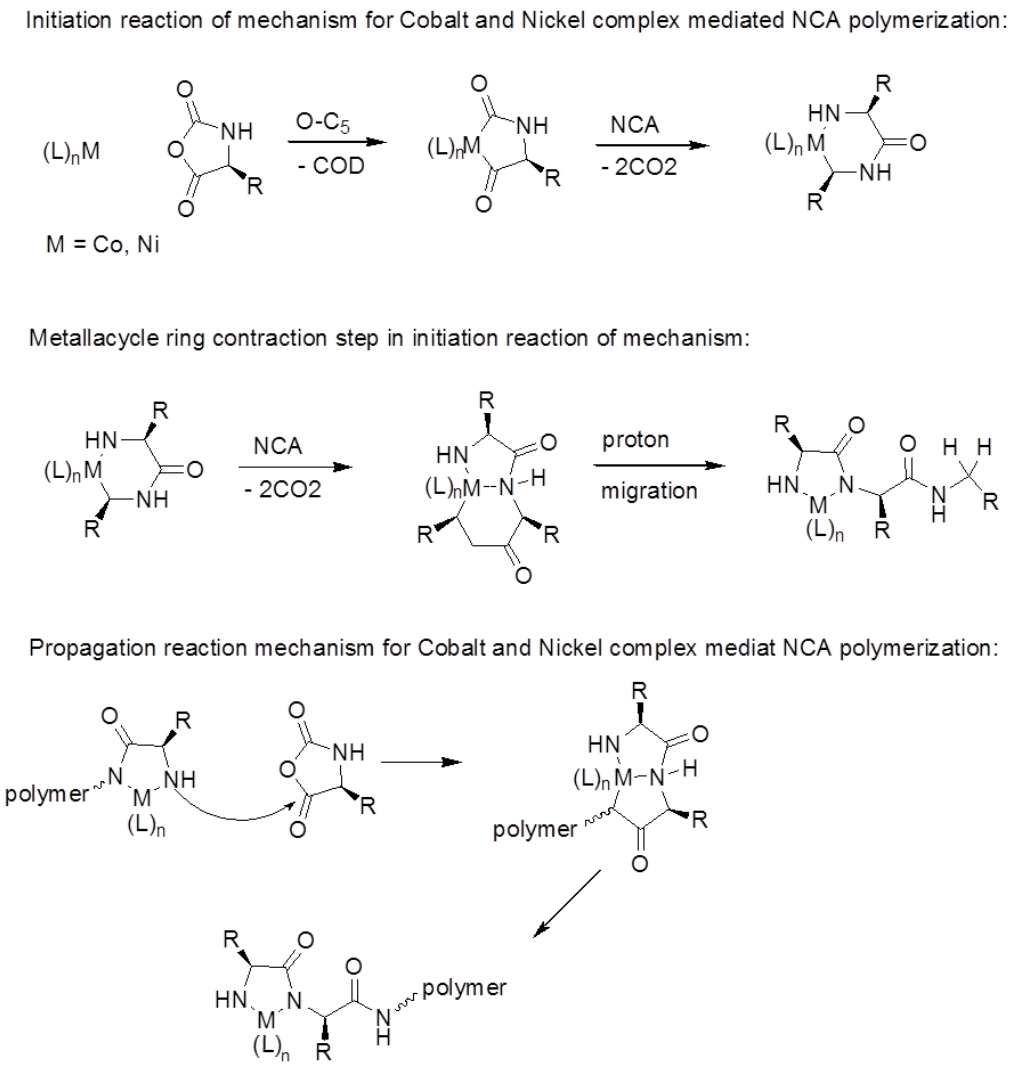

Scheme 1.4: Transition metal mediated NCA polymerization proposed by Deming and co-workers.[42]

In 2004, in an another novel approach to minimize chain termination reactions in NAM, Vayaboury and co-workers[60] studied polymerization of ε-trifluoroacetyl-L-lysine NCA (TFA-Lys NCA) in DMF by lowering the reaction temperature and using Schlenk techniques under nitrogen. SEC and non-aqueous electrophoresis of reaction mixture, revealed an increase in the number of living chains from 22 to 99% by lowering reaction temperature from 20 to 0 °C. It was envisioned that at 0 °C, the activation energy barrier of the propagating chain is lower than the side reaction, thus dominating the reaction kinetically. The drawback of prolonged reaction time of this technique can be eliminated by

combining HVT and LTT.[61] Applying both the techniques not only give excellent control over polymerization but also significantly reduce the reaction times. In 2007, Lu and Cheng[62] have explored silazane derivative mediated living NCA polymerization similar to the group transfer polymerizations (GTP) of acrylic monomers initiated by similar organosilicon compounds. The block co-polypeptides such as poly(*γ*-benzyl-L-glutamate)-*b*-poly(*ε*-carbobenzyloxy-L-lysine) (PBLG-*b*-PZLL) synthesized by sequential addition with this technique, showed narrow polydispersity indices and molecular weights as expected with quantitative yields. In a later study, this research group showed efficiency of other functional group bearing N-TMS amines such as benzyl amine, propargylamine, m-PEG200 amine as initiators for NCA polymerization. These functional groups are useful for further reactions such as click chemistry or ring opening metathesis polymerization.[63] The rare earth metal complexes can also be employed as NCA-ROP initiators to synthesize homo, block, and random co-polypeptides with low polydispersities and quantitative conversions.[64] Mechanistic investigation of this polymerization showed co-existence of the AAM and NAM paths by nucleophilic attack of a metal on the 5-CO and simultaneous deprotonation of the 3-NH of NCA.[65]

1.3.2 Surface Grafting of polypeptides

Synthetic polypeptide decorated hybrids are advantageous over the synthetic polymer hybrids in biocompatibility and biodegradability. As described earlier, 'grafting to' and 'grafting from' are the most commonly used techniques to form covalently attached polymer brushes onto solid surfaces. Likewise, anchoring of the polypeptides onto an inorganic surface can be achieved by the 'grafting to' approach where the end-functional, pre-formed synthetic polypeptide synthesized by NCA-ROP is tethered covalently to an appropriately functional surface using coupling chemistry. The main advantage of this technique is the possibility of comprehensive characterization of the polypeptides prior to the grafting resulting in hybrids with defined composition of brushes. However, since the steric hindrance and diffusion of peptide chains onto the surface are limiting factors, it often results in non-homogeneous, low density grafting of polypeptide brushes. In

comparison, the 'grafting from' technique involves ring opening polymerization of NCA from initiator immobilized solid surface. Covalently or non-covalently immobilized primary amines anchored to a solid support are predominantly used as an initiator. The surface initiated NCA-ROP results in the formation of high density, homogeneous polypeptide brushes. However, control over the molecular weight and molecular weight distribution remains a challenge in this technique resulting from difficulties in controlling the initiation and propagation rates from the surface immobilized initiators.[66] This drawback is offset by the high density of grafted polypeptides and the high density of functional groups resulting from it. This opens opportunities for rendering desired properties of hybrids materials useful for technological applications. Building on the versatility of both surface grafting techniques a wide range of organic and inorganic surfaces such as mesoporous and non porous silica',[67], silicon wafers[68,69,70,71], iron-oxide nanoparticles[72], gold surfaces[73,74,75], glass slides[76], macro porous polymeric structures[77], micro porous polymeric membranes have been decorated with synthetic polypeptides. The stimuli responsive properties of the surface grafted polypeptides have been used for applications such as molecular recognition, ion exchange and drug delivery systems.

1.3.2.1 Polypeptide Hybrids by 'Grafting-to' Technique

The ease of characterization of preformed polypeptide and well known thiolate-gold interaction resulted in an early report of disulphide end-functional poly(benzyl L-glutamate) (PBLG) grafting onto planer gold surfaces. Samulski and co-workers[78,79] employed N-terminus lipoic acid modified PBLG to graft it onto the gold surface. The chemisorption of disulphide end-functional PBLG through strong thiolate-gold interaction was demonstrated by FT-IR and water contact angle measurement. The chemisorbed helical PBLG showed tethering to gold surface with higher grafting density when compared to physically adsorbed non end-functional free PBLG. In a further report, the same group demonstrated use of electrostatic interaction to improve the grafting of helical PBLG onto a charged gold surface owing to the macroscopic dipole moment of PBLG.[80] An efficient tethering of PBLG helical rods through thiolate-gold interaction under the influence of an electrostatic field resulted in thicker films compared to their previous results. The

phenomenon of macroscopic dipole of helical PBLG and the strong intramolecular dipole interaction between the chains caused an anti-parallel alignment of the helical rods resulting in a double layered assembly of polypeptides on the substrate.

By employing helicogenic (e.g. $CHCL_3$) and non-helicogenic (e.g. DMSO) solvents to control the helicity of grafted PBLG, Higashi and co-workers[81] demonstrated the reversible assembly of single and double-layered PBLG onto gold surface. Further demonstration of utilizing helical macroscopic dipole moment to graft high molecular weight polypeptides (Mw: 27 kDa) with higher grafting density was shown by Williams and Gupta.[82,83] N-lipoyl-1,3-diaminopropane was used as an initiator for NCA-ROP to obtain helical PBLG with a free N-terminus exhibiting a macromolecular dipole moment with opposite direction reported previously. These polypeptides rapidly assemble onto the gold substrate with surface coverage influenced by molecular weight of PBLG, solvent and assembly time.

A different approach to graft polypeptides onto silicon surfaces was investigated by Chang and Frank.[69] Functional silanes were immobilized onto planer silicon surfaces to facilitate the grafting of the polypeptides. Three strategies were devised: In the first approach, the silicon substrate was functionalized with chloroformate using 3-(trichlorosilyl) propyl chloroformate. A preformed PBLG was anchored to the silicon surface by using the interaction of terminal amino group of polypeptide and chloroformate groups present on the surface. In an another approach, triethoxy silane end-functional PBLG was synthesized utilizing 3-(aminopropyl) triethoxysilane (APTES) as an initiator for NCA-ROP and subsequently attached to the silicon wafer. In a third approach, the silicon surface was decorated with APTES and a subsequent polymerization of BLG-NCA to graft PBLG from the silicon surface was carried out. Although all three approaches successfully demonstrated PBLG grafting onto to the surface they resulted in different polypeptide film thicknesses and grafting densities. The first approach showed low grafting density of polypeptide due to PBLG dipole interaction with the substrate resulting in chains lying parallel to the surface, eventually causing lower grafting density. The second approach revealed a higher grafting density of PBLG attributed to grafting of oligomeric PBLG chains formed due to condensation of silanol moieties prior to surface tethering. Despite the success of grafting of PBLG in all three approaches, the last ‘grafting from’ approach was

severely hampered by intermolecular interactions. The high rate of initiation resulted in densely packed oligomers with β–sheet structures, making the propagating amine inaccessible to the solvated monomers, inhibiting further film growth. Since this report, significant advances have been made in the 'grafting from' approach making it more attractive technique to synthesize polypeptide hybrids.

Similar to the planer surfaces, microporous membranes have also been investigated for the grafting of polypeptides to improve their properties. In an attempt to tune the separation properties of cellulosic membrane, Hollman and Bhattachrya[84] grafted pH responsive poly(L-glutamic acid) (PHLG) onto an aldehyde prefunctionalized macroporous membrane. A display of conformational change from helix to coil by PHLG depending on the microenvironment pH was used to control the hydraulic permeability and ion selectivity in dilute conditions. In an another demonstration of utilizing polypeptides to diversify the applications of single walled carbon nanotubes (SWNTs) poly(L-lysine) surface grafting was employed by Li and co-workers.[85] Primary amine groups on PLL side chain were coupled with carboxylic groups of oxidized SWNTs by well known carbodiimide coupling. The PLL functional SWNTs were then immobilized onto gold substrate followed by coupling of horseradish peroxide through remaining amine groups of PLL by using same carbodiimide coupling to construct biosensing electrode for H_2O_2.

Following polypeptide grafting onto the planer surfaces, spherical surfaces such as silica nanoparticles were also investigated for polypeptide tethering to improve properties and applicability. Russo and co-workers used copper catalyzed azide-alkyne click (CuAAC) to tether polypeptide to nanoparticle surface.[86] By employing propargylamine as an initiator for NCA-ROP, alkyl end functional poly(stearyl-L-glutamate) (PSLG) was synthesized followed by grafting onto azide-functionalized silica nanoparticles by azide-alkyne click chemistry. The surface grafted hydrophobic PSLG polypeptide improved the dispersion properties of silica nanoparticles in organic solvents like THF, toluene and $CHCl_3$.

Using a similar approach, Gupta and co-workers[87] grafted PLL onto silica nanoparticle surface to investigate the gene delivery and antimicrobial applications of the hybrids. The CuAAC coupling of propargyl end functional poly (ε-crbobenzyloxy-L-lysine) (PZLL) onto azidotriethoxysilane functional silica nanoparticles resulted in core-shell silica-

polypeptide nanoparticles. The group also successfully demonstrated grafting of amphiphilic block-co-polypeptide (L-lysine-b-L-leucine) from colloidal silica for antimicrobial applications against gram-positive and gram-negative bacteria. In an another demonstration of polypeptide grafting to silica nanoparticles by same research group, pH responsive PLGA was grafted from nano silica and its self-assembly to form 3D scaffolds by ice templating technique was investigated.[88] These scaffolds possessed lamellar structures with fish bone type architectures (**Fig.: 1.2**) and showed disassembly behavior upon contact with water. The mechanical strength of the scaffold was increased by crosslinking PLGA chains with poly(ethyleneimine) (PEI). These materials possess potential for applications in 3D scaffolds for tissue engineering. Like amorphous silica nanoparticles, mesoporous silica materials have also been grafted with PLL using similar CuAAC approach by Gupta and co-workers.[89] These PLL grafted mesoporous materials were able to maintain their porosity after conjugation and could be useful as platform materials for drug delivery applications.

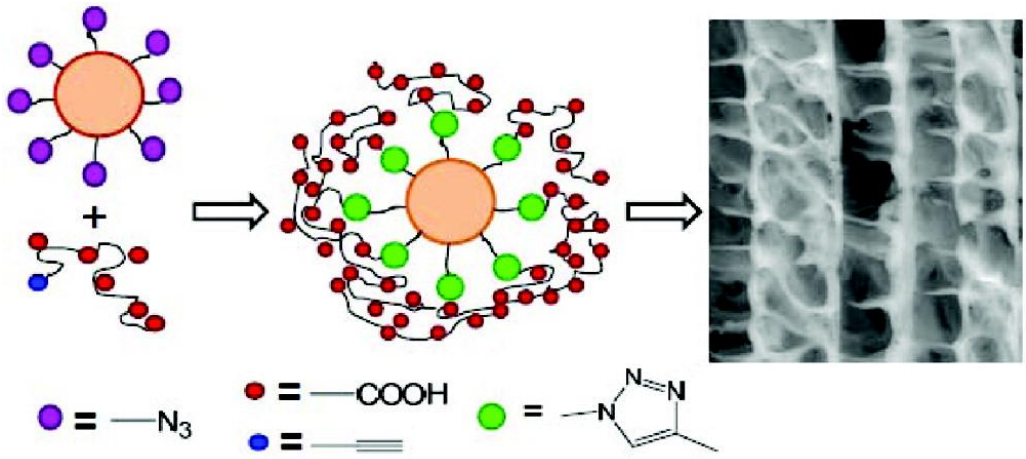

Figure 1.2: Silica-PLGA composites by azide-alkyne click and their macroporous assembly.[88]

1.3.2.2 Polypeptide Hybrids by 'Grafting- from' Technique

While the 'grafting to' technique allows the comprehensive characterization of the polypeptide prior to the surface grafting, its drawback is the generally low grafting efficiency arising from inherent steric hindrance. In comparison, 'grafting from' technique involves polymerization of NCA monomer by ROP from surface immobilized initiator to graft polypeptides. The later approach offers higher grafting efficiency and produces homogeneous polypeptide brushes. Amines or metal catalysts have predominantly been used as an initiator for surface initiated ring opening polymerization. Being nucleophilic, primary amines are excellent initiators for NCA-ROP proceeding via the normal amine mechanism (NAM). Under the confined conditions of a surface polymerisation it is possible that primary amines act as bases favouring the activated monomer mechanism (AMM). This can lead to non-grafted polypeptide chains in solution with high polydispersities. Since both the pathways might co-exist, it is essential to suppress the AAM to avoid free polymer formation and to ensure efficient polypeptide grafting from the surface.

Most commonly, an initiator is immobilized onto the surface by forming self-assembled monolayers (SAM) using organosulphide/thiol and alkyl/alkoxy silane coumponds onto gold and silicon surfaces, respectively. However, initiators are often densely packed and spacing between the adjacent initiating sites is smaller than a cross-sectional area of the grafted polypeptides (i.e. helix). Therefore, it was proposed that it is essential to control the spacing of initiating sites to offer enough space for native folding of the grafted polypeptide. Much work has been done on controlled spacing of initiating sites for example, the use of SAM with larger cross-sectional tripod structure[90], use of mixed composition of initiator bearing and non bearing SAM[91,92,93], micropattering of SAM by photolithography[94,95] or microcontact printing[96].

1.3.3 Surface Initiated NCA-ROP from Planar Surfaces

Menzel and co-workers[68] reported early studies on surface initiated ring opening polymerization (SI-ROP) of NCA-BLG from APTES functional silicon wafers. The number of initiating amine groups on the surface were varied by using a mixed SAM approach which showed a correlation with the grafted polypeptide film thickness and surface morphology. Typically, SAM composed of 40% initiator showed minimum surface roughness which only increased beyond this composition but the polypeptide film thickness remained unchanged. FT-IR measurements of the films showed helical confirmation of the PBLG chains.

Electrochemical properties of the ultrathin polypeptide films grafted from metal surface were studied by Jaworek and coworkers[97] to investigate the orientation of the helical strands. Grafting of PBLG from aluminium surface under the influence of the applied electrical field showed inverse-piezoelectric effect indicating parallel arrangement of the PBLG chains. Despite the observed inverse-piezoelectric coefficient, the voltage sensitivity exhibited by the films was comparable to the commercial piezoelectric materials indicating the potential of 'grafting from' approach to grow piezoelectric-active films from a variety of electrodes and flexible substrates.

Since surface initiated NCA-ROP in solution is observed to suffer from chain termination or other side reactions it often results in lower degree of polypeptide grafting and large proportion of monomer remains unreacted in solution. In 1996, an alternative method of melt surface initiated NCA-ROP was investigated by Wieringa and Schouten.[98] In this study, γ-methyl-L-glutamate (MLG) NCA was deposited onto APTES functionalized silicon wafers using a spin coating technique. The substrates were then heated above the melting point of the MLG-NCA (i.e., >105 °C) to increase the mobility of the monomers and to allow the NCA-ROP initiation by surface bound amine groups. Although complete monomer conversion was achieved in 30 mins. by this method, only 20% of the monomer was polymerized from the surface since NCA monomer can undergo thermal polymerization at elevated temperatures. In spite of low polypeptide grafting, the surface grafted PMLG brushes were shown to adopt purely α-helical structures while the non

grafted free polypeptides showed both α-helical and β-sheet confirmations. Another solvent free approach for grafting of polypeptides from amine functional planer surfaces was investigated by Frank and Chang[70] in 1997. PBLG chains were grafted from APTES functional silicon wafers through the vapour deposition polymerization. In VDP the vacuum reaction conditions (0.02-0.04 Torr) allow the NCA vaporization to occur at much lower temperatures than in the melt polymerisation and the monomers remains mobile in the gaseous phase until they condense onto the substrate. This method is advantageous over melt polymerization for reproducibility and its ease to vary local monomer concentration to obtain polypeptide films of tuneable thickness. Wang and Chang[99] introduced further improvements to the VDP method. By redesigning the reaction chamber and optimizing the reaction conditions the versatility and robustness of the improved VDP was demonstrated by surface grafting of homo and block co-polypeptide films of PZLL, PMLG, PPA and poly(-benzyl-L-aspartate) (PBLA).

A better controllable method of grafting polypeptides in solution from solid surfaces such as silicon and quartz wafers was studied by Schouten and co-workers.[100,101,102] SI-ROP of NCA-BLG and NCA-MLG was carried out from APTES functionalized silicon wafers and quartz slides in anhydrous N, N-dimethylformamide (DMF) at 40 °C. Most of the polypeptide growth occurred in the first 5 h of the reaction and polypeptide film thickness showed a pronounced dependence on monomer concentration in solution. The surface grafted polypeptides showed pure rigid α-helical confirmations with perpendicular orientation to the surface. The effect of monomer size onto helix orientation was studied by comparing helix-surface tilt angles (θ). PMLG with smaller methyl side group displayed a more upright orientation with higher tilt angle compare to PBLG (benzyl side group) attributed to higher grafting density combined with steric hindrance and unfavourable polar interactions. The authors also reported the first time synthesis of surface grafted block co-polypeptide films.[102] Due to the shorter reaction times, the chain termination and the formation of free polypeptides in solution are least favourable ensuring reactive amino end groups intact for further polypeptide growth. A diblock co-polypeptide composed of PBLG as first block and a second block of PMLG were synthesized from APTES functional silicon wafers. Polymerization of the BLG-NCA was carried out from the surface for short period of time (2 h). After removal of the unreacted monomer, the grafted PBLG chains

were used as macro-initiators for subsequent polymerization of MLG-NCA. Using X-ray photoelectron spectroscopy (XPS) it was found that maximum grafting density for PBLG was not achieved within an hour of reaction and polymerization of the second monomer NCA-MLG at this stage leads to formation of PMLG helices in between the preformed PBLG brushes. Following the studies of helical orientation on planer surfaces, Schouten and co-workers[103] investigated the reversible inversion of helical screw sense of surface grafted polypeptide by means of external stimuli. SI-ROP of β-phenethyl-L-aspartate N-carboxyanhydride from APTES functional quartz surface yields poly(β-phenethyl-L-aspartate) (PPELA) films with right handed helical confirmation. Inversion of the helical screw of grafted chains to left-handed π-helical conformation takes place upon annealing of the films at 150 °C for 30 min. The inversion is completely stable under any conditions of further temperature changes. Reversal of the helical screw inversion to the original only takes place upon immersion of the annealed films into helicogenic solvent (e.g. $CHCl_3$). The inversion of the helical orientation is repeatable over many cycles of annealing and solvent treatment. The authors also devised a chemical crosslinking procedure to preserve the desired helical conformation.[104]

The effect of macrodipole moment of pre-grafted polypeptide onto the rate of polymerization of growing polypeptide chain was studied by Higashi and co-workers.[105] Modified PBLG with disulphide moieties at C-terminus (PBLG-C-SS) and N-terminus (PBLG-N-SS) were synthesized and grafted onto the gold surfaces. The resulting PBLG films showed opposite macrodipole moments. The polypeptide uncovered surface area of the films was subsequently amine functionalized using a mixed SAM approach. ROP of BLG-NCA from the initiator immobilized gold surface experienced the influence of direction of macrodipole moment of the pre-adsorbed PBLG chains. The rate of NCA-ROP from the gold surface in the presence of the pre-adsorbed PBLG-N-SS increased by ten folds compared to in the absence of the pre-adsorbed polypeptide. The authors attributed the increase in rate of polymerization to the macrodipole moment of PBLG-N-SS which is anti-parallel to the direction of growing PBLG chain favouring the formation of PBLG with higher degree of polymerization (DP:95). On the other hand, the PBLG-C-SS showed a parallel macromolecular dipole moment to the direction of growing polypeptide chain resulting in grafting of PBLG with lower degree of polymerization (DP:15).

Recently, in an attempt to create non-fouling polypeptide films onto planer surfaces, Klok and co-workers[106] polymerized oligo(ethyleneglycol) modified L-lysine from APTES functional silicon, quartz and glass surfaces. The success of polymerization was confirmed by XPS analysis and circular dichroism (CD) measurements which confirmed the α-helical confirmation of the grafted polypeptides. When investigated for the nonspecific adsorption of the fluorescently labelled proteins such as bovine serum albumin (BSA) and fibrinogen (FBG), the non-fouling polypeptide coated substrates exhibited significant reduction in fluorescence intensity compared to non-coated surfaces.

1.3.4 Surface initiated NCA-ROP from non-planar surfaces

The earliest report of polypeptide grafting from colloidal silica particles was done by Harmann and co-workers[107] in 1974. The ROP of L-alanine NCA (Ala-NCA) and L-leucine NCA (Leu-NCA) was carried out from aminophenyl functionalized silica particles at 15 °C in dioxane. The polypeptides thus formed by ROP could not be separated from silica particles by extraction technique, which led to the conclusion of the covalent attachment of the polypeptides onto the silica particles. Colloidal silica polypeptide hybrids with 20 to 85% unextractable polypeptide content were obtained by this method. Similarly, carbon black surfaces functionalized with amino, methyl amino and dimethyl amino moieties were investigated for NCA-ROP of MLG-NCA by Sone and co-workers.[108] As a result of better initiation, primary amine functionalized carbon black particles presented higher grafting efficiencies compared to other amines. Despite incomplete studies of uniformity of the polypeptide grafting due to limitation of synthetic tools and characterization techniques, the report conclusively proved the use of 'grafting from' technique to obtain surface-tethered polypeptides.

In 1999, Russo and co-workers reported synthesis of organophilic silica colloids by surface initiated ring opening polymerization.[67] Homopolypeptide decorated silica nanoparticles were synthesized by polymerization of BLG-NCA from APTES decorated Stöber silica nanoparticles (~100 nm) (**Fig.: 1.3**). In this report, the authors could demonstrate surface

initiation of NCA-ROP but were not able to quantitatively graft polypeptides onto the nanoparticle surface. Observed polypeptide shell thickness was much smaller than the thickness calculated by geometrical considerations. This was attributed to the chain termination reactions on the surface and free initiator induced solution polymerization to form free polymer. Covalent attachment of polypeptides to the surface was proven by characterization with techniques like FT-IR, TGA, SEM, DLS after repeated washings of nanoparticles with DMF followed by centrifugation to remove unbound polypeptide. When analyzed by thermo gravimetric analysis, polypeptide shell could account for 20% of the total composite mass. The same research group continued their work by exploring polypeptide silica composites and further studied silica-poly(ε-carbobenzyloxy-L-lysine) (PCBL) composites.[109] Unlike the first reported PBLG-silica composites, PCBL grafted core-shell particles showed distinct α-helical confirmation of the homopolypeptides. The chiral polypeptide decorated silica particles with appropriate size showed a spontaneous ability to from crystals, which showed the similar optical properties as achiral polymer decorated particles.

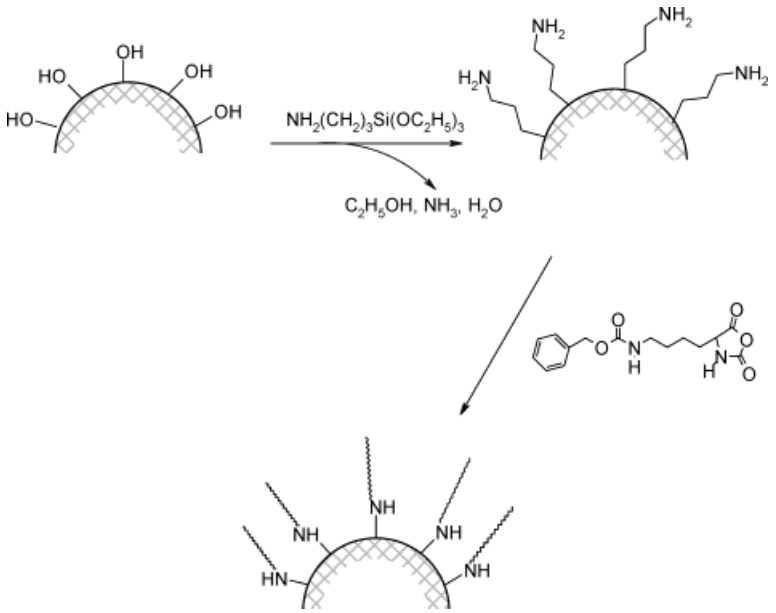

Figure: 1.3: Production of Silica-PolypeptideColloidal Composite Particles.[67]

In 2010, in an elaborated study of synthetic polypeptide-silica hybrids synthesized by immobilized initiator induced NCA polymerization, the same research group attempted to

show ‘livingness’ of the polymerization technique by sequential re-addition of monomers resulting in an additional shell growth (**Fig.: 1.4**).[110] CBL-NCA was polymerized from APTES decorated silica nanoparticle surface using DMF as a solvent at room temperature. After complete polymerization of initial monomer, a new batch of monomer was added to the polymerization solution. When analyzed by DLS for hydrodynamic radii, nanoparticles showed relative increase in the shell thickness in accordance with the monomer addition. To avoid previously seen chain termination reaction attributed to steric crowding of polypeptides, the same researchers have used amine functional and amine non-functional (reactive and passive) silanes to decorate nanoparticle surface. Due to passivation of the particle surface with non-functional silane, the grafting density of the synthetic polypeptides onto the surface dramatically reduced and the composite particles revealed ‘spiky’ appearance when analyzed by TEM (**Fig.: 1.4**). Despite the good control over the polymerization, the authors could not control the free polymer formation. This led to a discrepancy of mass conversion of NCA and actually tethered polypeptide.

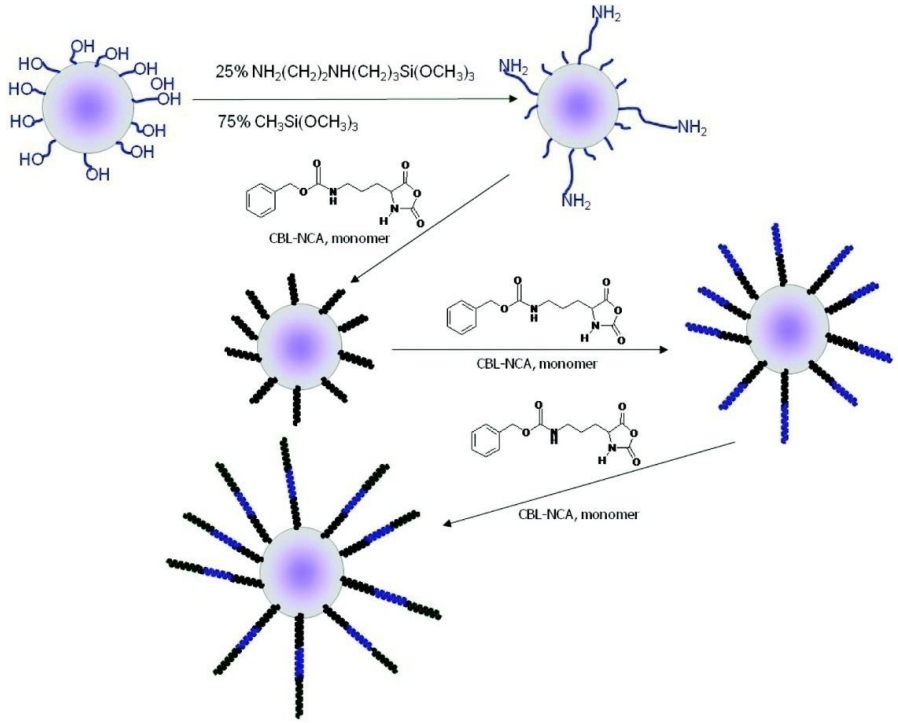

Figure 1.4: Production of Si-PCBL core-shell particles by sequential addition of monomer.[110]

SI-RIOP to graft polypeptides has also been employed from ordered mesoporous silica (OMS) to improve properties of OMS for desired applications. SI-ROP of ZLL-NCA and Ala-NCA was carried out from aminopropyltrimethoxysilane (APTMS) functionalized mesoporous silica nanoparticles by Lunn and Shantz.[111] The porosity of resultant polypeptide-OMS composites was found to be lower than polypeptides nongrafted OMS attributed to high grafting density of polypeptide brushes onto the surface. Moreover, the grafting density of the polypeptide could be varied as a function of initiator density, pore size, pore topology and type of monomer.

Other than inorganic surfaces, recently Heise and co-workers[77] employed the SI-ROP to macroporous polymeric monolith to demonstrate the grafting of polypeptide chains to tailor the bioconjugation properties of the monoliths (**Fig.: 1.5**). The porous polymers synthesized within high internal phase emulsion (polyHIPE) are an interesting class of materials with high surface to volume ratio making them useful for the applications in tissue engineering, 3D cell culture, filtration/separation techniques, etc. The authors synthesized amine functional polyHIPE by polymerizing styrene, divinylbenzene and 4 vinylbenzylamine in water at 70 ^{o}C with the help of surfactant Span-80. The primary amine moieties present on the surface of resultant polyHIPE-NH_2 were used as initiating sites for SI-ROP of BLG-NCA and ZLL-NCA to form high density brushes of PBLG and PZLL respectively. Subsequent deprotection of the side chain functionalities of the grafted polypeptide brushes resulted in high density functional group coatings rendering pH responsive properties to polyHIPE. Furthermore, authors employed deprotected polypeptide coatings (eg. –COOH functional PLGA) for the bioconjugation of enhanced green fluorescent protein (eGFP) and fluorescein isothiocyanate (FITC).

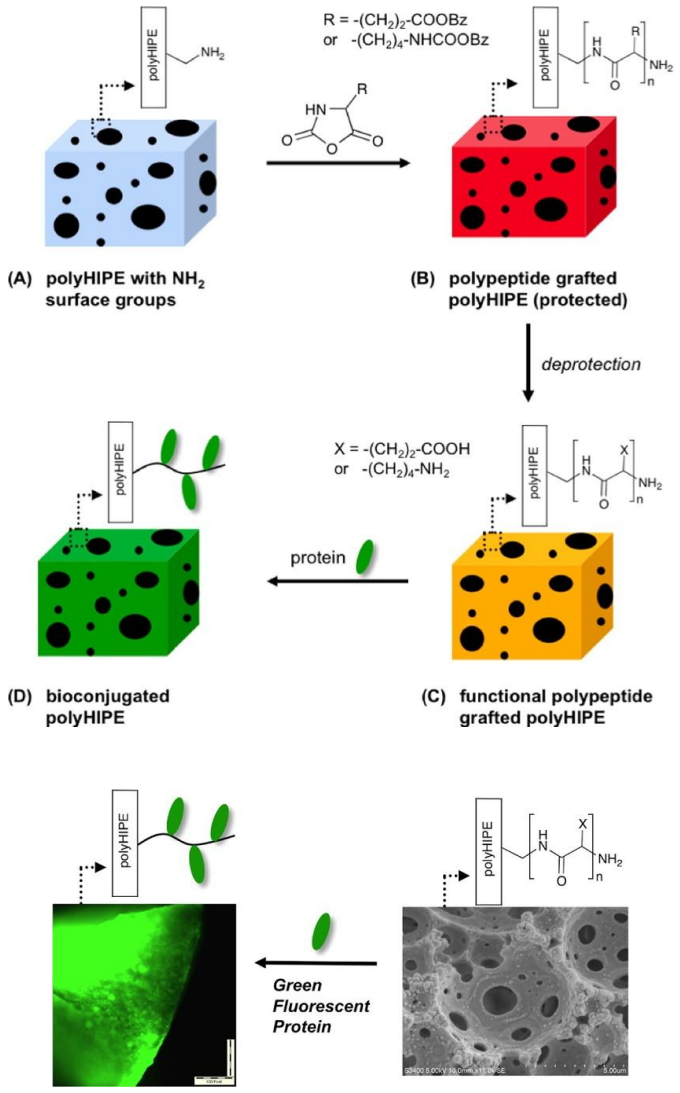

Figure 1.5: Synthetic pathways to polypeptide-grafted polyHIPE and subsequent bioconjugation.[77]

Multiwalled carbon nanotubes (MWNT's) have also been decorated with polypeptides using surface-initiated NCA-ROP. Hua and co-workers[112] synthesized amine functional MWNT's by reacting carboxyl functional oxidised MWNT's with excess 1,6 diaminohexane, followed by surface-initiated ROP of NCA-ZLL from amine moieties. The deprotection of resultant PZLL grafted MWNT's resulted in water dispersible PLL-grafted MWNT's. This approach can address the problem of processability of carbon nanotubes,

which are interesting materials for technological applications such as molecular wires, sensors, probes, and biological electronic devices.

Magnetic nano and micro particles possesses unique physico-chemical properties like superparamagnetism, high saturation field, high field irreversibility and high surface to volume ratio could find applications in biomedical technology. In recent years, attempts have been made to enhance properties and to impart unique functionalities to these nanomaterials by employing surface-initiated NCA-ROP. Yang and co-workers[113] prepared magnetic-silica polypeptide hybrids by polymerizing NCA-BLG from nanoparticle surface. Firstly, Magnetite (Fe_3O_4) particles prepared by solvothermal process were encapsulated in silica shell by sol-gel reaction followed by silanization with APTES to impart amine functionality to the nanoparticle surface. These primary amine moieties were used as an initiator to polymerize NCA-BLG from the particle surface to afford the magnetic-silica polypeptide hybrids. The hybrids showed enhanced colloidal dispersion stability (more than 3 days), though magnetic separation of the colloids could be achieved (t= 10 s) the presence of the external magnetic field.

Silica coatings onto magnetic particles might reduce the magnetic properties of the particles limiting their use in certain applications. Fernandez-Garcia and co-workers[72] designed a new strategy for functionalization of magnetic nanoparticles by employing self-polymerization of dopamine onto nanoparticle surface to introduce amine functionalities. These amine groups were then used for surface initiated polymerization of NCA-BLG to graft PBLG chains onto particle surface. Followed by the deprotection of the PBLG chains, the resultant pH responsive nanoparticles were conjugated to the model drug procaine to investigate the applications of the nanoparticles for magnetic resonance imaging (MRI) and drug delivery. Following the similar approach, magnetic-peptide-metal nanohybrids also been prepared.[114] To the PBLG grafted magnetic nanoparticles, catechol functionality was imparted to the polypeptide shell by aminolysis with dopamine. Gold nanoparticles were then formed in polypeptide shell *in situ* by allowing gold ions to interact with the catechol functionalities followed by reduction with sodium borohydride. The catalytic activity of the gold-decorated magnetic-polypeptide hybrids to reduce 4-nitrophenolate ions to 4-aminophenol was investigated. The hybrids displayed high catalytic efficiencies

(conversions up to 95% in 25 min), the ability of magnetic separation and the nanoparticles could be reused over 8 times without significant loss of catalytic activity.

1.4 Conclusion and Scope of Thesis

With the advancements of surface grafting techniques to synthesize nanoscale polypeptide hybrids, an exciting platform has been opened to design and synthesize the new class of hybrid biomaterials. A wide range of functionality, capability of undergoing conformational changes and phase transition in response to the chemical and physical changes of the microenvironment are strong arguments for candidature of polypeptide-based hybrids for biomedical applications. As summarized here, researchers have taken the advantages of these aspects and tried to develop a range of hybrids with desired properties. While in the early stage focus has mostly been on surface grafting of polypeptide films and its characterization, recently efforts have been made to answer the challenges associated with surface initiated NCA-ROP such as suppression of side reactions and formation of non-grafted materials. The aim of the presented research work is to design a facile synthetic strategy to graft polypeptides from nanoparticle surfaces. Minimal formation of the free polymer could be the key factor to graft dense polypeptide shell onto inorganic nanoparticle surface. This could be achieved by careful decoration of nanoparticle surfaces with primary amine initiators and dry, inert reaction conditions. First platform of the research will be to develop SI-NCA-ROP technique from silica nanoparticle surface. NCAs of various amino acids will be polymerized by SI-ROP to check the versatility of the technique. In later platform, new materials with sophisticated architecture and complex properties highly desired for applications like imaging, theranostics will be developed by employing the developed polymerization technique from iron oxide nanoparticle surfaces.

1.5 References

1. R. A. Petros and J. M DeSimone, *Nature Rev. Drug Disc.*, 2010, **9**, 615.

2 .G-R. Tan, S-S. Feng, D. T. Leong, *Biomaterials*, 2014, **35**, 3044.

3. C-N. Lok, T. Zao, J-J. Zhang, I. W-S. Lin, C-M. Che, *Adv. Mater*, 2014, DOI: 10.1002/adma.201305617.

4. C. Wang, M. Zhao, Y-R. Liu, X. Luan, Y-Y. Guan, Q. Lu, D-H. Yu, F. Bai, H-Z. Chen, C. Fang, *Biomaterials*, 2014, **35**, 1215.

5. F. Qui, D. Wang, Q. Zhu, G. Tong, Y. Lu, D. Yan, X. Zhu, *Biomacromolecules*, 2014, **DOI:** 10.1021/bm401891c.

6. E. C. Dreadan and M.L Al-Sayed, *Acc. Chem. Res.*, 2012, **45**, 1854.

7. L. Dykman and N. Khlebtsov, *Chem. Soc. Rev.*, 2012, **41**, 2256.

8. C. Wu, T. Schneider, M. Zeigler, J. Yu, P. G. Schiro, D. R. Burnham, J. D. McNeill, D.T. Chiu, *J. Am. Chem. Soc.*, 2010, **132**, 15410.

9. Y. Chen, H. Chen, J. Shi, *Adv. Mater*., 2013,**23**, 3144.

10. D. Ling and T. Hyeon, *Small*, 2013, **9**, 1450.

11. C. Xu and S. Sun, *Adv. Drug Delivery Rev.*, 2013, 65, 732.

12. E. Fantechi, C. Innocenti, M. Zanardelli, M. Fittipaldi, E. Falvo, M. Carbo, V. Shullani, L. D. C. Mannelli, C. Ghelardini, A. M. Ferretti, A. Ponti, C. Sangregorio, P. Ceci, *ACS Nano*, 2014, **DOI:** 10.1021/nn500454n

13. R. Ladj, A. Bitar, M. Eissa, Y. Mugnier, R. L. Dntec, H. Fessi, A. Elaissari, *J. Mater. Chem. B*, 2013, **1**, 1381.

14. T. M. Allen, P. R. Cullis, *Adv. Drud. Deliv. Rev.*, 2013, **65**, 36

15. J. Nicolas, S. Mura, D. Brambilla, N. Mackiewicz, P. Couvreur, *Chem. Soc. Rev.*, 2013, **42**, 1147.

16. M. Gonçalves, D. Maciel, D, Capelo, S. Xiao, W. Sun, X. Shi, J. Rodrigues, H. Tomás, Y. Li, *Biomacromolecules*, 2014, **15**, 492.

17. M. Elsabahy, K. L. Wooley, *Chem. Soc. Rev.*, 2012, **41**, 2545.

18. Z. Liu, B. Zhao, C. Guo, Y. Sun, F. Xu, H. Yang, Z. Li, *J. Phys. Chem. C*, 2009, **113**, 16766.

19. A. C. Balazs, T. Emrick, T. P. Russell, Science, 2006, 314, 5802

20. J. L. Vivero-Escoto, R. C. Huxford-Phillips, W. Lin, *Chem. Soc. Rev.*, 2012, **41**, 2673.

21. T-H. Tran-Thi, R. Dagnelie, S, Crunaire, L. Nicole, *Chem. Soc. Rev.*, 2011, **40**, 621.

22. H. MoK and T. G. Park, *Maccromole.Biosci.*, 2012**,** **1**, 40.

23. V. V. Gizburg, *Macromolecules*, 2013, 46, 9798

24. K. G. Neoh and E. T Kang, *Polym. Chem.* 2011, **2**, 747.

25. S. Mahouche-Chergui, S. Gam-Derouich, C. Mangeneya, M. M. Chehimi, *Chem. Soc. Rev.*, 2011,**40**, 4143.

26. Y. Zhu, H. S. Sundaram, S. Liu, L. Zhang, X. Xu, Q. Yu, J. Xu, S. Jiang, *Biomacromoleculs*, 2014, **DOI:** 10.1021/bm500209a.

27. R. Barbey, L. Lavanant, D. Paripovic, N. Schüwer, C. Sugnaux, S.Tugulu, H.-A. Klok, *Chem. Rev.*, 2009, **109**, 5437.

28. K. Matyjaszewski, *Macromolecules*, 2012, **45**, 4015.

29. J. Moraes, K. Ohno, T. Maschmeyer, S. Perrier, *Chem. Commun.*, 2013,**49**, 9077.

30. D. Cimen, T. Caykara, *J. Appl. Polym. Sci.*, 2013, **129**, 383.

31. L. Ghannam, J. Parvole, G. Laurelle, J. Francois, L. Billon, *Polym. Int*., 2006, **55**,1199.

32. S. H. Wibowo , A. Sulistio , E. H. H. Wong , A. Blencowe, G. G. Qiao, *Chem. Commun.*, 2014, DOI: 10.1039/C4CC00293H.

33. L. Carlsson, S. Utsel, L. Wågberg, E. Malmströmab, A. Carlmark, *Soft Matter*, 2012,**8**, 512.

34. H. Tian, Z. Tang, X. Zhuang, X. Chen,X. Jing, *Pro. in Poly. Sci.*,2012, **37**, 237.

35. H. Lu, J. Wang, Z. Song, L. Yin, Y. Zhang, H. Tang, C. Tu, Y. Lin, J. Cheng, *Chem. Commun.*, 2014, **50**, 139.

36. H. E CL, X. L. Zhuang, Z. H. Tang, H. Y. Tian, X. S. Chen, *Adv. Healthcare Mater.*, 2012, **1**, 48.

37. R. J. Mart, R. D. Osborne, M. M. Stevens, R. V. Ulijn, *Soft Matter*, 2006, **2**, 822.

38. J.Huang, and A. Heise, *Chem. Soc. Rev.*, 2013, 42, 7373.

39. T. J. Deming, *Prog. Polym. Sci.*, 2007, **32**, 858.

40. J. M. Collins, K. A. Porter, S. K. Singh, G. S. Vanier, *Org. Lett.*, 2014, **16**, 940.

41. S. Cavalli, F. Alaberico, A. Kros, *Chem. Soc. Rev*., 2010, **39**, 241.

42. (a) T. J. Deming, *Nature*, 1997, **390**, 386. (b) T. J. Deming, *J. Am. Chem. Soc.*, 1998, **120**, 4240.

43. H.R. Kricheldorf, *Angew. Chem. Int. Ed*., 2006, **45**, 5752.

44. N. Hadjichristidis, H. Iatrou, M. Pitsikalis, G. Sakellariou, *Chem. Rev.*, 2009**, 109**, 5528.

45. G. J. M. Habraken, A. Heise, P. D. Thornton, *Macromol. Rapid Commun.,* 2012, **33**, 272.

46. (a) H. Leuchs, *Ber. Dtsch. Chem. Ges.*, 1906, **39**, 857. (b) H. Leuchs and W. Manasse, *Ber. Dtsch. Chem. Ges.*, 1907, **40**, 3235. (c) H. Leuchs and W. Geiger, *Ber. Dtsch. Chem. Ges*., 1908, **41**, 1721.

47. T. Curtius and W. Siebe, *Ber. Dtsch. Chem. Ges. B*, 1921, **54**, 1430.

48. F. Wessely, *J. Physiol. Chem.*, 1925, **146**, 72.

49. A. C. Farthing and R. J. W. Reynolds, *Nature*, 1950, **165**, 647.

50. (a) W. H. Daly and D. S. Poche´, *Tetrahedron Lett.*, 1988, **29**, 5859. (b) R. Katakai,Y. J. Iizuka, *Org. Chem.*, 1985, **50**, 715. (c) A. Nagai, D. Sato, J. Ishikawa, B. Kudo, H. Ochiai, T. Endo, *Macromolecules*, 2004, **37**, 2332.

51. D. Ballard and C. Bamford, *J. Chem. Soc.*, 1956, 381.

52. M. Szwarc, *Adv. Polym. Sci.*, 1965, **4**, 1.

53. M. Szwarc , M. Levy , R. Milkovich, *J. Am. Chem. Soc.*, 1956, 78, 2656.

54. T. J. Deming, *Macromolecules*, 1999, **32**, 4500.

55. T. J. Deming and S. Curtin, *J. Am. Chem. Soc.*, 2000, **122**, 5710.

56. Y. Peng, S. Lai, C. Lin, *Macromolecules*, 2008, **41**, 3455.

57. I. Dimitrov and H. Schlaad, *Chem. Commun.*, 2003, **23**, 2944.

58. T. Aliferis, H. Iatrou, N. Hadjichristidis, *Biomacromolecules*, 2004, **5**, 1653.

59. T. Aliferis, H. Iatrou, N. Hadjichristidis, *J. Polym. Sci. Part A*, 2005, **43**, 4670.

60. W. Vayaboury, O. Giani, H. Cottet, A. Deratani, F. Schue´, *Macromol. Rapid Commun.*, 2004, **25**, 1221.

61. G. J. M. Habraken, K. H. R. M. Wilsens, C. E. Koning, A. Heise, *Polym. Chem*., 2011, **2**, 1322.

62. H. Lu and J. Cheng, *J. Am. Chem. Soc.*, 2007, **129**, 14114.

63. H. Lu and J. Cheng, *J. Am. Chem. Soc.*, 2008, **130**, 12562.

64. H. Peng, J. Ling, Z. Q. Shen, *J. Polym. Sci. Part A: Polym. Chem.*, 2012, **50**, 1076.

65. H. Peng, J. Ling, Y. Zhu, L. X. You, Z. Q. Shen, *J. Polym. Sci. Part A: Polym. Chem.*, 2012, **50**, 3016.

66. J. Huang and A. Heise, *Chem. Soc. Rev.*, 2013, **42**, 7373.

67. B. Fong and P. S. Russo, *Langmuir*, 1999, **15**, 4421.

68. A. Heise, H. Menzel, H. Yim, M. D. Foster, R. H. Wieringa, A. J. Schouten, V. Erb and M. Stamm, *Langmuir*, 1997, **13**, 723.

69. Y-C. Chang and C. W. Frank, Langmuir, 1996, 12, 5824–5829

70. Y-C. Chang and C. W. Frank, Langmuir, 1998, 14, 326–334

71. B. J. Sparks, J. G. Ray, D. A. Savin, C. M. Stafford and D. L. Patton, *Chem. Commun.*, 2011, **47**, 6245.

72. G. Marcelo, A. Muñoz-Bonilla, J. Rodríguez-Hernández and M. Fernández-García, *Polym. Chem.*, 2013, **4**, 558.

73. M. Prabaharana, J. J. Grailerb, S. Pillaa, D. A. Steeberb, S. Gong, *Biomaterials*, 2009, **30**, 6065.

74. J-Y. Shim, V. K. Gupta, *J. Colloid. and Interface Sci.*, 2007, **316**, 977.

75. M. Niwa, T. Murata, M. Kitamastu, T. Matsumoto, N. Higash, *J. Mater. Chem.*, 1999, **9**, 343.

76. S. H. Wibowo, E. Wong, A. Sulistio, A. Blencowe and G. G. Qiao, *Aust. J. Chem.*, 2014 DOI:10.1071/CH13519.

77. F. Audouin, M. Fox, R. Larragy, P. Clarke, J. Huang, B. O'Connor and A. Heise, *Macromolecules*, 2012, **45**, 6127.

78. E. P. Enriquez, K. H. Gray, V. F. Guarisco, R. W. Linton, K. D. Mar and E. T. Samulski, *Seattle, Washington*, USA, 1992.

79. E. P. Enriquez, K. H. Gray, V. F. Guarisco, R. W. Linton, K. D. Mar and E. T. Samulski, *J. Vac. Sci. Technol. A*, 1992, **10**, 2775.

80. C. G. Worley, R. W. Linton and E. T. Samulski, *Langmuir*, 1995, **11**, 3805.

81. M. Niwa, T. Murata, M. Kitamastu, T. Matsumoto and N. Higashi, *J. Mater. Chem.*, 1999, **9**, 343.

82. A. J. Williams and V. K. Gupta, *J. Phys. Chem. B*, 2001, **105**, 5223.

83. A. J. Williams and V. K. Gupta, *Thin Solid Films*, 2003, **423**, 228.

84. A. M. Hollman and D. Bhattacharyya, *Langmuir*, 2002, **18**, 5946.

85. Y. Zhang, J. Li, Y. Shen, M. Wang and J. Li, *J. Phys. Chem. B*, 2004, **108**, 15343.

86. S. S. Balamurugan, E. Soto-Cantu, R. Cueto and P. S. Russo, *Macromolecules*, 2010, **43**, 62.

87. M. Kar, P. S. Vijayakumar, B. L. V. Prasad and S. S. Gupta, *Langmuir*, 2010, **26**, 5772.

88. M. Kar, M. Pauline, K. Sharma, G. Kumaraswamy and S. Sen Gupta, *Langmuir*, 2011, **27**, 12124.

89. M. Kar, B. Malvi, A. Das, S. Panneri and S. S. Gupta, *J. Mater. Chem.*, 2011, **21**, 6690.

90. J. K. Whitesell and H. K. Chang, *Science*, 1993, **261**, 73.

91. M. Higuchi, T. Koga, K. Taguchi and T. Kinoshita, *Chem. Commun.*, 2002, 1126.

92. M. Higuchi, K. Ushiba and M. Kawaguchi, *J. Colloid Interface Sci.*, 2007, **308**, 356.

93. A. Heise, H. Menzel, H. Yim, M. D. Foster, R. H. Wieringa, A. J. Schouten, V. Erb and M. Stamm, *Langmuir*, 1997**, 13**, 723.

94. S. Britland, E. Perez-Arnaud, P. Clark, B. McGinn, P. Connolly and G. Moores, *Biotechnol. Prog.*, 1992, **8**, 155.

95. Y. Wang and Y. C. Chang, *Adv. Mater*., 2003, **15**, 290.

96. T. Kratzmüller, D. Appelhans and H.-G. Braun, *Adv. Mater.*, 1999, **11**, 555.

97. T. Jaworek, D. Neher, G. Wegner, R. H. Wieringa and A. J. Schouten, *Science*, 1998, **279**, 57.

98. R. H. Wieringa and A. J. Schouten, *Macromolecules*, 1996, **29**, 3032.

99. Y. Wang and Y.-C. Chang, *Langmuir*, 2002, **18**, 9859.

100. R. H. Wieringa, E. A. Siesling, P. F. M. Geurts, P. J. Werkman, E. J. Vorenkamp, V. Erb, M. Stamm and A. J. Schouten, *Langmuir*, 2001, **17**, 6477.

101. R. H. Wieringa, E. A. Siesling, P. J. Werkman, H. J. Angerman, E. J. Vorenkamp and A. J. Schouten, *Langmuir*, 2001, **17**, 6485.

102. R. H. Wieringa, E. A. Siesling, P. J. Werkman, E. J. Vorenkamp and A. J. Schouten, *Langmuir*, 2001, **17**, 6491.

103. J. Luijten, E. J. Vorenkamp and A. J. Schouten, *Langmuir*, 2007, 23, 10772.

104. J. Luijten, D. Y. Groeneveld, G. W. Nijboer, E. J. Vorenkamp and A. J. Schouten, *Langmuir*, 2007, **23**, 8163.

105. M. Niwa, Y. Kuwagaki, S. Yamaguchi and N. Higashi, *Angew. Chem. Int. Ed.*, 2003, **42**, 1839.

106. J. Wang, M. I. Gibson, R. Barbey, S.-J. Xiao and H.-A. Klok, *Macromol. Rapid Commun.*, 2009, **30**, 845.

107. V. E. Dietz, N. Fery and K. Hamann, *Angew. Makromol. Chem.*, 1974, **35**, 115.

108. N. Tsubokawa, K. Kobayashi and Y. Sone, *Polym. J.*, 1987, 19, 1147

109. B. Fong, P.S. Russo, *Langmuir*, 2004, **20**, 266.

110. E. Sotu-Kantu, S. Turksen-seluck, J. Qiu, Z. Zhou, P.S. Russo, *Langmuir*, 2010, **26**, 15604.

111. J. D. Lunn and D. F. Shantz, *Chem. Mater.*, 2009, **21**, 3638.

112. J. Li, W.-D. He, L.-P. Yang, X.-L. Sun and Q. Hua, *Polymer*, 2007, **48**, 4352.

113. D. Liu, Y. Li, J. Deng and W. Yang, *React. Funct. Polym.*, 2011, **71**, 1040.

114. G. Marcelo, A. Muñoz-Bonilla and M. Fernández-García, *J. Phys. Chem. C*, 2012, **116**, 24717.

Chapter 2

Polypeptide Core-Shell Silica Nanoparticles with High Grafting Density by N-Carboxyanhydride Ring Opening Polymerization

This chapter has been published in : *Polym. Chem.*, 2012, **3**, 1267-1275.

Abstract

Silica nanoparticles were furnished with a functional polypeptide shell to create a pH-responsive inorganic-organic hybrid material. Free amine groups present on silica nanoparticles initiated the *N*-carboxyanhydride (NCA) polymerization of particular amino acid NCAs directly onto the inorganic support, offering a convenient method to functionalize silica core nanoparticles with a uniformly dense polypeptide shell. Poly(γ-benzyl-L-glutamate) (PBLG), poly(ε-carbobenzyoxy-l-lysine) (ε-CBZ-PLL), and S-*tert*-butyl protected polycysteine (tB-PLC) were grafted from the silica core both independently as homopolypeptides, and simultaneously to form a copolypeptide shell, highlighting the versatility that the grafting mechanism possesses. The grafting of PBLG was investigated in detail at 0 °C and 20 °C to determine any differences in the size and uniformity of the polypeptide shell formed. Dynamic light scattering (DLS) analysis revealed a correlation between the thickness of the uniform organic shell and the amount of amino acid in the monomer feed, with higher linearity at the lower polymerization temperature. Size Exclusion Chromatography (SEC) analyses of degrafted PBLG confirmed the DLS results. A high grafting density of around 0.4 PBLG chains per nm^2 was calculated highlighting the control afforded in this approach to polypeptide grafting. Subsequent deprotection of the PBLG homopolypeptide shell afforded pH-sensitive poly(glutamic acid) (PGA) coupled silica nanoparticles. The selective release of a model rhodamine B dye was demonstrated to emphasize the potential that these hybrid nanomaterials have for the *on-demand* release of payload molecules in response to a targeted pH trigger

2.1 Introduction

The organic functionalization of inorganic materials offers potential to develop novel inorganic-organic hybrid materials capable of displaying a range of desired behaviors.[1] In particular, the use of nanostructured silica is of special interest as it permits a wide range of functionality arising from its unique optical, electrical and physical properties. Tailoring the material surface properties, through its designed chemical modification, has been demonstrated in a variety of applications ranging from simple fillers to highly active components in biomedical devices including anti-microbial agents,[2,3] biodiagnostic devices[4] and drug delivery mechanisms.[5,6] Advanced biomedical applications necessitate that the surface groups must provide several key functions to enhance the materials effectiveness. Surface conjugation with markers or biomolecules, enhanced biocompatibility and increasingly stimuli responsiveness are important factors that may be engineered into the design of the material to improve its performance. Stimuli-responsive materials possess the capability to change their macroscopic properties upon changes in targeted external stimuli such as temperature,[7] light,[8] ionic concentration,[9] electric/magnetic field,[10,11] and enzyme selectivity.[12,13] Recent developments concerning this category of materials have been vast with suggested applications found in fields including the targeted release of therapeutic agents,[14] biodiagnostics,[15] and chronic wound healing.[16] In addition, pH-responsive materials have been devised and developed with the aim of manipulating differing pH levels that exist within distinct organs and disease states within the human body. Such differences dictate that polymeric materials possessing the capability to respond to different environmental pH levels are suitable candidates as drug carriers in medicinal applications.

Polymer conjugation to the silica nanoparticle surface by initiating polymerization from an immobilized initiator (grafting from) is a promising way to generate a high grafting density of a functional organic shell onto an inorganic surface.[17,18] In particular, radical polymerization methods have been employed for the surface modification of silica nanoparticles in this manner including conventional radical polymerization, atom transfer radical polymerization (ATRP), reversible addition-fragmentation chain transfer

polymerization (RAFT), and nitroxide-mediated Polymerization (NMP). The main advantages of these techniques include excellent control over the grafting thickness and a large choice of readily available monomers, which allows the introduction of various functional groups to the silica nanoparticle surface. A drawback is that radical polymerization is limited to vinyl polymers, while in many applications there is a need for biocompatibility and sometimes biodegradability. An alternative method is the use of synthetic polypeptides, which offer biocompatibility in conjunction with a degree of functional diversity. The functionality offered by the polypeptide can be readily tuned dependent on the particular amino acid groups selected from the pool of natural and non-natural amino acids available.

Our interest is in the synthesis of functional, stimuli-responsive, polypeptide nanoparticles for sensor and biomedical applications. We reported poly(γ-benzyl-L-glutamate) (PBLG)/polystyrene core-shell nanoparticles obtained by the combination of controlled radical and NCA polymerization.[19,20] Recently "grafting to" approaches of alkyne terminal synthetic polypeptides onto azide functional silica nanoparticles by employing copper catalyzed 'click' chemistry were reported.[21,22] The disadvantage of this approach is the usually lower grafting density due to increasing steric hindrance with increasing grafting density. This can be circumvented by the "grafting from" approach, which has been extensively utilized in the synthesis of polypeptide brushes on planar silicon wafers by ring opening polymerization of NCA in solution,[23-29] melt[30] and by vapor deposition polymerization.[31-38] Research by the group of Russo demonstrated that the "grafting from" approach of PBLG can also successfully be applied from silica nanoparticles.[39] Further work demonstrated the grafting of poly(ε-carbobenzyoxy-l-lysine) (ε-CBZ-PLL) from the silica nanoparticle surface with special emphasis on controlling the polypeptide shell thickness by sequential monomer addition.[40] However, the grafting did not appear to be completely uniform in all cases and only very low mass increases (the grafting efficiency was calculated as 1.85% after four grafting steps) were observed despite the excessive addition of NCA monomer. This was stated to be either due to the monomer not reacting, or the formation of unbound polymer.

In order to expand the range of stimuli-responsive polypeptide decorated nanoparticles, we have investigated the direct grafting of various polypeptide and copolypeptide shells from silica nanoparticles by *N*-carboxyanhydride (NCA) polymerization at both 0 °C and 20 °C to ascertain optimal grafting conditions. Free amine groups present on silica nanoparticles act to initiate the polymerization of NCAs directly onto the silica support, offering a convenient method to functionalize inorganic silica core nanoparticles with a dense polypeptide shell (**Scheme 2.1**). A clear aim of this work is to produce uniform polypeptide shells whilst eliminating the generation of non grafted polypeptide, thus enabling the efficient generation of high molecular weight polypeptides grafted from silica nanoparticles surfaces. The hydrodynamic diameters of the polypeptide-silica conjugates were measured to determine a correlation between the dimensions of the functionalized nanoparticles formed and the amount of NCA monomer present in the monomer feed, and to confirm the lack of ungrafted polypeptide associated to the completed product. The molecular weight and polydispersity of the grafted chains could be determined by GPC following the etching of the silica core to provide a comprehensive analysis of the polymerization whilst demonstrating the extensive control that the polymerization methodology affords. Finally, we demonstrate the ability to use these nanoparticles as carrier vehicles in a pH-responsive release application.

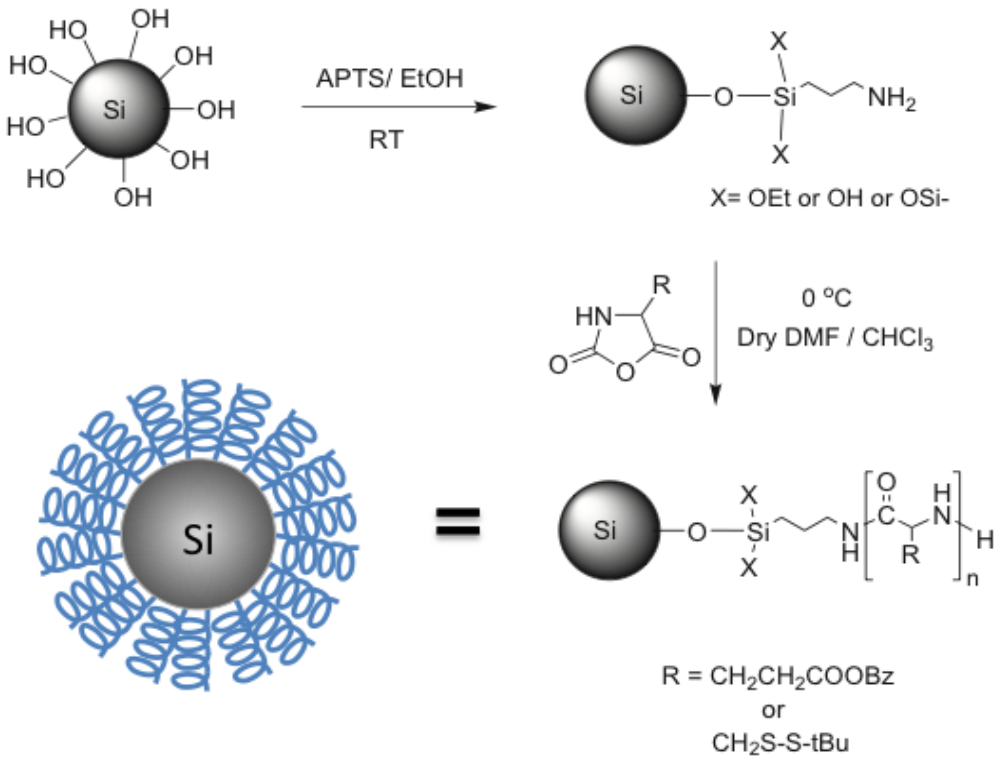

Scheme 2.1: Schematic representation of amino functionalization of silica nanoparticles (Si) with 3-aminopropyltrimethoxysilane (APTS) and the facile grafting of a polypeptide from the silica nanoparticle surface by the ring opening polymerization of an amino acid NCA in DMF. R: CH_2CH_2COOBz (PBLG); R: CH_2S-StBu (tBPLC) and R: $CH_2CH_2CH_2CH_2NHCOOBz$ (e-CBZ-PLL).

2.2 Results and Discussion

2.2.1 Synthesis of peptide grafted silica nanoparticles

The synthetic strategy for the conjugation of peptides to silica nanoparticle surfaces is shown in Scheme 2.1. Silica nanoparticles (~120 nm diameter) were initially modified with APTS at room temperature to generate primary amine groups on the nanoparticle surface.[41] The success of this modification was verified by elemental analysis, which revealed that the silica nanoparticles contained 0.72 % nitrogen content by mass while no nitrogen was detected on the unmodified nanoparticles. DLS measurements in ethanol revealed an increase in hydrodynamic diameter from 122 nm to 136 nm, indicating multilayer formation of APTS on the silica nanoparticle surface.[42] This means that a large fraction of the amino groups are not exposed at the particle surface and cannot take part in the initiation of the NCA. Consequently, a molar monomer to initiator ratio cannot be calculated and instead a constant NCA to silica particle mass ratio was used in the polymerizations. The primary amine groups of covalently attached APTS exposed on the nanoparticle surface were then utilized to initiate the ring opening polymerization of the NCA of a desired amino acid, resulting in polypeptide grafting from the nanoparticle surface. In order to verify the versatility of the grafting approach, the attachment of three amino acid NCAs, γ-benzyl-L-glutamate (BLG), ε-carbobenzyoxy-l-lysine (ZLL), and S-*tert*-butyl protected polycysteine (tBLC), was carried out at 0 °C both independently to give each homopolymer, and in the case of BLG and tBLC simultaneously to form the random copolymer. These amino acids were selected because following their deprotection useful functional groups (thiol: cysteine, amine: lysine and carboxylic acid: glutamic acid) are introduced into the polypeptide that may be used for subsequent chemical modification, stimuli responsiveness and (bio)conjugation. It has been widely reported within the literature that carrying out NCA polymerizations at 0 °C suppresses both unfavorable side reactions and premature chain termination.[43-45] Consequently, a study was undertaken whereby the NCA of BLG was additionally polymerized at 20 °C to determine any

disparity in polypeptide uniformity and molecular weight between the product formed at this temperature and the product formed at 0 °C.

Due to the good solubility of NCA-BLG and NCA-ZLL in DMF the grafting reactions of these monomers were carried out in this solvent. During the course of the polymerization, the DMF solution remained homogenous and the silica nanoparticles were recovered by precipitation in diethyl ether and centrifugation. Initially, unbound polypeptide formed during the grafting process as reported by Russo *et al.*[39,40] The presence of such material is detrimental to the system proposed; the polypeptide shell thickness cannot be accurately determined and the effectiveness of the hybrid materials as vehicles for the controlled release of payload molecules is diminished. We speculate that it may be caused by traces free APTS initiating the NCA in solution. Consequently, exhaustive washing of the silica nanoparticles in THF prior to the NCA polymerization resulted in the absence of any free polymer as analyzed by TGA. After washing with THF and drying under vacuum the success of the grafting reaction was investigated by NMR, FTIR, TGA and TEM. **Figure 2.1 b** shows an example of an ATR-FTIR spectrum of PBLG grafted silica nanoparticles (NP-g-PBLG) and the NCA-BLG monomer (**Figure 2.1 a**). The latter reveals strong peaks at 1772 cm^{-1} and 1880 cm^{-1} that are attributed to the C=O groups of the anhydride. A third characteristically strong peak at 3331 cm^{-1} is attributed to the secondary amine present in the anhydride ring. These typical NCA peaks were not present in the spectrum corresponding to silica nanoparticles after the grafting. Instead, the IR spectra of the polypeptide-conjugated silica nanoparticles reveals peaks characteristic of PBLG, i.e. the peptide carbonyl group of amide I and amide II at 1652 cm^{-1} and 1547 cm^{-1} (**Figure 2.1 b**). The position of these peaks also suggests that PBLG adopts an α-helical conformation in the dry state.[46] Moreover, the broad peak at 3291 cm^{-1} is due to N-H stretching of amide linkage, the carbonyl group within the benzyl ester can be assigned at 1732 cm^{-1}, and the very broad peak at 1040 cm^{-1} is due to the Si-O-Si bonds present within silica nano-particles.

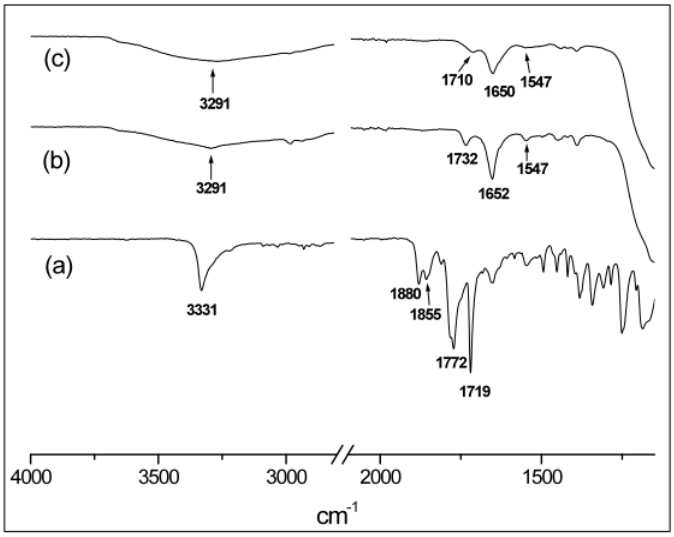

Figure 2.1: FTIR spectra of (a) NCA-BLG (b) NP-*g*-PBLG (c) Benzyl deprotected NP-*g*-PGA.

A series of control experiments were then carried out specifically to further verify covalent polypeptide grafting from the silica nanoparticles. Most significant in that respect was an experiment in which amine functional nanoparticles were mixed with free PBLG. Following this, the material was washed several times with THF and recovered by centrifugation, i.e. treated in an identical multi-step washing process. No PBLG IR signals were detected signifying the lack of any unbound polypeptide in the system. The same negative result was obtained when the grafting process was carried out with silica nanoparticles that lack amino groups. These control experiments provide strong evidence that the characteristic IR and NMR signals indeed stem from PBLG grafted to the silica nanoparticles.

The hydrodynamic diameters of PBLG-conjugated nanoparticles created in reactions carried out at 0 °C and 20 °C were measured to determine any diversity in the dimensions or polydispersities of the products created (**Figure 2.2**). The results exhibit the control over size of the PBLG-silica nanoparticles dictated by the ratio of NCA monomer to silica nanoparticles; a higher ratio results in larger functionalized nanoparticles as expected. When the reactions were carried out at 0 °C a significant increase in hydrodynamic radii from 172 to 236 nm (PDI: 0.04-0.09) was observed when ratio was increased from 1 to 3,

respectively. At 20 °C a similar increase in hydrodynamic size from 150 nm to 210 nm (PDI: 0.04-0.13) was measured by DLS when ratio was raised from 0.5 to 2. In particular, the data corresponding to the 0 °C reactions converges towards linearity, suggesting better control over polypeptide grafting offered by this reaction condition in agreement with results obtained in solution. The DLS observations are in agreement with results obtained from thermo-gravimetric analysis (TGA) where an increasing polymer weight loss was measured with increasing NCA to nanoparticles ratio (**Figure 2.3**).

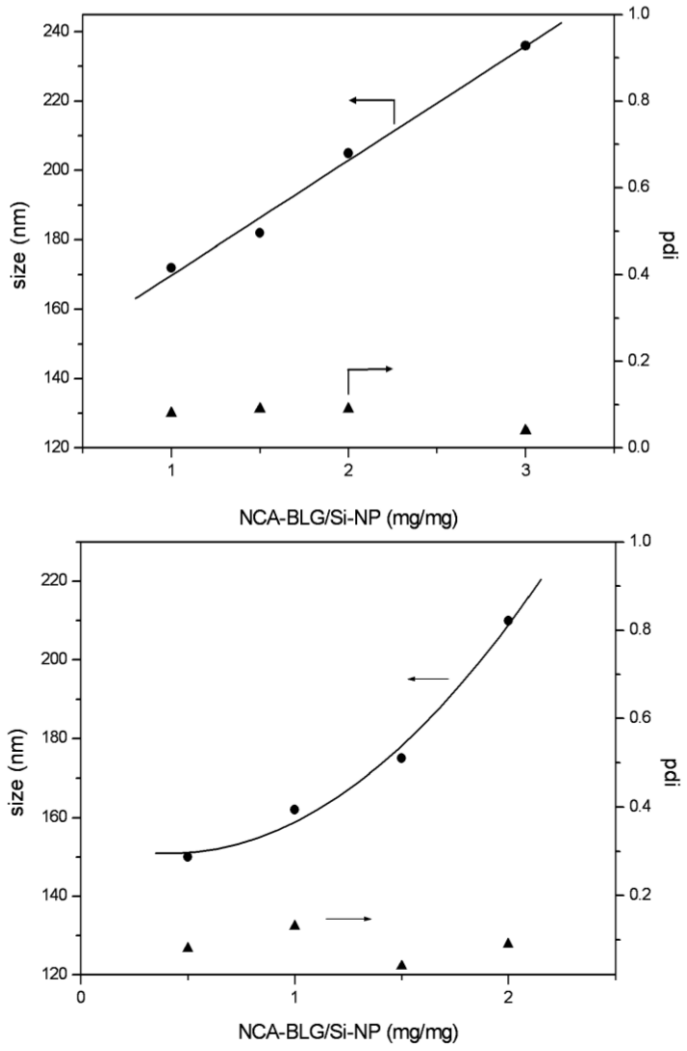

Figure 2.2: Size and polydispersity index (PDI) obtained by DLS of PBLG grafted silica nanoparticles for polymerization reactions carried out at 0 (top) and 20 °C (bottom).

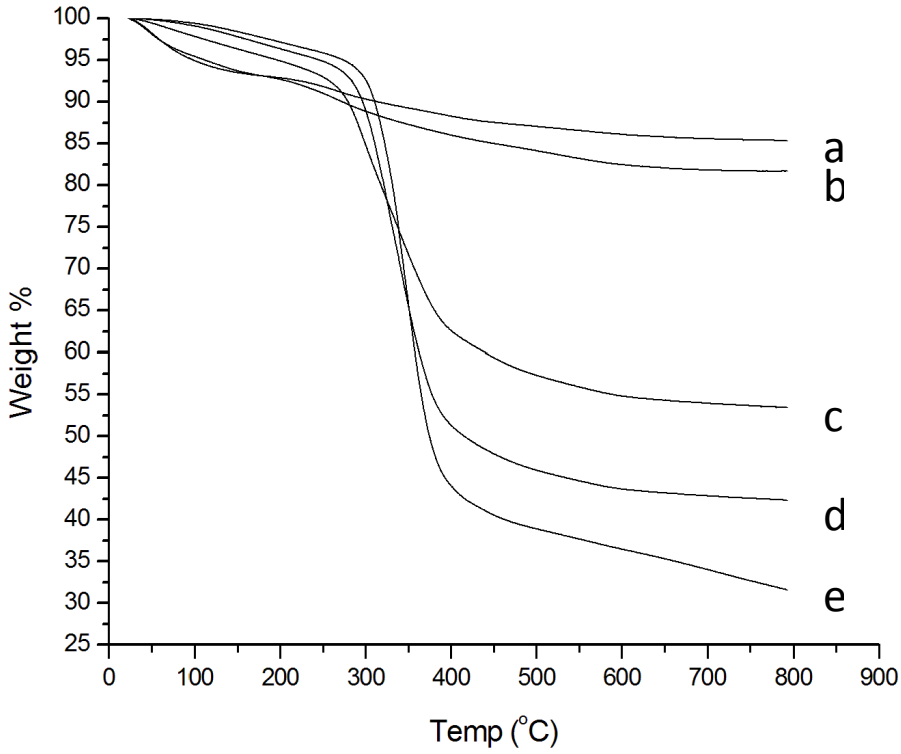

Figure 2.3: TGA Analysis of (a) Si NP-OH (b) Si NP-NH_2 (c) Si NP-*g*-PBLG (mass ratio 1:1), (d) Si NP-*g*-PBLG (mass ratio 1:2), (e) Si NP-*g*-PBLG (mass ratio 1:3). All polymerization carried out at 0 °C.

In a preliminary attempt to gain information regarding the molecular weight of the grafted PBLG achieved at both 0 °C and 20 °C, hydrofluoric acid was used to etch the silica core from the PBLG shell to enable the analysis of the polypeptide by GPC (**Table 2.1**). In both cases extensive control over the polymerizations were afforded with the molecular weights of the polypeptides generated increasing proportionally with the increase in BLG NCA within the monomer feed. Polypeptides possessing enhanced molecular weights were generated when the reactions were done at 20 °C.

Table 2.1: GPC molecular weights and PDIs of PBLG degrafted from selected silica nanoparticles.

Sample	NCA-BLG/Si NP Mass Ratio	Reaction Temperature (°C)	Mn (g/mol)	PDI
Si NP-PBLG 1	1:1	0	7700	1.4
Si NP-PBLG 2	2:1	0	16100	1.4
Si NP-PBLG 3	3:1	0	20700	1.4
Si NP-PBLG 4	1:1	20	8700	1.4
Si NP-PBLG 5	1.5:1	20	15000	1.2
Si NP-PBLG 6	2:1	20	20100	1.3

Molecular weight measurements of degrafted PBLG from the silica nanoparticles surface along with TGA results of these hybrids enable us to determine the grafting density. The grafting density of APTS initiator G_{APTS} onto silica nanoparticles was found to be 2.4 APTS per nm^2. Polymer grafting density G_{PBLG} of PBLG grafted onto silica nanoparticles at 0 °C with varying molecular weights was found to be in the range of 0.4 polymer chains per nm^2. Considering that the radius of a PBLG helical rod was reported to vary within the range of 0.8-1.3 nm depending on the conformation of the side chain (cross-section area: 2.0-5.8 nm^2) this suggests a high grafting density under the conditions applied.[47-49] To our knowledge this is the first time that GPC data and grafting density concerning silica nanoparticle-grafted PBLG has been disclosed in the academic literature.

To demonstrate the versatility that the system possesses to graft a range of homopolypeptides to silica nanoparticles, tBLC was chosen as a second amino acid to form a polypeptide conjugated to silica nanoparticles owing to its potential to utilize the cysteine thiol for further reactions in future studies.[51] In an analogous fashion to that demonstrated for the conjugation of PBLG to the silica nanoparticles, the NCA of tBLC was formed and nanoparticle initiated polymerization was done to yield the desired silica NP-*g*-PtBLC product. Due to the limited solubility of the tBLC peptide in a wide range of solvents, several experiments were carried out which resulted in chloroform ($CHCl_3$) being selected for use in the grafting of tBLC to the nanoparticle surface. Characterization of silica NP-*g*-PtBLC nanoparticles by ATR-FTIR showed the presence of two peptide conformations, β-sheet (amide I C=O stretching absorbs at 1633 cm^{-1}) and random coil (amide I absorbs at 1657 cm^{-1}). Due to the lower solubility of the cysteine homopolypeptide, a lower weight ratio (100 mg silica NP-NH_2:100 mg NCA-tBLC) of NCA-tBLC to amine functionalized silica was employed and resulted in the grafting of a cysteine homopeptide shell with lower thickness compared to that observed for the polypeptide shell of NP-g-PBLG as analyzed by TEM.

ZLL was chosen as the final amino acid to graft from the silica nanoparticle surface to afford silica NP-*g*-PZLL following the nanoparticle-initiated polymerization. The extent of peptide grafting was determined by TGA revealing a hybrid material consisting of 70% inorganic core surrounded by 30% organic shell by mass. Deprotection of the CBZ

protecting group further reduces the organic part of the hybrid material, leaving a final product with a mass composition of 80% silica core surrounded by 20% PLL shell. Upon deprotection cationic polylysine offers a pH-responsive shell to the particles that may be employed further for biotinylation or anti-microbial applications. Characterization of the particles by ATR-FTIR revealed the amide I and amide II bands at 1651 cm^{-1} and 1535 cm^{-1} in addition to a peak at 1698 cm^{-1} representative of the C=O present in the carbobenzyloxy protecting group (**Figure 2.4 a**). Following the deprotection of the lysine R group this peak is lost, signifying the generation of free amine groups (**Figure 2.4 b**). These deprotected lysine silica hybrids (NP-*g*-PLL) are highly hydrophilic and readily disperse in water to form homogeneous clear suspensions as the side chain amino group residue present in lysine has a pK_a of 10.53. The hydrodynamic radii of PLL grafted silica nanoparticles particles were found to be 182 nm measured by DLS in pH4 aqueous solution.

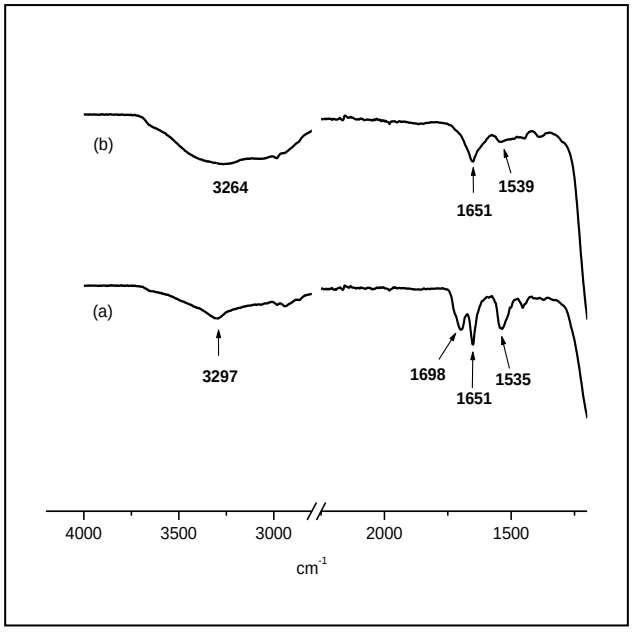

Figure 2.4: FTIR spectra of (a) NP-*g*-PZLL (b) NP-*g*-PLL (after deprotection).

To further demonstrate the adaptability of the polymerization technique, core-shell nanoparticles were then produced consisting of a silica nanoparticle core surrounded by a copolypeptide poly(BLG-*co*-tBLC) shell. The copolypeptide shell was grafted to the silica core in the molar ratio of 80:20 (BLG:tBLC). As the molar ratio of BLG was significantly

greater than that of tBLC, the silica conjugated copolypeptide displayed a similar IR absorption spectrum to that of PBLG grafted silica particles. While difficult to quantify, ^{1}H-NMR analysis suggests the presence of both amino acids in the particle shell due to the appearance of benzyl ester (7.19 ppm and 4.96 ppm) and t-butyl peaks (1.18 ppm) protons.

TEM was used to image the peptide silica hybrid particles and revealed distinct core-shell morphologies. An inorganic silica core appears darker than the grafted organic peptide shell due to the difference in density. Comparison of TEM images in **Figure 2.5 a**, **b**, **c** of peptide grafted hybrid silica nanoparticles with image (**d**) of amino functionalized bare particles confirms the successful ring opening polymerization of NCA by the amino functional group present on the APTS functionalized silica particles. The average particle size as estimated by TEM measurements of these peptide grafted silica hybrid particles was found to be in the range of 150-170 nm with a shell thickness of 10-20 nm. This concisely agrees with DLS measurements, which showed a hydrodynamic radius of 170 nm. The nanohybrid materials also showed a perfect core-shell structure, highlighting the uniform grafting of the copolypeptide from the silica nanoparticle surface.

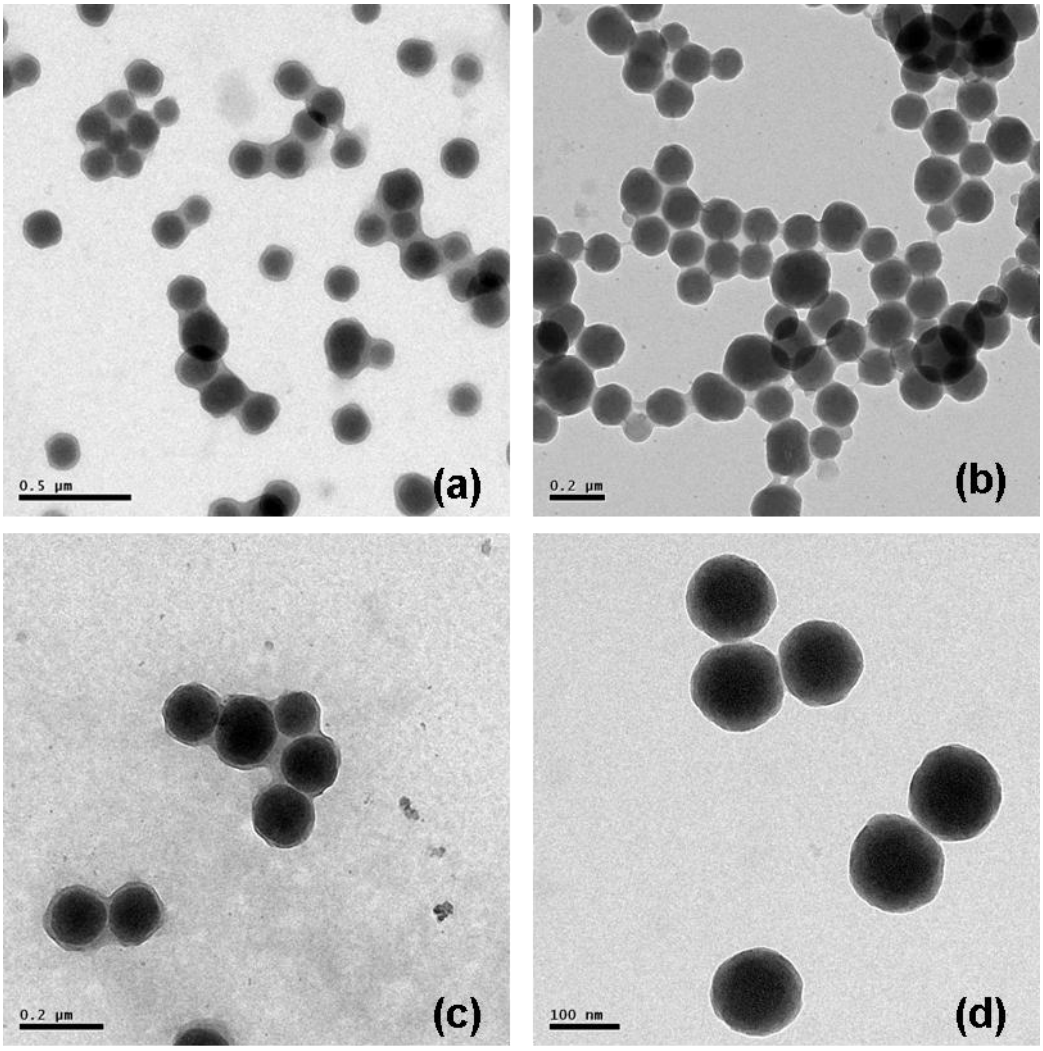

Figure 2.5: TEM images of peptide grafted silica nano particles (a) NP-*g*-PBLG (b) NP-*g*-PtBLC (c) NP-g-PLG (d) NP-OH.

The conversion of the silica nanoparticle-conjugated PBLG polypeptides to pH-responsive grafted PGA polypeptides was achieved by the deprotection of the PBLG benzyl ester groups directly on the silica nanoparticles by HBr/AcOH treatment. The progress of this reaction was monitored by FTIR spectroscopy, which showed the disappearance of the ester peak at 1732 cm^{-1} and the appearance of a peak at 1710 cm^{-1} corresponding to the carboxylic acid generated (**Fig.: 2.1 c**). This process produced free carboxylic acid groups, which renders the nanoparticles pH-sensitive and potentially allows further biomodification of the nanoparticles. Newly formed carboxyl functionalized peptide silica hybrid particles

when dispersed in solutions of different pH values showed pH-responsive behaviour. This process is usually associated with helix-coil transition at pH 5.7. However, it has been shown that the transition point of end grafted poly(glutamic acid) shifts to the alkaline side suggesting that the grafted polymer favors the helical state.[50] In contrast, when in an acidic pH environment, phase separation of the peptide chains occurs which results in aggregate formation. DLS studies of NP-*g*-PGA nanoparticles at different pH levels confirmed the above results. The hydrodynamic radius of completely solvated silica NP-*g*-PGA at pH 10 was found to be 170 nm.

It was hypothesized that PGA grafted silica nanoparticles could be employed for the pH-triggered release of payload molecules. As a model system, the pH-directed release of hydrophobic rhodamine B was chosen to prove this concept. The entrapment of rhodamine B molecules within the hybrid structure was achieved by allowing the diffusion of rhodamine B into the hybrid particles at pH 2 at which the nanoparticles form aggregates. Confocal microscopy was utilized to demonstrate the ability of PGA decorated silica nanoparticles to release guest rhodamine B molecules as a result of an increase in the solution pH value. When immersed in a solution of pH 2 the dye is completely localized within the nanoparticle aggregates (**Figure 2.6**, left). From the image it cannot unambiguously been concluded whether the dye is entrapped within the aggregated nanoparticle structures or in the collapsed shell of the hybrid structure. However, the dye is clearly concentrated in the hydrophobic part of the hybrid clusters and cannot be removed by dialysis. Payload release is only achieved when the surrounding solution is replaced by one with a pH value capable of generating a swollen negatively charged PGA shell. In this instance a buffer solution of pH 10 was employed and the rapid diffusion of rhodamine B particles from the hosts' interior occurred (**Figure 2.6**, right). This result signifies that the nanomaterials formed through the highly controlled NCA surface polymerization technique are therefore rendered pH-responsive and have the potential for use as pH-responsive payload delivery vehicles for the on-demand release of hydrophobic payloads.

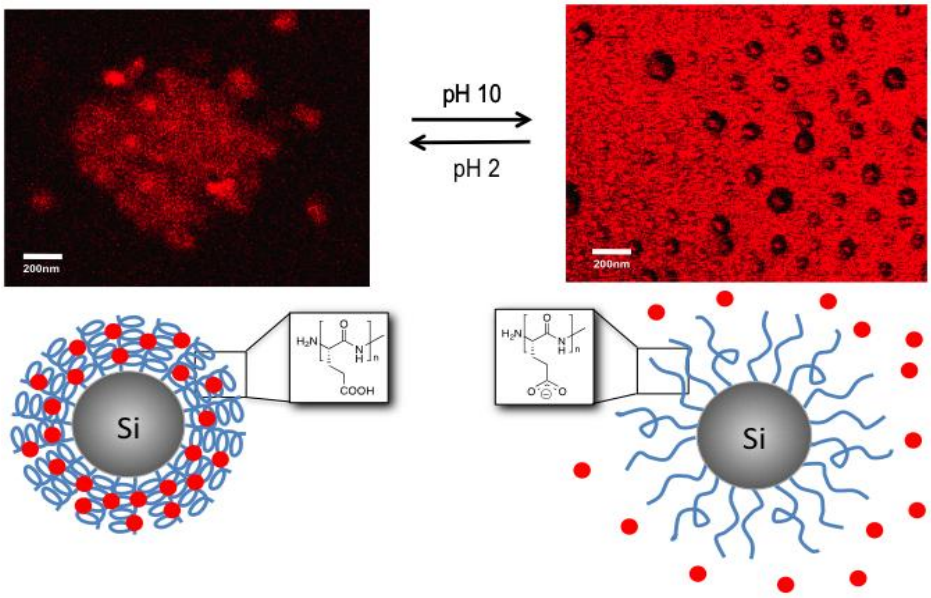

Figure 2.6: Top: Confocal images of pH responsive entrapment and release of Rhodamine B from poly(glutamic acid) functional nanoparticles. Bottom: A schematic representation detailing the pH-triggered release of guest rhodamine molecules due to change in the hydrophilicity of the poly(glutamic acid) shell. Scale bars represent 200 nm.

The second concept, *i.e.* the availability of PGA grafted nanoparticles for bioconjugation, was proven by the attachment of green fluorescent protein (GFP) in PBS buffer using NHS coupling chemistry. The reaction solution was thoroughly washed after GFP conjugation to ensure the removal of all unbound GFP. The GFP conjugated nanoparticles were fully dispersible in water and fluorescent microscopy images taken from the nanoparticle solution after attachment of the GFP clearly show the green fluorescence (**Fig. 2.7**). It has to be noted that due to their small size individual nanoparticles cannot be visualized by this technique and cluster formation was intentionally promoted by using high concentrations in the sample preparation. The fluorescent particles visible in the image thus represent clusters of nanoparticles of otherwise dispersed GFP conjugated nanoparticles.

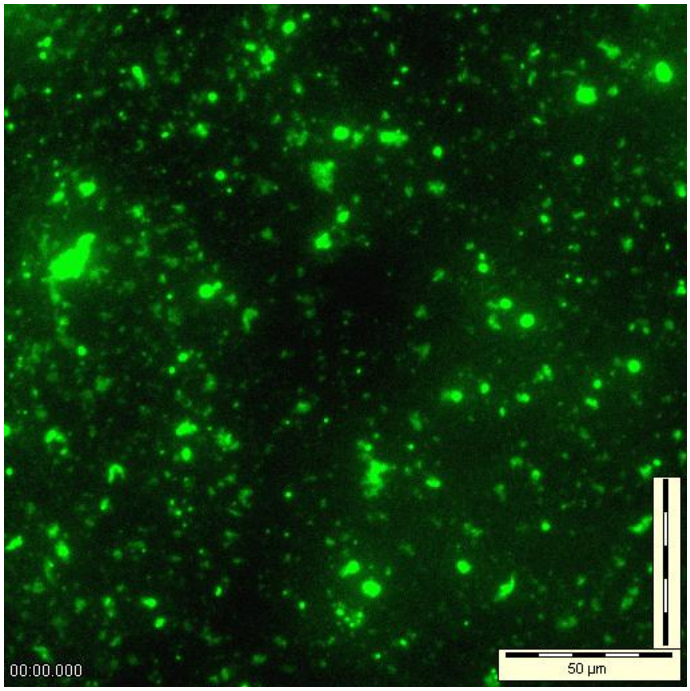

Figure 2.7: Fluorescence Microscopy Image of Si NP-g-PLG-GFP conjugates.

2.3 Conclusion

The work detailed in this article suggests and validates a facile method for the grafting of polypeptide chains from the surface of amine-functionalized silica nanoparticles. Primary amine groups present on the nanoparticles were used to initiate the ring opening polymerization of the NCAs of BLG, PZLL and tBLC independently as homopolypeptides, and BLG and tBLC simultaneously to form a copolypeptide. The results suggest that this methodology for polymerization has the potential to be applied to other natural and non-natural amino acids capable of forming an NCA as a technique to functionalize silica nanoparticles with a functional (co)polypeptide shell. All reactions gave a uniform and covalently bound polypeptide shell. Extensive washing of the silica nanoparticles prior to polypeptide grafting eliminated the production of non-covalently bound polypeptide in the final product, and thus enabled a very high grafting efficiency relative to previous studies. Further, the molecular weight of the polypeptide casing could be readily controlled by altering the monomer: initiator in the reaction with grafting densities around 0.4 chains per

nm^2. Comparison between BLG grafting carried out at 0 °C and 20 °C suggested that the lower temperature afforded core-shell structures possessing hydrodynamic diameters that increased proportionally with increased BLG NCA in the monomer feed. TEM analysis confirmed that the structures formed possessed a core-shell inorganic-organic hybrid composition. We believe that this is the first time that such control has been demonstrated analytically for the grafting of polypeptides from silica nanoparticles. Deprotection of the benzyl ester from PBLG grafted silica nanoparticles gave rise to pH-responsive core-shell hybrid nanoparticles. Selective release of particle-entrapped rhodamine B molecules was demonstrated when the surrounding solution pH was changed from pH 2 to pH 10, offering a mechanism for the pH triggered release of payload molecules. Grafting of two or more peptides with side chains containing different functional groups may lead to multifunctional hybrid nanoparticles.

2.4 Experimental Section

Materials: α-pinene 98%, bis(trichloromethyl) carbonate (triphosgene) 99%, tetraethyl orthosilicate (TEOS) puriss 99%, aminopropyltriethoxy silane (APTS), hydrobromic acid solution (HBr/AcOH) purum 33% in acetic acid (AcOH), Hydrofluoric acid (HF) 48 wt % in water, dimethylformamide (DMF) (anhydrous), ethyl acetate (anhydrous), chloroform (CHCl3), ethanol and n-heptane were purchased from Sigma-Aldrich and used without any further purification unless otherwise stated. γ-Benzyl-L-glutamate (BLG), N6-Carbobenzyloxy-L-lysine (ZLL) and S-tert-butyl-L-cysteine (tBLC) were supplied by Bachem and converted into the corresponding NCAs following a literature procedure.51 Dialysis membrane, Spectra/Por 6 (molecular weight cut-off: 1000 Da) was supplied by Spectrum Labs. Laboratory grade diethyl ether was purchased from VWR. DMF and ethyl acetate were stored under an inert, dry atmosphere.

Methods: ^{1}H and ^{13}C nuclear magnetic resonance (NMR) spectra were recorded at room temperature with a Bruker Avance 400 (400 MHz) and a Bruker Avance Ultrashield 600 (600 MHz). $CDCl_3$ was used as solvent and the signals were referred to the signal of residual protonated solvent signals. Tetramethylsilane (TMS) was used as an internal standard for $CDCl_3$. Elemental Analysis was performed on a CE440 Elemental Analyser from Exeter Analytical. A Perkin-Elmer Spectrum 100 was used for collecting attenuated total reflectance Fourier transform infrared (ATR-FTIR) spectra in the spectral region of 650−4000 cm^{-1}. The spectra were obtained from 4 scans with a resolution of 2 cm^{-1}. A background measurement was taken before the sample was loaded onto the ATR unit for measurements. TEM images were obtained using a JEOL 2100 TEM scan instrument (at an accelerating voltage of 200 kV) for samples deposited on carbon-coated (400 mesh) copper grids. The preparation of samples for transmission electron microscopy (TEM) analysis involved depositing a drop (15 μL) of the nanoparticle solution in $CHCl_3$, onto the grids and allowing the solvent to evaporate prior to imaging. All confocal microscopy experiments were carried out at room temperature. A Zeiss LSM 510 confocal microscope with an Ar^{+} laser was employed to visualize the release or entrapment. A 63x oil immersion

objective was used with an NA of 1.4. The excited light (514 nm) was passed through an 80/20 beam splitter. Collected light was passed through an 80/20 beam splitter to a 560 nm dichroic filter. Following this the reflected light was further filtered with a 505 nm longpass filter and the transmitted light filtered with a 575 nm longpass filter. The pinhole size used was 60 μm. Image analysis was performed using Image J software. The dynamic light scattering (DLS) experiments of peptide grafted nanoparticles in different pH solutions were performed at 25 °C on a Zetasizer Nano ZS particle analyzer (Malvern Instruments) using a detection angle of 173° and a 4 mW He−Ne laser operating at a wavelength of 633 nm. Size exclusion chromatography (SEC) analysis using DMF (0.1M LiBr) as eluent was done using PSS GRAM analytical (300 and 100 Å, 10μ) columns on an Agilent 1100 series equipped with a Wyatt Optilab rEX refractive index detector thermostated at 40 °C and a Wyatt DAWN HELEOS-II multi angle light scattering detector (MALS). Molecular weights and polydispersity index (PDI) were calculated from the MALS signal by the ASTRA software (Wyatt) using a dn/dc value of 0.118 mL/g for PBLG in DMF.[52] Before SEC analysis was performed, the samples were filtered through a 0.2 μm PTFE filter (13 mm, PP housing, Whatman).

The grafting density of APTS (G_{APTS}) and PBLG (G_{PBLG}) was calculated following a literature procedure using data from TAG analysis and the molecular weights of the degrafted PBLG.[53] The following equations were applied where *W%* is the weight loss between 150 and 800 °C from TGA analysis, M_n is the number average molecular weight of degrafted PGLG from GPC analysis, S_{sp} is the surface specific area of the nanoparticle and N_A is Avagadro's number. S_{sp} was calculated using the density of silica (2.27 g/cm^3) under the assumption of a sphere: S_{sp} = 132 nm^2/g for APTS functionalized nanoparticles (radius = 62 nm) and S_{sp} = 101 nm^2/g for PBLG grafted nanoparticles (radius = 68 nm).

$$G_{APTS} = \left\lfloor \left(\frac{W\%_{Si+APTS}}{100 - W\%_{Si+APTS}} - \frac{W\%_{Si}}{100 - W\%_{Si}} \right) \Big/ M_{APTS} \times S_{sp} \right\rfloor \times N_A$$

$$G_{PBLG} = \left\lfloor \left(\frac{W\%_{PBLG+Si+APTS}}{100 - W\%_{PBLG+Si+APTS}} - \frac{W\%_{Si+APTS}}{100 - W\%_{Si+APTS}} \right) \Big/ Mn_{PBLG} \times S_{sp} \right\rfloor \times N_A$$

Synthesis of silica nanoparticles: Silica nanoparticles were obtained by the Stöber method.[54] In a round bottom flask tetraethyl orthosilicate (16.90 g, 81.12 mmol) was mixed for 1 minute in 163.9 mL of ethanol. To this limpid, colourless, solution 13 mL of 28-30% ammonia solution was added (1 minute mixing). The solution turned into a dense milky suspension in 20 minutes (no mixing during this time). This solution was left for 10 days at room temperature and then used. The average particle size obtained by above procedure was 110-120 nm determined by DLS.

Synthesis of amino functionalised silica nanoparticles: Bare silica nanoparticles (1 g) were dispersed in 10 mL ethanol by ultrasonication for 10 min. resulting in milky fine suspension. A 90 mL solution ethanol/water 95/5 V/V was acidified to pH 5.0 by adding acetic acid glacial 60 µL and then APTS 4.2 g (19 mM) was added dropwise. The resulting clear colorless solution was kept under magnetic stirring (400 rpm) during 5 min. at room temperature in order to allow hydrolysis to occur and to form reactive silanols.

The bare silica nanoparticle suspension was added dropwise to the silanol solution under magnetic stirring and the resulting pale milky suspension was stirred at room temperature for 2h. The suspension was then centrifuged at 4830 RCF for 30 min. The supernant liquid was clear and colorless and the decanted solid was white. This solid was washed 3 times with ethanol, resuspended in anhydrous THF and acetone followed by centrifugation. Amino functionalized silica particles were then dried in vacuum oven at 110 °C for 1 h and stored in airtight container.

Ring opening polymerization of NCA-BLG from silica nanoparticles: The polymerization was carried out with different weight ratios of NCA to silica nanoparticles. The following describes a typical procedure. Amino functionalized silica nanoparticles (100 mg) were added to a dry Schlenk tube containing NCA-BLG (217 mg, 0.828 mmol). The Schlenk tube was purged with dry nitrogen gas and placed in an aqueous salt solution maintained at 0 ºC. Anhydrous DMF (10 mL) was then injected into the tube and the mixture stirred for 96 h. The peptide-grafted particles were then precipitated into cold and

dry diethyl ether (200 mL) before being washed four times with dry diethyl ether. These peptide grafted silica nanoparticles were then washed with 10 mL THF, centrifuged and the final nanoparticle solution (2 mL) was then precipitated in 25 mL diethyl ether. The particles were then washed twice with dry diethyl ether to remove traces of THF and dried under vacuum before being stored in the refrigerator. Yield: 185 mg.

Ring opening polymerization of NCA-ZLL from silica nanoparticles: Amino functionalized silica nanoparticles (100 mg) were added to a dry Schlenk tube containing NCA-ZLL (200 mg, 0.653 mmol). The Schlenk tube was purged with dry nitrogen gas and placed in an aqueous salt solution maintained at 0 ºC. Anhydrous DMF (10 mL) was then injected into the tube and the mixture stirred for 96 h. The peptide-grafted particles were then precipitated into cold and dry diethyl ether (200 mL) and washed with dry diethyl ether and 10 mL THF and centrifuged. The procedure was repeated three times and the final nanoparticle solution (2 mL) was then precipitated in 25 mL diethyl ether. The particles were then washed twice with dry diethyl ether to remove traces of THF, and dried under vacuum before being stored in refrigerator. Yield: 165 mg.

Ring opening polymerization of NCA-tBLC from silica nanoparticles: Amino functionalized silica nanoparticles (100 mg) were added to a dry Schlenk tube containing NCA-tBLC (100 mg, 0.425 mmol). The Schlenk tube was purged with dry nitrogen gas and placed in an aqueous salt solution maintained at 0 ºC. Anhydrous cold $CHCl_3$ (10 mL) was then injected into the tube and the mixture stirred for 96 h. The peptide-grafted particles were then precipitated in cold, dry diethyl ether (200 mL) before being washed with dry diethyl ether and 10 mL $CHCl_3$ and centrifuged. The procedure was repeated four times and the final nanoparticle solution (2 mL) was then precipitated in 25 mL diethyl ether. The particles were then washed twice with dry diethyl ether to remove traces of $CHCl_3$, and dried under vacuum before being stored in the refrigerator. Yield: 130 mg.

Ring opening copolymerization of NCA-BLG/NCA-tBLC from silica nanoparticles: Amino functionalized silica nanoparticles (100 mg) were added to a Schlenk tube. NCA-BLG (174.3 mg, 0.662 mmol) and NCA-tBLC (38.97 mg, 0.166 mmol) were then added to the nanoparticles. The Schlenk tube was purged with dry Nitrogen gas and placed in an aqueous salt solution maintained at 0 ºC. Anhydrous cold $CHCl_3$ (10 mL) was then injected into the tube and the mixture was stirred for 96 h. The peptide-grafted particles were then precipitated in cold and dry diethyl ether (200 mL). The obtained precipitated particles were washed with dry diethyl ether and 10 mL THF and centrifuged. The procedure was repeated three times and the final nanoparticle solution (2 mL) was then precipitated in 25 mL diethyl ether. The particles were then washed twice with dry diethyl ether to remove traces of THF, and dried under vacuum before being stored in refrigerator. Yield: 185 mg.

Deprotection of silica NP-*g*-PBLG: PBLG grafted Silica nanohybrids (100 mg) were stirred in 5 mL HBr/AcOH (33% HBr in AcOH) solution for 3 h. This mixture was then precipitated in 50 mL cold diethyl ether. The resultant deprotected poly(glutamic acid) grafted silica nanoparticles (silica Np-g-PGA) were then washed with fresh diethyl ether four times to ensure the complete removal of deprotecting reagents. Yield: 75 mg.

Deprotection of silica NP-*g*-PZLL: PZLL grafted Silica nanohybrids (100 mg) were stirred in 5 mL HBr/AcOH (33% HBr in AcOH) solution for 3 h. This mixture was then precipitated in 50 mL cold diethyl ether. The resultant deprotected poly(Lysine) grafted silica nanoparticles (NP-g-PLL) were then washed with fresh diethyl ether four times to ensure the complete removal of deprotecting reagents. Yield: 75 mg.

Rhodamine B loading of silica NP-*g*-poly(L-glutamic acid): Silica NP-g-PGA nanoparticles (50 mg) were dispersed in a 5 mL solution of rhodamine B (2 mg/10 mL) at pH 2. The solution was stirred for 2 h to allow diffusion of the dye into the peptide shell. The rhodamine B loaded nanoparticle solution was then dialyzed in a 1,000 Da molecular

weight cut off membrane against a pH 2 solution for 3 days to ensure the complete removal of adsorbed rhodamine B on the particle surface if any. The dye-loaded particles were then separated from the supernatant by centrifugation (6,000 R.P.M for 30 minutes using a using a 6 x 2 mL centrifuge rotor).

Etching of the silica core: In a Teflon vial, 0.5 mL of hydrofluoric acid solution was added to 3 mL dispersion of 10 mg PBLG grafted silica particles in THF and stirred overnight to ensure complete etching of silica by hydrofluoric acid. The reaction mixture was then added to polyethylene centrifuge tube and degrafted PBLG was precipitated by adding 10 mL deionized water followed by centrifugation at 9000 rpm for 10 min. Traces of HF was then removed by dissolving degrafted material in 0.5 mL THF and re-precipitation in 5 ml deionized water. The product was then centrifuged at 6000 rpm for 5 min. Repetitive washings and centrifugation were done with fresh deionized water until the washing solution had shown the same pH as the deionized water used for washing. The free polymer was dried in vacuum oven at 40 ^{0}C to remove traces of water. Yield: 1.5 mg.

2.5 References

1. K. G. Sharp, *Adv. Mater.*, 1998, **10**, 1243.

2. J. Jang and Y. Kim, *Chem. Commun*., 2008, 4016.

3. J. Song, H. Kong, and J. Jang, *Chem. Commun*., 2009, 5418.

4. C. M. Stafford, A. Y. Fadeev, T. P. Russell and T. J. McCarthy, *Langmuir*, 2001, **17**, 6547.

5. D. J. Bharali, I. Klejbor, E. K. Stachowiak, P. Dutta, I. Roy, N. Kaur, E. J. Bergey, P. N. Prasad, and M. K. Stachowiak, *Proc. Natl. Acad. Sci. U.S.A.*, 2005, **102**, 11539.

6. P. D. Thornton, and A. Heise, *J. Am. Chem. Soc*., 2010, **132**, 2024.

7. H. Xu, F. Meng, and Z. Zhong, *J. Mater. Chem*., 2009, **19**, 4183.

8. F. Benito-Lopez, R. Byrne, A. M. Răduţă, N. E. Vrana, G. McGuinness and D. Diamond, *Lab Chip*, 2010, **10**, 195.

9. J. Huang, X. Hu, W. Zhang, Y. Zhang, and G. Li, *Colloid Polym. Sci.*, 2008, **286**, 113.

10. R. Shankar, T. K. Ghosh and R. J. Spontak, *Adv. Mater*., 2007, **19**, 2218.

11. R. J. Ping Mart, K. Liem, and S. J. Webb, *Chem. Commun*., 2009, 2287.

12. P. D. Thornton, and A. Heise, *Chem. Commun*., 2011, **47**, 3108.

13. C. J. Duxbury, I. Hilker, S. M. A. de Wildeman and A. Heise, *Angew. Chem. Int. Ed.*, 2007, **46**, 8452.

14. P. D. Thornton, R. J. Mart, S. J. Webb and R. V. Ulijn, *Soft Matter*, 2008, **4**, 821.

15. T. Asefa, C. T. Duncan, and K. K. Sharma, *Analyst*, 2009, **134**, 1980.

16. R. V. Ulijn, N. Bibi, V. Jayawarna, P. D. Thornton, S. J. Todd, R. J. Mart, A. M. Smith and J. E. Gough, *Mater. Today*, 2007, **10**, 40.

17. B. Radhakrishnan, R. Ranjan and W. J. Brittain, *Soft Matter*, 2006, **2**, 386.

18. H. Zhou, S. Wu, and J. Shen, *Chem. Rev*., 2008, **108**, 3893.

19. R. J. I. Knoop, M. de Geus, G. J. M. Habraken, C. E. Koning, H. Menzel and A. Heise, *Macromolecules*, 2010, **43**, 4126.

20. F. Audouin, R. J. I. Knoop, J. Huang, A. Heise, *J. Polym. Sci. A: Polym. Chem.*, 2010, **48**, 4602.

21. M. Kar, P. S. Vijayakumar, B. L. V. Prasad and S. S. Gupta, *Langmuir*, 2010, **26**, 5772.

22. S. S. Balamurugan, E. Soto-Cantu, R. Cueto and P. S. Russo, *Macromolecules*, 2010, **43**, 62.

23. M. L. C. M. Oosterling, E. Willems and A. J. Schouten, *Polymer*, 1995, **36**, 4463.

24. A. Heise, H. Menzel, H. Yim, M. D. Foster, R. H. Wieringa, A. J. Schouten, V. Erb and M. Stamm, *Langmuir*, 1997, **13**, 723.

25. R. H. Wieringa, E. A. Siesling, P. F. M. Geurts, P. J. Werkman, E. J. Vorenkamp, V. Erb, M. Stamm and A. J. Schouten *Langmuir*, 2001, **17**, 6477.

26. T. Jaworek, D. Neher, G. Wegner, R. H. Wieringa, and A. J. Schouten, *Science*, 1998, **279**, 57.

27. J. Luijten, D. Y. Groeneveld, G. W. Nijboer, E. J. Vorenkamp, and A. J. Schouten, *Langmuir*, 2007, **23**, 8163.

28. J. Luijten, E. J. Vorenkamp, and A. J. Schouten, *Langmuir*, 2007, **23**, 10772.

29. J. Wang, M. I. Gibson, R. Barbey, S. J. Xiao and H. A. Klok, *Macromol. Rapid Commun.*, 2009, **30**, 845.

30. R. H. Wieringa and A. J. Schouten, *Macromolecules*, 1996, **29**, 3032.

31. Y. Chang and C. W. Frank, *Langmuir*, 1998, **14**, 326.

32. W. W. Zheng and C.W. Frank, *Langmuir*, 2010, **26**, 3929.

33. Y. Wang and Y. C. Chang, *Macromolecules*, 2003, **36**, 6511.

34. J. Wu, Y. Wang, C. Chen and Y. Chang, *Chem. Mater*., 2008, **20**, 6148.

35. H. Duran, K. Ogura, K. Nakao, S. D. B. Vianna, H. Usui, R. C. Advincula and W. Knoll, *Langmuir*, 2009, **25**, 10711.

36. D-Y. Wang, T-S. Teng, Y-C. Wu, Y-C. Lee, K. H. Chen, C-H. Chen, Y-C. Chang and C-C. Chen, *J. Phys. Chem.*, 2009, **113**, 13498.

37. C. Yang, Y. Wang, S. Yu and Y. Chang, *Biomacromolecules*, 2009, **10**, 58.

38. C-T. Yang, Y. Wang and Y-C. Chang, *Biomacromolecules*, 2010, **11**, 1308.

39. B. Fong and P. S. Russo, *Langmuir*, 1999, **15**, 4421.

40. E. Soto-Cantu, S. Turksen-Selecut, J. Qiu, Z. Zhou and P. S. Russo, *Langmuir*, 2010, **26**, 15604.

41. B. Mu, T. Wang and P. Liu, *Ind. Eng. Chem. Res*., 2007, **46**, 3069.

42. M. Van de Waterbeemd, T. Sen, S. Baigini and I. J. Bruce, *Micro & Nano Letters*, 2010, **5**, 282.

43. W. Vayaboury, O. Giani1,H. Cottet, S. Bonaric, F. Schué, *Macromol. Chem. Phys.*, 2008, 209, 1628.

44.G. J. M. Habraken, M. Peeters, C. H. J. T. Dietz, C. E. Koning and A. Heise, *Polym. Chem.*, 2010, **1**, 514.

45.G. J. M. Habraken, K.H.R.M. Wilsens, C.E. Koning and A. Heise, *Polym. Chem.*, 2011, **2**, 1322.

46.T. Wang and P. Liu, *Ind. Eng. Chem. Res*., 2007, **46**, 3069.

47. N. Higashi, T. Koga and M. Niwa, *Langmuir*, 2000, **16**, 3482.

48. Y-C. Chang and C.W. Frank, *Langmuir*, 1996, **12**, 5824.

49. J. Helfrich and R. Hentschke, *Macromolecules*, 1995, **28**, 3831.

50. Y. Yang and Y. C. Chang, *Macromolecules*, 2003, **36**, 6503.

51. G. J. M. Habraken, C. E. Koning, J. P. A. Heuts and A. Heise, *Chem. Commun*., 2009, **24**, 3612.

52. L. M. DeLong and P. S. Russo, *Macrolmolecules*, 1991, **24**, 6139.

53. P. Pasetto, H. Blas, F. Audouin, C. Boissiere, C.Sanchez, M. Save and B. Charleux *Macromolecules*, 2009, **42**, 5983.

54. W. Stöber, A. Fink and E. Bohn, *J. Colloid Interface Sci*., 1968, **26**, 62.

Chapter 3

Stable Aqueous Dispersions of Glycopeptide Grafted Magnetic Nanoparticles of Selectable Functionality

This chapter has been published in *Angew. Chem. Int. Ed.* 2013, **52**, 3164-3167

Measurement of the magnetic properties of nanoparticles has been performed in Dr. Brougham's laboratory.

Abstract

Surface initiated NCA ring opening polymerization from spherical surfaces is a robust technique to graft high density polypeptide shell onto nanoparticle core. The ‘grafting-from’ NCA ring opening polymerization of clickable amino acid and its subsequent click glycosylation to produce aqueous suspensions of glycopeptide grafted magnetic nanoparticles is presented. The novel materials have high sugar density, optimal dispersion and T_1-weighted MRI properties, and bio-recognition ability. The approach can be used to attach any type or combination of functionalities and the density of functional groups is not limited by particle surface area.

3.1 Introduction

Bio-nanomaterials have received increasing attention over the last decade, due to their potential to advance medical science by providing novel solutions for disease diagnostics and treatment.[1] However, the engineering of bio-nanomaterials imposes considerable challenges, as significant design criteria and properties, dictated top-down by the specific application, must be met. MRI-trackable magnetic nanoparticles (MNPs), and their assemblies, capable of targeting specific cell types, *e.g.* cancer cells, for image-guided treatment are increasingly being investigated.[2] Typical design criteria for MNPs are of biomedical nature, including cellular selectivity (bio-recognition), extended blood circulation times and biocompatibility, there are also practical considerations such as processability and scalability. Additional, MRI specific criteria, include colloidal stability and high image contrast. The efficacy of a MNP suspension for generating contrast by enhancing, or suppressing, local MRI signal is quantified by the spin-lattice (r_1) and spin-spin (r_2) relaxivities, respectively. These are the water relaxation enhancement per millimolar concentration of iron. For T_1-weighting applications (localized signal enhancement), r_1 must be high, and r_2 and the ratio r_2/r_1 must be low. Particle aggregation increases the r_2 value, so T_1-weighting can only be achieved by ensuring full MNP dispersion and long-term colloidal stability.

Monosaccharides offer colloidal stability through charge and steric interactions along with the possibility of cellular targeting and so have been used to stabilize MNPs. Recently MNP clusters were prepared by encapsulation of alkyl-stabilized MNPs using poly(maleic anhydride-alt-1-octadecene) followed by EDC coupling of aminated sugars.[3] Detailed analysis of the effect of coating on cellular uptake showed that high grafting density is critical for avoiding non-specific cellular interaction. However, the encapsulation approach resulted in extensive aggregation, as is usually the case, limiting the possibility of T_1-weighting application. Aggregation was exploited in a recent report where clickable monosaccharides were used to stabilize MNP clusters using complex peptide linkers,[3] allowing differentiation of cancer cells by quantitative profiling of carbohydrate binding through changes in T_2 (local signal suppression). In a prominent recent example, a range of phosphonate-functionalized sugars were used to fully disperse MNPs and the effect of

MNP size on the T_1-weighting and hyperthermic properties *in vitro* were investigated.[4] However, only one sugar per linker was possible, limiting the total sugar density.

Hence there is a need for platform technologies that maximize the surface density of functional monosaccharides while allowing full MNP dispersion. Multifunctional polymers have potential to address the first issue; there have been two recent reports of *grafting-onto* for MNP modification with glycopolymers. However, dispersion proved not to be possible. In the first example glycosylated polyacrylate was grafted onto silica-coated iron-oxide MNPs.[5] While cellular uptake of the micron scale aggregates was confirmed, the magnetic component was quite dilute. In the second example some improvement in colloidal control was achieved using glucosylated poly(pentafluorostyrene) derivatives, to produce suspensions of hydrodynamic size (d_{hyd}) ranging from 100–300 nm.[6] However, the polydispersity index (PDI) from dynamic light scattering was quite high (>0.22) suggesting non-uniform particles.

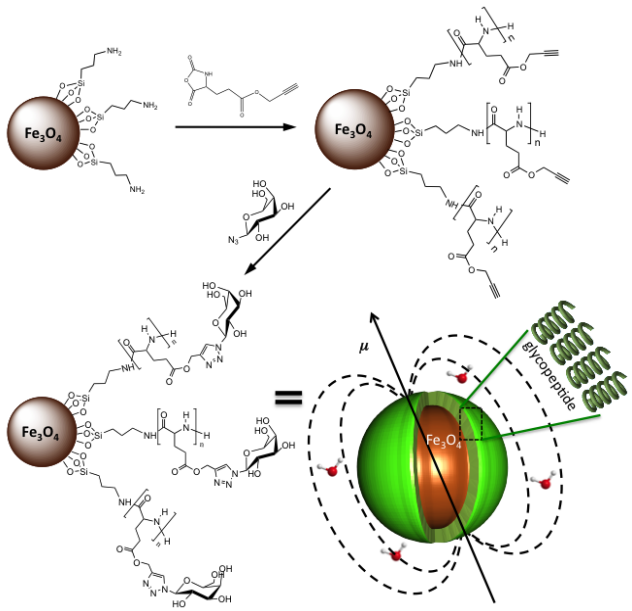

Scheme 3.1: Synthesis of glycopeptide-grafted magnetic nanoparticles GP-MNPs.

Here we describe for the first time combination of a polymer *grafting-from* approach with glycosylation by *click* chemistry for preparing MNPs with high surface density of monosaccharides. We hypothesized that this would promote dispersibility and, based on the

important role of carbohydrates in cell interaction/recognition,[7] introduce bio-recognition. The polymers are synthetic polypeptides and thus rely on natural degradable building blocks (amino acids). This is the first report of glycopeptide-grafted superparamagnetic Fe_3O_4 nanoparticles (GP-MNP), which exhibit excellent water dispersibility, optimal T_1–weighting properties and selective binding.

3.2 Result and Discussion

The synthetic protocol (Scheme 1) involves the preparation of highly crystalline Fe_3O_4 MNPs using the surfactant-free non-hydrolytic organic phase method.[8] The MNPs were further functionalized with 3-aminopropyl-trimethoxysilane (APTS), which has been show to be an efficient initiator in the polymerization of amino acid N-carboxyanhydrides from silica nanoparticles.[9] After APTS decoration the MNPs were fully dispersible in non-polar solvents. The particle core diameter was calculated to be d_{core} = 8.3 ± 2.0 nm from Transition Electron Microscopy (TEM) images (Figure 1) with d_{hyd} = 12.9 nm (PDI 0.14) in $CHCl_3$. The surface amine initiated ring-opening polymerization of propargyl-L-glutamate NCA[10] afforded polypeptide grafted MNPs with click-able alkyne groups. The success of the grafting process was verified by FTIR analysis; displaying distinct amide I and II bands at 1649 and 1544 cm^{-1}, characteristic of the α-helical conformation, and by the glutamic ester carbonyl band at 1725 cm^{-1}. Glycosylation was achieved by Huisgens' "*click*" reaction of azide-functionalized galactose to the surface bound poly(propargyl-L-glutamate). FTIR spectra (**Fig.: 3.1**) show strong galactose OH-signals at 3296 cm^{-1} suggesting a high galactose content in agreement with our previous studies.[11]

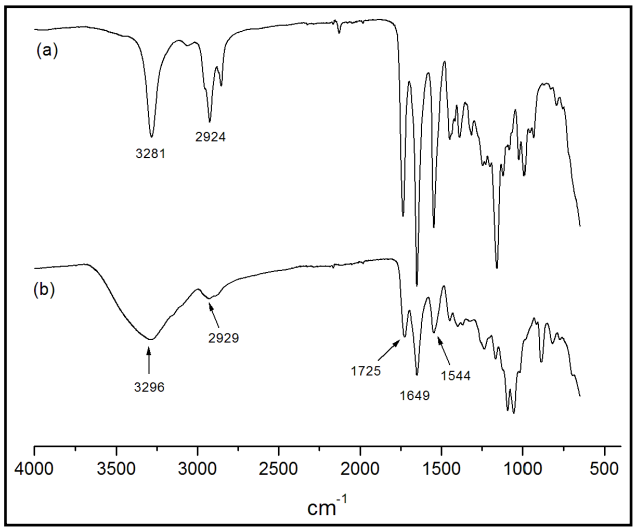

Figure 3.1: ATR-IR spectrum of (a) peptide grafted magnetic nanoparticles (b) glycopeptides grafted magnetic nanoparticles (GP-MNP).

The resulting glycopeptide-grafted particles were easily dispersible in water, further highlighting the successful synthetic protocol and extensive glycosylation. In water we find d_{hyd} = 15.5 nm (PDI 0.12) by DLS and this value did not change over a period of months. The low PDI values strongly suggest that the stable suspensions are composed of fully dispersed MNPs, critical for bio-application. This is consistent with the TEM analysis which showed excellent quality MNPs with particle core diameters d_{core} of 8.3 ± 2.0 nm (**Fig.: 3.2**).

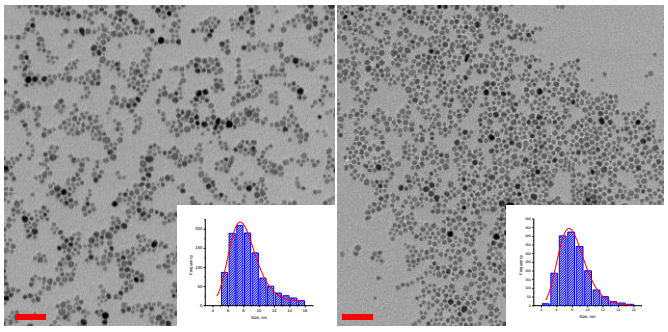

Figure 3.2: Representative transmission electron micrographs and statistical analyses for; (lhs) APTS functionalized Fe_3O_4 NPs (d_{TEM} 8.8 ± 2.7 nm), and (rhs) GP-MNPs (d_{TEM} 8.3 ± 2.0 nm). The scale bars represent 50 nm.

Stability of suspensions in water and salt was confirmed by dynamic light scattering (**Fig.: 3.3** and **Fig.: 3.4)**. As the serum suspensions are unsuitable for DLS, stability was confirmed by the complete absence of any aggregation over several months, as confirmed by eye and by Fe determination (**Fig.:3.5**).

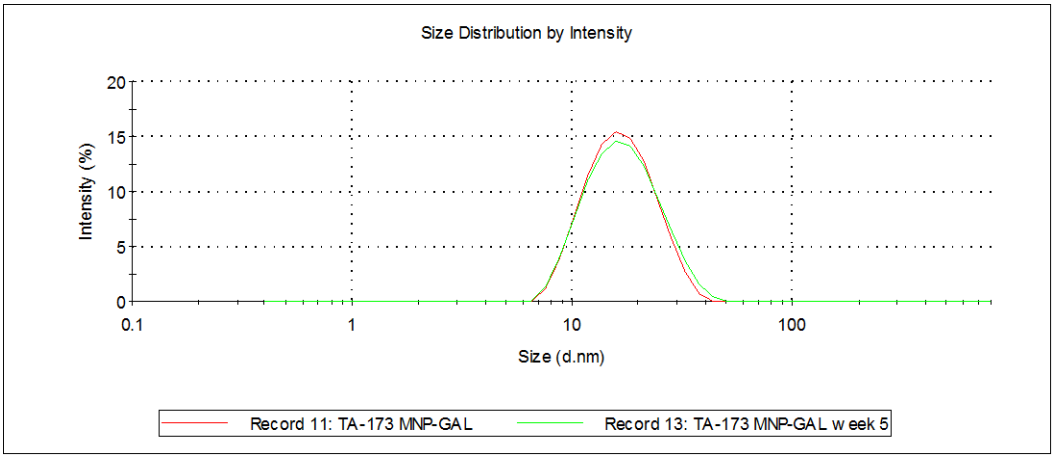

Figure 3.3: DLS data for a typical GP-MNP suspension (mM range) in pure H_2O (red) and the same suspension re-analysed five weeks later (green). The hydrodynamic properties are unchanged.

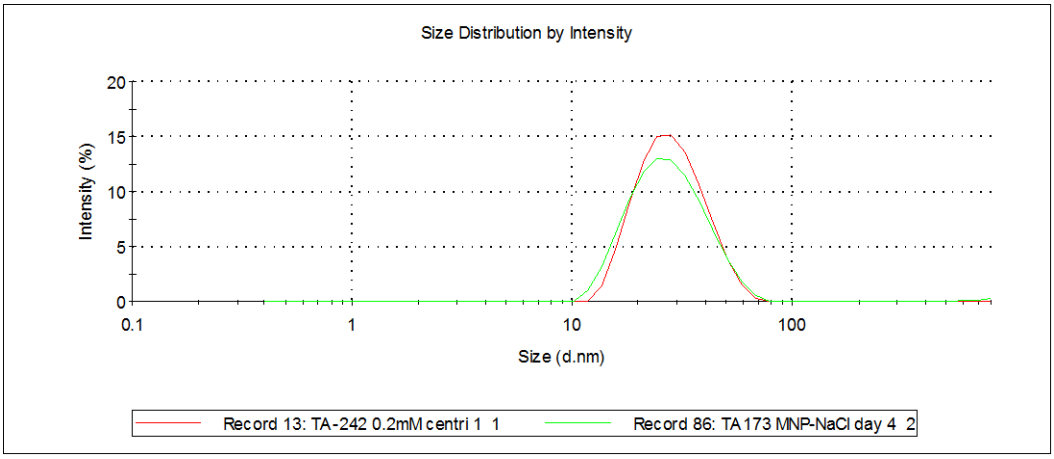

Figure 3.4: DLS data for a typical GP-MNP suspensions (mM range) in pure H_2O (red) and the same suspension, at a concentration of 0.14 mM NaCl, after standing for four days (green). The hydrodynamic properties are unchanged.

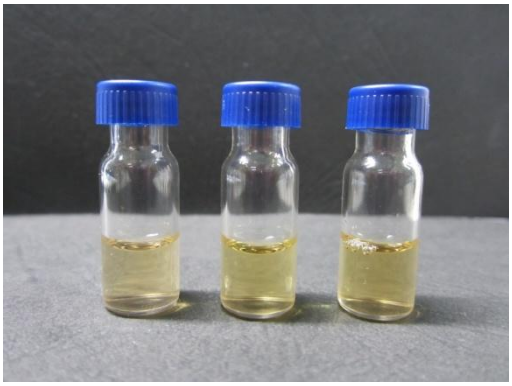

Figure 3.5: Typical GP-MNP suspensions, at Fe = 0.25 mM, in pure water (left), in serum after 1 day (centre), and in serum after two months (right).

The efficacy of GP-MNP dispersions for generating image contrast was studied primarily by fast field-cycling NMR relaxometry, or NMRD. The technique involves measurement of r_1 as a function of field strength (and hence ^{1}H Larmor frequency). The profiles provide insight into the magnetic order of the particles in the dispersion, using the ^{1}H relaxation of water as a local probe.[12] Specifically, NMRD provides information on the diffusion lifetime of the solvent in the particles environment (and hence core size), on the dynamics of the moment in its local magnetocrystalline field (τ_N, the Néel correlation time and ΔE_{anis}), and on the saturation magnetization (M_s) of the particles.

A typical NMRD profile of a GP-MNP dispersion is shown in **Fig.: 3.6**. The presence of a mid-frequency minimum is highly characteristic of superparamagnetic MNPs in suspension. The solid line included in Figure 2 is a simulation using SPM theory,[13] which provides very good agreement with experimental data. The values obtained from this analysis are d_{core} = 10 nm (slightly higher than TEM), M_s = 59 emu.g^{-1}, ΔE_{anis} = 1.6 GHz τ_N = 16 ns. The low anisotropy energy and rapid Néel motion confirm the superparamagnetism, and hence dispersion, of the MNPs. SPM theory is known to produce slight overestimates in core size, but quantitative M_s values. [12(a),14] The slight mid-frequency discrepancy arises due to a change in the relaxation mechanism in this range, which has been described.[15]

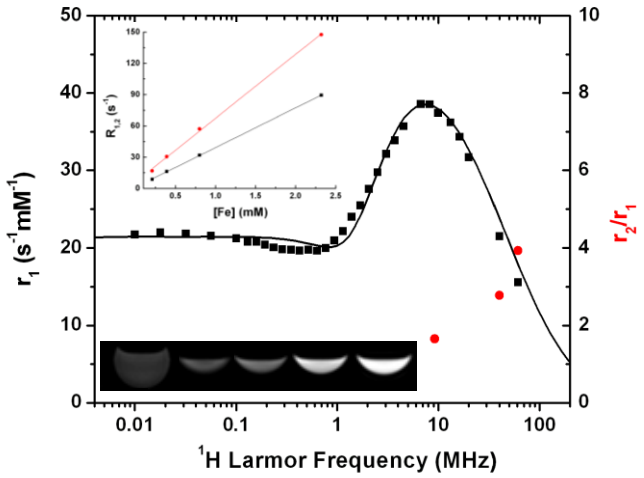

Figure 3.6: ^{1}H relaxation profile (■) and relaxivity ratios (●), recorded at 298 K in H_2O, for a GP-MNP suspension, d_{hyd} 15.5 nm (PDI 0.12). The solid line is a simulation generated using SPM theory,[15] the parameters used were; d_{core} 10 nm, M_s 59 emu.g^{-1}, □E_{anis} 1.3 GHz, □$_N$ 16 ns, see text. The upper inset shows the determination of relaxivity (■ r_1) and (● r_2), at 9.25 MHz. The lower inset is a T_1-weighted image, recorded at 120 MHz. From the left; 0.0, 0.008, 0.04, 0.2, 1.0 mM Fe.

The utility of the GP-MNP dispersions for MRI is demonstrated by the values of the relaxivities, r_1 and r_2. GP-MNP have high r_1 of 16 $s^{-1}mM^{-1}$ and low r_2 of 62 $s^{-1}mM^{-1}$ at the typical clinical frequency of 61 MHz (1.5 T), giving an r_2/r_1 ratio of 3.9. In particular the low ratio further demonstrates that GP-MNPs are fully dispersed in water without any aggregation. The relaxivities confirm the applicability of the suspensions for T_1–weighted imaging at 60 MHz. Furthermore, the image, inset to Figure 6, demonstrates strong signal enhancement, under T_1-weighting, at 120 MHz. Hence GP-MNP may be useful over the human clinical MRI range. The relaxivities also show that the polymer chains have minimal effect on the interaction of the magnetic moments with bulk water.

Most known MNP-based positive contrast agents are of slightly smaller size and hence lower r_2/r_1, but also lower r_1. Citrate stabilized MNP dispersions, of d_{hyd} 7 nm were considered as T_1-agents for MRI angiography, r_1 10.9 $s^{-1}mM^{-1}$, r_2/r_1 is 2.4.[16] The medium-term stability in blood was an issue, presumably due to desorptive loss of citrate. PEGylated Fe_3O_4 MNPs of the same core size, from ligand exchange of oleate, were also considered,[17] with similar results; r_1 7.3 $s^{-1}mM^{-1}$, r_2/r_1 2.4. However, on increasing the

molecular weight of the polymer, as would be required for optimal steric stabilization and to achieve "*stealth*" effects *in vivo*, partial aggregation occurred, compromising the T_1-weighting properties. By comparison, in our case the larger core used results in a favourable increase in r_1, partially offset by an increase in r_2/r_1, however the T_1-weighting potential remains. The grafting-from/click-functionalization strategy provides a robust and adaptable chemistry ensuring optimal colloidal properties (*i.e.* preventing particle aggregation which is the key limitation for maintain good T_1-weighting[17]) but also opening up new potential for targeting. In this regard it is important to emphasise that the surface chemistry we have described can be used for any APTS coated iron oxide or metal ferrite MNP of any size.

To demonstrate specific targeting we used galactose functionalized GP-MNP for binding to *Ricinus communis Agglutinin* (RCA_{120}) lectin.[18] **Fig.: 3.7** shows that a magnet has no effect on the GP-MNP dispersion in water (~1.5 mM) due to the small size of the dispersed particles. The addition of RCA_{120} causes particle aggregation through selective multivalent binding with the lectin and attraction to the magnet. When additional galactose was added to the aggregated particles competitive binding with free galactose resulted in the re-dispersion of MNPs. When the same experiment was carried out with Concanavalin A lectin (Con A), which is selective for glucosyl and mannosyl but unable to bind galactosyl residues, no aggregation was observed, highlighting the specific binding properties of the GP-MNPs.

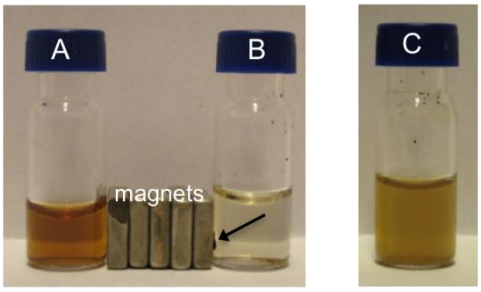

Figure 3.7: Dispersion of glycopeptide grafted MNPs in water (1-2 mM) before (A) and after the addition of lectin RCA_{120} (B). The addition of lectin causes particle aggregation through selective multivalent binding and attraction to the magnet (arrow). (C) Re-dispersion of MNPs through addition of free galactose.

It should be emphasized that there are no technical limits to the types, or indeed the combinations, of functional groups that can be used. This differentiates the current work from other approaches to fully disperse MNPs in water, which include stabilization with low or intermediate molecular weight ligands. The most prominent of the former are citrate stabilized dispersed MNPs, which have been assessed for clinical application,[16] however desorption limited colloidal stability and there was no potential for targeting. MNP stabilization with bio-derived ligands of intermediate molecular weight and lower charge (properties that reduce macrophage uptake), can be achieved by exchanging alkyl ligands, on MNPs synthesized by the thermal decomposition, with bi-functional silanes[19] or phosphate-modified PEG[18]. However, yields can be low and the ligand density is often limited, in some cases compromising water stability. More recently, we reported a novel grafting-to approach, using epoxy linker chemistry, for binding amine bearing polymers or amino acids, yielding fully dispersed MNP suspensions.[8(b)] Polymerization and MNP phase-transfer (from THF to water) was achieved in a single step, which limited the possibility for targeting with active functionalities. Indeed those limitations provided the motivation for the approach presented here.

3.3 Conclusion

We have reported first time instance of glycopeptide decorated magnetic nanoparticles by 'grafting from' technique. The main advantage of these techniques is non-limited availability of functional groups unlike monolayerd nanoparticles. Versatile azide-alkyne click to graft various sugars renders aqueous dispersiblity accompanied by bio-recognition ability. The particles showed exceptional dispersion properties useful for MR imaging as T_1-weighed contrast agents accompanied by prolonged stability in aqueous media.

3.4 Experimental Details

All material were obtained from Sigma-Aldrich and used as received unless otherwise noted. All anhydrous solvents mentioned were stored under dry inert atmosphere. Laboratory grade diethyl ether was purchased from VWR. 1-Azido-1-deoxy-β-D-galactopyranoside was synthesized according to a literature procedure.[11(a)]

Methods: The TEM measurements were performed using TECNAI G2 TEM operating at an accelerating voltage of 120 kV. Attenuated total reflectance (ATR) infrared spectra were recorded on a Spectrum GX FT-IR System (Perkin Elmer; Norwalk, CT, USA), under accumulation of 8 scans using a ZnSe trough plate crystal. Dynamic light scattering (DLS) experiments were performed at 25 °C on a Malvern NanoZS (Malvern Instruments, Malvern UK) which uses a detection angle of 173°, and a 3 mW He-Ne laser operating at a wavelength of 633 nm. The hydrodynamic diameter and the polydispersity index (PDI) values were obtained using cumulants analysis. PDI values below 0.2 indicate a monodisperse suspension. The frequency dependence of the water ^{1}H relaxation, at 25 °C, was recorded over the frequency range 0.01–20 MHz using a Spinmaster FFC- 2000 Fast Field Cycling NMR Relaxometer (Stelar SRL, Mede, Italy). The system operated at a measurement frequency of 9.25 MHz for ^{1}H, with a 90° pulse of 7 μs. A re-conditioned Bruker WP80 electromagnet was used at 40 and 61 MHz. T_2 was measured using the CPMG pulse sequence. Total iron content was determined by ICP-AES using a Varian Liberty 220ICP. Suspensions were prepared for determination by acid dissolution. MRI images were recorded at 3T (120 MHz) using a gradient echo sequence with TE = 2.3 ms, TR 134 ms, flip angle 80^{o}, voxel size 0.45x0.45x3.00 mm.

Synthetic Procedures

Synthesis of APTS functional Fe_3O_4 nanoparticles: Magnetite nanoparticles were synthesized using a modification of the method reported by Pinna *et al.*[20] In a typical synthesis, Iron (III) acetylacetonate (2 g) and benzyl alcohol (20 mL) were placed in flask

and the mixture heated to reflux (200 °C) for 7 h under nitrogen. The resulting black brown nanoparticles were washed twice with ethanol using magnetic separator (Dynamag). APTS (50 μL) in chloroform (2 mL) was added to wet Fe_3O_4 nanoparticles and tumbled for an hour. The nanoparticles were precipitated in methanol to remove excess APTES and redispersed in chloroform.

Synthesis of γ–propargyl L-glutamate hydrochloride: Propargyl ester of glutamic acid was synthesized by literature procedure by Hammond *et al*[10] with some modifications. In a 250 mL three necks round bottom flask 5 g (34 mmol) L-glutamic acid and 165 mL propargyl alcohol was added. The mixture was stirred under nitrogen atmosphere and refluxed at 40 °C. Over 1 hour 8.64 mL (64 mmol) chlorotrimethylsilane was added drop wise to this mixture and stirred overnight until all glutamic acid solid disappears. This clear reaction mixture was precipitated in diethyl ether and washed with fresh diethyl ether until a white solid was obtained. This crude product was then purified to remove traces of propargyl alcohol by refluxing in anhydrous ethanol at 40 °C and precipitation in diethyl ether. Propargyl glutamate hydrochloride thus obtained was washed with diethyl ether and dried under vacuum. Yield - 6.48 g (86%). ^{1}HNMR (400 MHz, D_2O) = 2.20 (m, 2H, CH_2), 2.63 (dt, 2H, CH-CO), 2.86 (t, 1H, C≡CH), 3.99 (t, 1H, CH), 4.70 (d, 2H, CH_2CO)

Synthesis of N-carboxyanhydride of γ-propargyl -L-glutamate: NCA-PLG was synthesized following the procedure from *Poche et al*[21] with minor modifications. To anhydrous ethyl acetate (50 mL), γ-propargyl-L-glutamte (1.5 g, 6.13 mmol) was added and refluxed at an ambient temperature. After addition of triphosgene (0.61 g, 2.04 mmol) the reaction mixture was refluxed for 5 hours under nitrogen atmosphere. The clear reaction mixture was cooled to 4 °C in a fridge and washed with water (50 mL), saturated sodium bicarbonate (50 mL) and brine solution (50 mL) all cooled to 4 °C. The organic solvent was dried with magnesium sulphate and evaporated to get viscous oil. Yield - 0.82g (54%). ^{1}H NMR (400 MHz, $CDCl_3$) δ=2.10-2.36 (dm, 2H, CH_2), 2.53 (t, 1H, C≡CH), 2.62 (t, 2H, CHCO), 4.4 (t, 1H, CH), 4.72 (d, 2H, CH_2CO), 6.2 (s, 1H, NH).

Grafting of polypropargyl-L-glutamate from MNP-APTS surface: To 250 mg NCA-PLG in a Schlenk tube, 5 mL suspension of amino functionalised magnetic nanoparticles (MNP-APTS) (15 mg/mL) in anhydrous chloroform was added under nitrogen atmosphere. The reaction mixture was stirred for 72 hours at room temperature and completion of polymerization reaction was confirmed with ATR-IR spectroscopy. Poly(propargyl glutamate) grafted magnetic nanoparticles were precipitated in excess diethyl ether and separated as dry product. The dry magnetic particles were suspended in an anhydrous DMSO (5 mL) and stored at room temperature under nitrogen atmosphere for further use.

Glycosylation of Polypropargyl glutamate grafted magnetic nanoparticles (GP-MNP): In a Schlenk tube, to 5 mL suspension of PPLG grafted magnetic nanoparticles (1.12 mmol alkyne, considering 100% conversion of monomer to polymer and 100% grafting of polymer on MNP surface) in an anhydrous DMSO, 1-azido-1-deoxy-B-D-galactopyranoside (344.5 mg, 1.68 mmol, 1.5 equiv to alkyne) and triethylamine (78.05 µL, 0.56 mmol, 0.5 equiv to alkyne) were added. The suspension was degassed by purging dry nitrogen gas for 30 min. After addition of triphenylphosphine copper(I) bromide ($(PPh_3)CuBr$) (104 mg, 0.112 mmol, 0.1 equiv of alkynes) the reaction mixture was purged again with nitrogen for 30 min. The reaction mixture was then stirred at 30 °C for 72 hours by placing in oil bath. Glycosylated magnetic particles were then precipitated twice in anhydrous THF (30 mL) and recovered by magnetic capturing. To remove traces of click catalyst and DMSO, GP-MNPS's were further washed three times with fresh THF (20 mL). Dry GP-MNP's were then suspended in DI water to make suspension of desired concentration and store in fridge.

Lectin Binding Experiment: In a typical lectin binding experiment, to a 0.5 mL (~1.5 mM) suspension of glycosylated magnetic nanoparticles in DI water, 100 µL (2 mg/mL) Lectin from Ricinus communis (castor bean) Agglutinin RCA_{120} was added resulting in instantaneous aggregation of nanoparticles. Addition of excess free galactose (100 µL (10 mg/mL)) resuspends the nanoparticle to form homogeneous suspension. A control experiment was performed with addition of 100 µL (2 mg/mL) Concanavalin A from *Canavalia ensiformis* (Jack bean) to the nanoparticle suspension.

3.4 References

1. M. E. Davis, Z. Chen, D. M. Shin, *Nat. Rev. Drug Disc.* **2008**, *7*, 771-782. R. A. Petros, J. M. DeSimone, *Nat. Rev. Drug Disc.*, 2010, **9**, 615.

2. J. Xie, G. Liu, H. S. Eden, H. Ai, X. Chen, *Acc. Chem Res.*, 2011, **44**, 883.

3. K. El-Boubbou, D. C. Zhu, C. Vasileiou, B. Borhan, D. Prosperi, W. Li, X. Huanga, *J. Am. Chem. Soc.*, 2010, **132**, 4490.

4. L. Lartigue, C. Innocenti, T. Kalaivani, A. Awwad, M. Sanchez Duque, Y. Guari, J. Larionova, C. Guerin, J. G. Montero, V. Barragan-Montero, P. Arosio, A. Lascialfari, D. Gatteschi, C. Sangregorio, *J. Am. Chem. Soc.*, 2011, **133**, 10459.

5. A. Pfaff, A. Schallon, T. M. Ruhland, A. P. Majewski, H. Schmalz, R. Freitag, A. H. E. Müller, *Biomacromolecules*, 2011, **12**, 3805.

6. K. Babiuch, R. Wyrwa, K. Wagner, T. Seemann, S. Hoeppener, C. Remzi Becer, R. Linke, M. Gottschaldt, J. Weisser, M. Schnabelrauch, U. S. Schubert, *Biomacromolecules*, 2011, **12**, 681.

7. D. P. Gamblin, E. M. Scanlan, B. G. Davis, *Chem. Rev.*, 2009, **109**, 131.

8. (a) N. Pinna, S. Grancharov, P. Beato, P. Bonville, M. Antonietti, M. Niederberger, *Chem. Mater.*, 2005, **17**, 3044. (b) T. Ninjbadgar, D. F. Brougham, *Adv. Funct. Mater.*, 2011, **21**, 4769.

9. (a) B. Fong and P. S. Russo, *Langmuir*, 1999, **15**, 4421. (b) T. Borase, M. Iacono, S. I. Ali, P. D. Thornton, A. Heise, *Polym. Chem.*, 2012, **3**, 1267.

10. A. C. Engler , H. Lee , P. T. Hammond, *Angew. Chem. Int. Ed.*, 2009, **48**, 9334.

11. (a) J. Huang, G. Habraken, F. Audouin, A. Heise, *Macromolecules*, 2010, **43**, 6050. (b) J. Huang, C. Bonduelle, J. Thévenot, S. Lecommandou, A. Heise, *J. Am. Chem. Soc.*, 2012, **134**, 119.

12. (a) E. Taboada , E. Rodriguez , A. Roig , J. Oro , A. Roch , R. N. Muller, *Langmuir*, 2007, **23**, 4583. (b) C. J. Meledandri , J. K. Stolarczyk , D. F. Brougham, *ACS Nano*, 2011, **5**, 1747. (c) C. J. Meledandri, D. F. Brougham, *Analytical Methods*, 2012, **4**, 331.

13. A. Roch, R. N. Muller, P. Gillis, *J. Chem. Phys.*, 1999, **110**, 5403.

14. (a) C. J. Meledandri, J. K. Stolarczyk, S. Ghosh. D. F. Brougham, *Langmuir*, 2008, **24**, 14159. (b) L. Xiao, J. Li, D. F. Brougham, E. K. Fox, N. Feliu, A. Bushmelev, A. Schmidt, N. Mertens, F. Kiessling, M. Valldor, B. Fadeel, S. Mathur, *ACS Nano*, 2011, **5**, 6315.

15. S. Laurent, D. Forge, M. Port, A. Roch, C. Robic, L. Vander Elst, R. N. Muller, *Chem. Rev.*, 2008, **108**, 2064.

16. M. Taupitz , S. Wagner , J. Schnorr , I. Kravec , H. Pilgrimm , H. Bergmann-Fritsch , B. Hamm, *Invest. Radiol.*, 2004, **39**, 394.

17. U. I. Tromsdorf, O. T. Bruns, S. C. Salmen, U. Beisiegel, H. Weller, *Nano Lett.*, 2009, **9**, 4434.

18. S. G. Spain and N. R. Cameron, *Polym. Chem.*, 2011, **2**, 1552.

19. R. De Palma, S. Peeters, M. J. Van Bael, H. Van den Rul, K. Bonroy, W. Laureyn, J. Mullens, G. Borghs, G. Maes, *Chem. Mater.*, 2007, **19**, 1821.

20. N. Pinna , S. Grancharov , P. Beato , P. Bonville , M. Antonietti ,M. Niederberger, *Chem. Mater.*, 2005, **17**, 3044.

21. D. S. Poche , M. J. Moore , J. L. Bowles, *Synth. Commun.*, 1999, **29**, 843.

Chapter 4

Glycopeptide Grafted Magnetic Nanoparticles with Combined Targeting, siRNA Loading and Imaging Properties

(Manuscript in preparation)

Measurement of the magnetic properties of nanoparticles has been performed in Dr. Brougham's laboratory.

Abstract

A novel approach to design glyco-polypeptide grafted superparamagentic iron oxide nanoparticle MRI contrast agents with vector ability for anionically charged biomolecules such as siRNA has been described. These glyco-polypeptide grafted iron oxide nanoparticles have excellent aqueous dispersibilty applicable for T_1- weighted positive magnetic resonance imaging. These hybrid nanoparticles display high positive ζ potential useful for siRNA complexation arsing from its poly(lysine) component whereas glycan mediated specific bio-recognition ability from glycosylated polypeptide component. This approach can be used to design new theranostics with choice of targeting ligands owing to ease of variety of coupling chemistry possibilities.

4.1 Introduction

Next generation nanomedical devices require the development of new smart materials that combine several functionalities in one component. Combined diagnostic modalities of the diseased tissue and targeted therapeutic delivery are desired elements of 'one package' materials referred to as theranostics.[1,2] The challenge in the development of these materials lies in the efficient packaging of imaging, targeting and therapeutic elements on the nanoscale.[3] Particularly promising is the combination of magnetic resonance imaging (MRI) trackable nanoparticles with functional polymers as it allows compatibilizing the different functions by careful molecular design.[4,5,6]

Superparamagnetic iron oxide nanoparticles (SPIONs) have recently drawn increased interest as MRI agents due to their low cytotoxicity.[7,8] Maximum contrast through localized signal enhancement (T_1-weighting) can be achieved by ensuring full MNP dispersion and long-term colloidal stability.[9] Colloidal stabilization of SPIONs by surface modification with hydrophilic molecules including polymers has been reported but none of them have an active role in targeting or drug delivery.[10] Glycosylated polypeptide-based materials show considerable promise as they are directly modelled on natural glycoproteins.[11] The latter play a significant role in various physiological and pathological events, which makes glycochemistry an attractive tool in the design of materials for active targeting.[12] We have recently disclosed a new concept combining MNP imaging with targeting by grafting glycosylated (galactose) polypeptides from the MNP surface.[13] These particles displayed exceptional colloidal stability, selective binding ability towards glycan specific lectins and a potential to employ as T_1 weighed MRI contrast agents.

Herein we report the efficient synthesis of novel colloidal theranostic nanoparticles with combined MRI contrast function, selective binding and siRNA carrying properties. The synthetic protocol, using controlled surface polypeptide synthesis, permits extensive control over the positioning of targeting and drug cargo compartments so as to obtain an optimized molecular design.

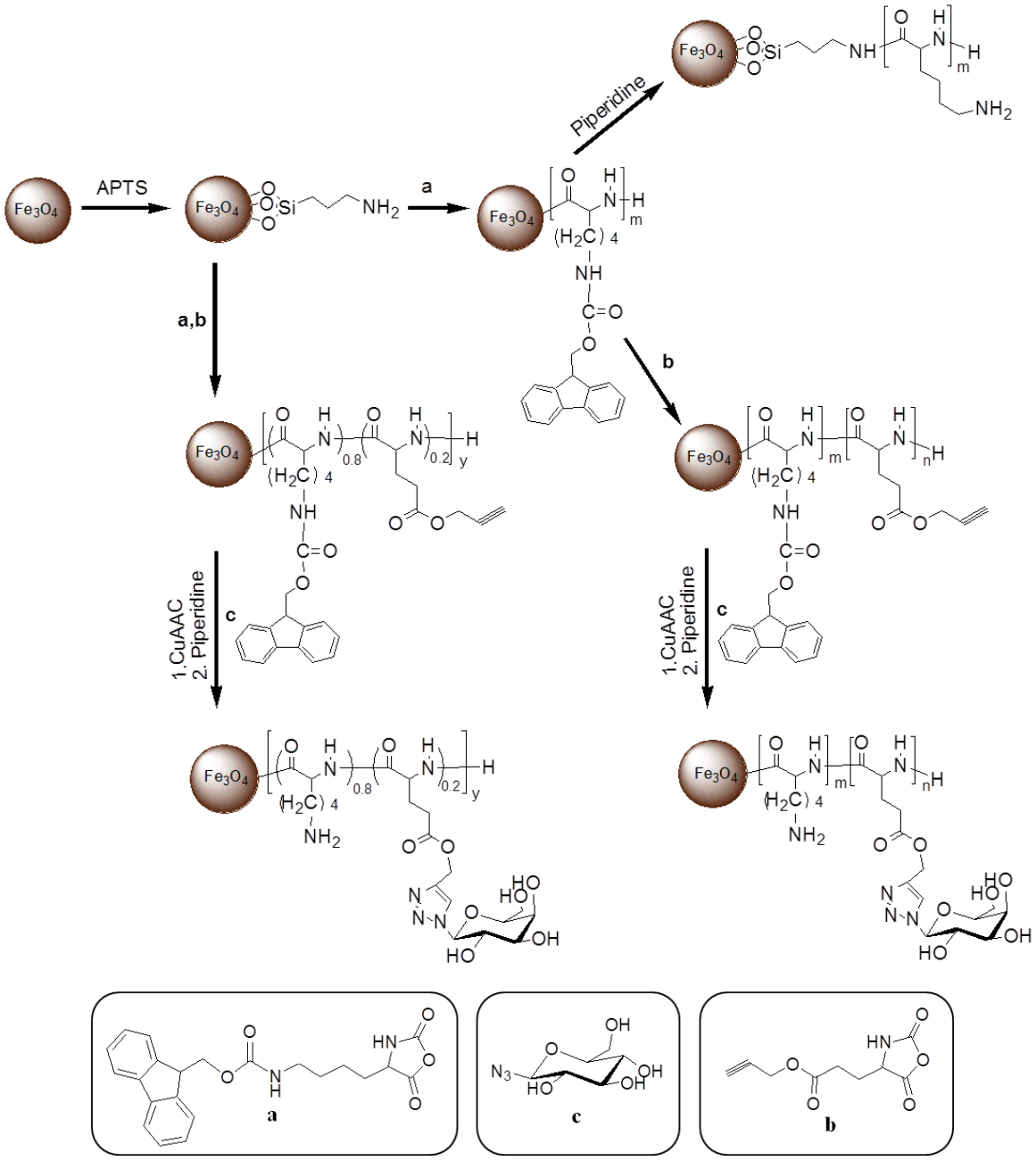

Scheme 4.1: Schematic representation of PLL, PLL-*b*-(PPLG-*c*-Gal) and PLL-*r*-(PPLG-*c*-Gal) grafting from APTS functionalized iron oxide nanoparticles. a. NCA-(Fmoc-L-lysine), b. NCA-(propargyl-L-glutamate), c. 1-Azido-1-deoxy-β-D-galactopyranoside.

4.2 Result and Discussion

MNPs were functionalized with polypeptides comprising two different amino acids, namely lysine for siRNA binding[14], and propargyl glutamate for attachment of galactose by click chemistry.[15,16] The weight composition of the lysine to propargyl glutamate in the grafted polypeptide was kept 4:1 to design polypeptide with higher cationic charge density as it was envisioned that few sugar will be sufficient for lectin specific targeting and to enhance water dispersibility. In order to compare the influence of molecular architecture two distinct arrangements were targeted with the same polypeptide weight composition. In the first one both amino acid NCA were polymerized simultaneously resulting in a statistical arrangement of both amino acids on the MNP surface (**Scheme: 4.1**). In the second arrangement a block structure was targeted with PLL forming the inner block and the glycosylated PPLG the outer block. While the statistical structure is synthetically more straightforward, it was rationalized that a block structure would provide distinct compartments for siRNA polyplexes close to the MNPs surface surrounded by glycosylated periphery available for interaction with biological receptors.

Statistical copolymerization was carried out with NCA of fluorenylmethyl-oxycarbonyl protected L-lysine (NCA-FLL) and NCA of propargyl-L-glutamate (NCA-PLG) (4:1 w/w) from aminopropyl trimethoxysilane (APTS) functional iron-oxide nanoparticle surfaces (8 nm) at room temperature. ATR-IR analysis of the resulting nanoparticles confirmed the successful grafting of the polypeptides evident from the presence of a propargyl alkyne band at 2127 cm^{-1} and a characteristic Fmoc carbonyl band at 1693 cm^{-1} (**Fig.: 4.1a**). Notably, propargyl ester carbonyl band (1733 cm^{-1}) and Fmoc carbonyl bond bands were merging in this statistical arrangement. Block co-polypeptide PFLL-*b*-PPLG were grafted from the magnetic nanoparticles by sequential addition of the monomers at 0 °C to prevent termination reactions.[17] PFLL was chosen as the first block and after 24 h complete monomer conversion was confirmed by ATR-IR by the absence of anhydride peaks at 1772 and 1880 cm^{-1}. The second monomer, NCA-PLG, was then added to form the second block. Analogous to the statistical copolymers, ATR-IR spectra displayed two defined peptide bands characteristic of the PPLG ester carbonyl (1733 cm^{-1}) and a less intense band

for the Fmoc-carbonyl (1693 cm^{-1}) of PFLL (**Fig.: 4.2 b**). When analyzed by TGA, the statistical copolypeptide (PFLL-*s*-PPLG) showed organic content of 80 % **(Fig.: 4.3)** whereas the nanoparticles containing the first poly(Fmoc-L-lysine) block, i.e. MNP-*g*-PFLL, revealed a weight loss of 67.0 % between 150 to 650 °C accounting for the PFLL shell. After polymerization of the second propargyl-L-glutamate block (PFLL-*b*-PPLG) the organic content raised to 80 % (**Fig.: 4.4**). This is in an agreement with the targeted block length ratio of 4:1.

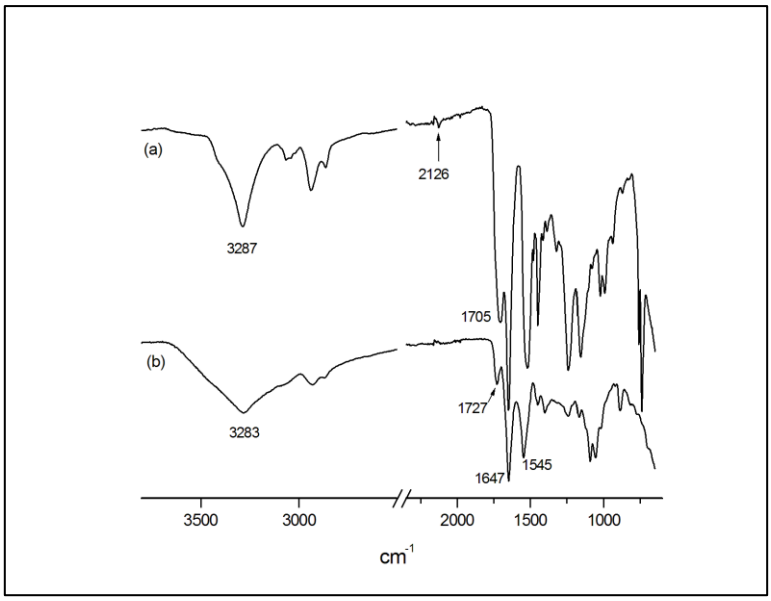

Figure 4.1: ATR-IR Spectrum of (a) MNP-*g*-PFLL-*s*-PPLG (b) MNP-*g*-PLL-*s*-PPLG-*c*-Gal.

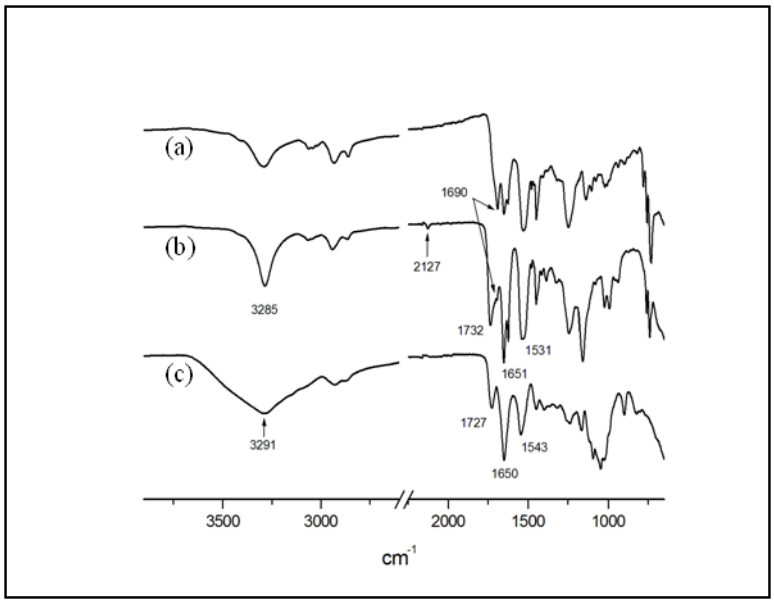

Figure 4.2: ATR-IR Spectrum of (a) MNP-*g*-PFLL (b) MNP-*g*-(PFLL-*b*-PPLG) (c) MNP-*g*-(PLL-*b*-(PPLG-*c*-Gal)).

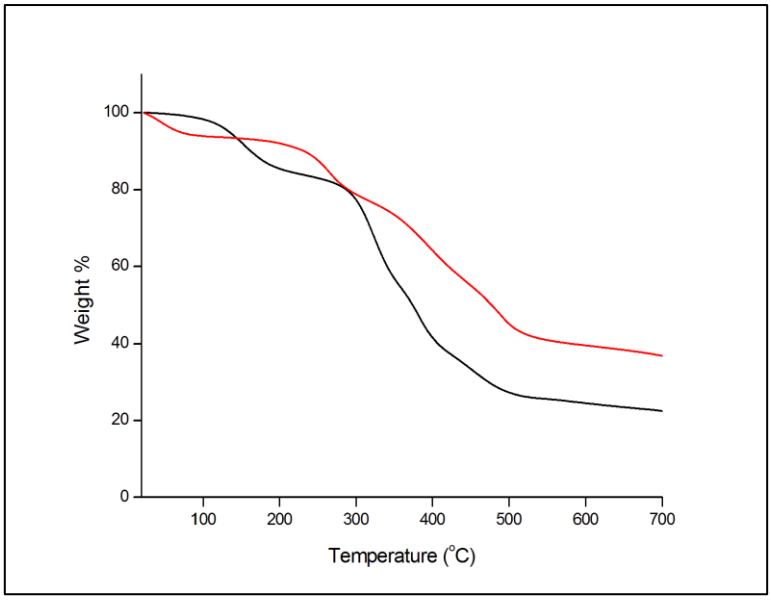

Figure 4.3: Thermogravimetric analysis of MNP-*g*-(PLL-*s*-(PPLG-*c*-Gal)) at various modification stages as MNP-*g*-(PFLL-*s*-PPLG) and MNP-*g*-(PLL-*s*-(PPLG-*c*-Gal)) indicated by black and red line, respectively.

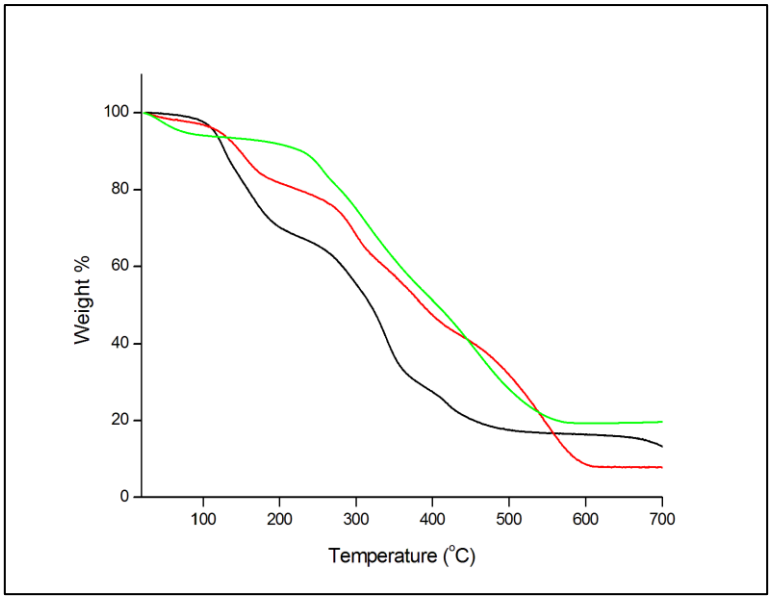

Figure 4.4: Thermogravimetric analysis of MNP-*g*-(PLL-*b*-(PPLG-*c*-Gal)) at various modification stages as MNP-*g*-PFLL, MNP-*g*-(PFLL-*b*-PPLG) and MNP-*g*-(PLL-*b*-(PPLG-*c*-Gal)) indicated by black, red and green lines respectively.

The propargyl-L-glutamate of both statistical and block decorated MNPs were glycosylated with azido galactose using copper catalyzed Huisgen's click chemistry. Because of the good solubility of the catalyst ($(PPh_3)_3CuBr$) and practically no solubility of the sugar in THF, repeated dispersion in DMSO and precipitation in THF was applied to remove all traces of copper catalyst. In a subsequent step, Fmoc was removed from PFLL by addition of pipyridine to the MNP suspension in DMF. The final products MNP-*g*-(PLL-*s*-(PPLG-*c*-Gal)) and MNP-*g*-(PLL-*b*-(PPLG-*c*-Gal)) were then recovered as dry products by lyophilization. TGA analysis of the final product MNP-*g*-(PLL-*b*-(PPLG-*c*-Gal)) revealed an organic content of 70 % (**Fig.: 4.4**). This overall decrease in organic content (~10%) after glycosylation (theoretical addition of 40 wt%) and Fmoc deprotection (theoretical removal of 52 wt%) is in agreement with the NCA-PFL to NCA-PLG feed ratio (200 mg to 50 mg respectively) suggesting quantitative glycosylation. TGA analysis of statistical statistical copolymer grafted magnetic nanoparticles revealed similar results. When analyzed by DLS, the poly(lysine)-*b*-glycopeptide decorated magnetic nanoparticles showed a hydrodynamic radius (d_{hyd}) of ~18 nm (**Fig.: 4.5**) and a PDI of 0.08, similar to poly(lysine) functional magnetic nanoparticles. The particle core diameter of both block

and statistical glyco-polypeptide grafted MNP's was calculated to be (8.2 ±2.0) nm based on TEM analysis. This difference is due to the fact that the polypeptide shell is in a hydrated and extended state for the DLS analysis while it is dry and collapsed in the TEM analysis. Both glycol-polypeptide grafted MNP's reveal excellent water dispersibility, which is prime requirement for the use as MRI contrast agents.

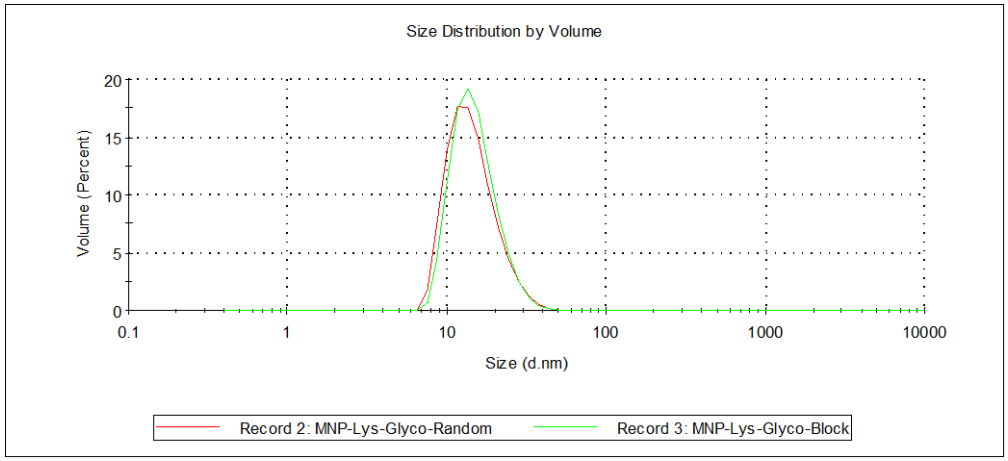

Figure 4.5: DLS data for hydrodynamic size determination of iron oxide nanoparticles decorated with MNP-*g*-(PLL-*b*-(PPLG-*c*-Gal)) (green) and MNP-*g*-(PLL-*s*-(PPLG-*c*-Gal)) (red).

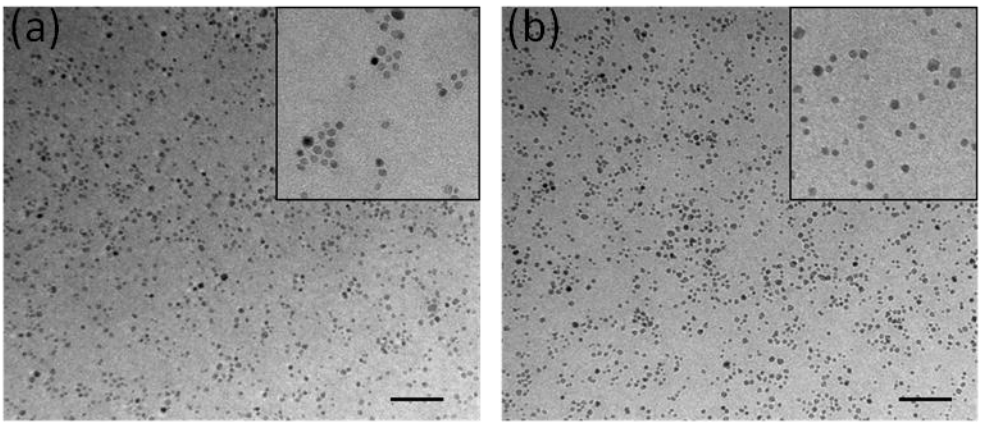

Figure 4.6: Representative transmission electron microscopy images of (a) MNP-*g*-(PLL-*s*-(PPLG-*c*-Gal)) and (b) MNP-*g*-(PLL-*b*-(PPLG-*g*-Gal)) grafted iron oxide nanoparticles. Inset shows zoomed images of well dispersed nanoparticles. The scale bar is 100 nm.

The efficiency of the poly(lysine)-co-glycopeptide (statistical and block) magnetic nanoparticles dispersions for generating image contrast in MRI was studied by fast field-cycling NMR relaxometry (NMRD).[18] Analysis of **Fig.: 4.7** shows that the NMRD profiles possess a characteristic shape confirming superparamagnetic behaviour of the particles. However, the clear differences suggest that incorporation of glycopeptide into the stabilising polymer has a significant effect on the low frequency relaxation. The frequency of the maximum, which is known to be largely affected by the size of the inorganic core, is constant (~8 MHz) which suggests the size of the magnetic core remains unchanged across the different samples. At high fields there is only a small increase in relaxivity (r_1) when the stabilising polymer is changed from PLL to PLL-*s*-(PPLG-*c*-Gal) to PLL-*b*-(PPLG-*c*-Gal). However, at the r_1 maximum, and at low frequency there are significant differences in the r_1 values; in this frequency range the relaxivity is largely determined by the saturation magnetization, M_s, and the Néel relaxation processes (magnetic moment reorientation) and hence is sensitive to the magnetocrystalline anisotropy. As the particles are fully dispersed these observations suggest that the ligands alter both M_s and the characteristic Néel correlation time, τ_N, of the individual particles. This is an unusual observation that requires some consideration. Simulation of the NMRD responses is ongoing in our collaborators laboratories.

Table 4.1: Physical properties of MNP dispersions.

	size (PDI)	**ζ**	**Relaxivity at 16.3mHz**	**Relaxivity at 61 mHz**
MNP sample	[nm]	[mV]	r1; r2; r2/r1 [$s^{-1}mM^{-1}$]	r1; r2; r2/r1 [$s^{-1}mM^{-1}$]
PLL	18.5 (0.18)	56	136.22;98.31;2.71	17.89;80.87;4.51
statistical	14.9 (0.12)	47	38.59;80.65;2.09	16.23;70.53;4.34
block	18.5 (0.09)	31	42.68; 81.09;1.9	16.91;78.08;4.6

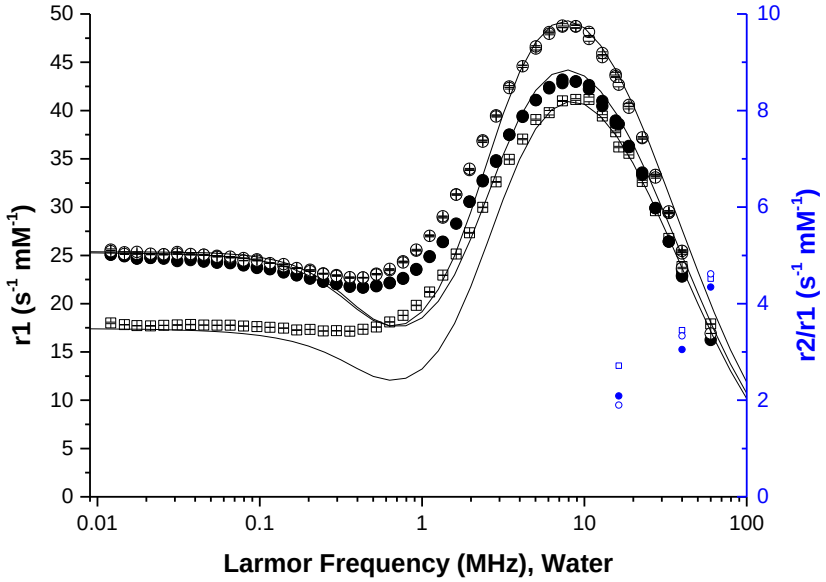

Figure 4.7 H^1 relaxation profile and relaxivity ratios recorded at 298 K in H_2O, for a MNP-*g*-PLL (□), MNP-g-(PLL-*s*-(PPLG-*c*-Gal)) (●) and MNP-*g*-(PLL-*b*-(PPLG-*c*-Gal)) (○) suspensions, d_{hyd}=18.5 nm (PDI 0.09).

Zeta (ζ) potential measurement of these glycopeptide-co-poly(lysine) grafted iron oxide nanoparticles revealed accumulative positive charge slightly lower than pure poly(lysine) grafted nanoparticles (**Table 4.1**) offering vector ability for anionically charged biomolecules. Small interfering RNA (siRNA) was used as model biomolecule to demonstrate vector ability of these glycopeptide-co-poly(lysine) grafted iron oxide nanoparticles. Block glyco-polypeptide grafted MNP suspensions of varying volume (1-10 µL) in DI water were mixed with fixed siRNA volume (1 µg) at increasing ratios and allowed to complex for 30 min. at room temperature. Gel elctrophoresis assays were used to demonstrate and confirm the ability of these nano vectors to successfully complex anionically charged siRNA. In the gel retardation assay (**Fig.: 4.8**), lane 1 shows the siRNA reference band whereas lane 2 shows complete complexation of siRNA with excess polyethylenimine (PEI) dendrimer, a commercial vector, by absence of siRNA band. In lanes 3 to 8 the fluorescence intensity of the siRNA band gradual decrease indicating an increasing complexation with increasing MNP/siRNA ratios. In lane 9 and 10 complete

complexation of siRNA with MNPs is evidenced by absence of a free (uncomplexed) siRNA band as also observed in case of excess PEI dendrimer (lane 2).

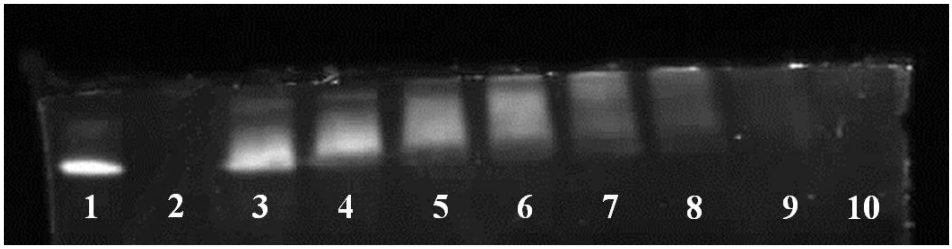

Figure 4.8: Polyacryl-amide gel electrophoresis image of siRNA complexed MNP-*g*-(PLL-*b*-(PPLG-*c*-Gal)) with increasing MNP amount. Lane 1 represents siRNA reference, lane 2 represents PEI complexed siRNA whereas lane 3 to 10 represent 1, 2, 4, 6, 8, 10, 15, 20 µL (2 mM) MNP suspension complexed with 1 µg siRNA respectively.

Specific targeting was demonstrated by using galactose functionalized magnetic nanoparticles and galactose specific letin *Ricinuscommunis Agglutinin* (RCA_{120}). As shown in **Fig.: 4.9 a**, an external strong magnet has no effect on the monodisperse aqueous dispersion of nanometer size magnetic nanoparticles (ca 1 mM). With the addition of the galactose specific lectin RCA_{120}, instantaneous aggregation of the magnetic nanoparticles through selective multivalent binding with the lectin was seen. In a control experiment, galactose non-binding lectin Canavalia ensiformis (jack bean) Concanavalin A did not show any aggregation of nanoparticles confirming the specificity of these nanoparticles towards galactose specific lectins. To further visualise this effect, FITC was reacted to some lysine amino groups. FITC-labelled PLL-*b*-(PPLG-*c*-Gal)) grafted magnetic nanoparticles suspension also showed specific targeted binding towards RCA_{120} by displaying fluorescent aggregates when observed under UV light. Addition of the aqueous solution of the free galactose to the aggregates resulted in redispersion of magnetic nanoparticles due to competitive binding of free galactose with the lectin. Similarly, successful complexation of siRNA with these glyco-polypeptide decorated nanoparticles was demonstrated using fluorescently tagged siRNA (**Fig.: 4.10**). The complexation with well dispersed nanoparticles displayed fluorescent aggregates capable of magnetic

capturing signifying increased total magnetization due to polyplexs formation (**Fig.: 4.10 b** (enhanced image)). The DLS analysis of these polyplexes revealed aggregates formation suggesting insufficient shielding of complexed siRNA by the glycopeptides block. Future studies of these siRNA delivery vehicles should focus on tailoring the length of outer glycopeptides shell to engineer the monodisperse siRNA vectors.

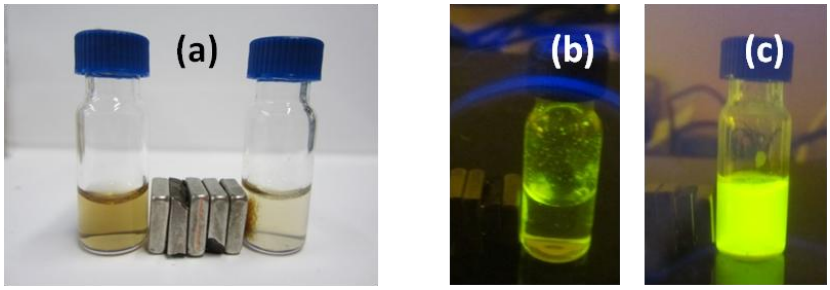

Figure 4.9: Photographic images showing selective and reversible binding of fluorescently tagged MNP's to lectin RCA_{120}.

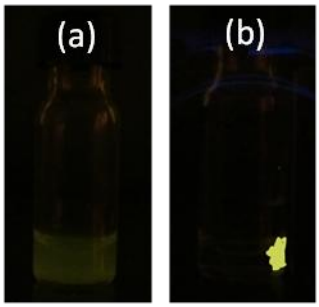

Figure 4.10: RCA_{120} specific binding of fluorescently tagged si-RNA complexed MNP-(PLL-*b*-(PPLG-*c*-Gal)) nanoparticles. (a) Si-RNA complexed nanoparticle dispersion in PBS buffer solution. (b) Magnetically captured nanoparticle aggregates after addition of RCA_{120}.

4.3 Conclusion

In conclusion, we have reported first instance of specific targeting superparamagnetic iron oxide nanoparticle useful for T_1 weighed MR imaging with high positive ζ potential, capable of siRNA complexation. The nanoparticles/siRNA complexes also showed specific binding towards targeted lectins highlighting their potential as theranostics. The ease of fluorescent tagging of nanoparticles could be useful for dual modal imaging. There is virtually no limit for the possibility of variety of sugar attachment or other clickable targeting moieties hence specific targeting due to versatility of the applied click chemistry.

4.4 Experimental Details

Materials

All material were obtained from Sigma-Aldrich and used as received unless otherwise noted. All anhydrous solvents mentioned were stored under dry inert atmosphere. Laboratory grade diethyl ether was purchased from VWR. 1-Azido-1-deoxy-β-D-galactopyranoside was synthesized according to a literature procedure.[19]

Methods: The TEM measurements were performed using TECNAI G2 TEM operating at an accelerating voltage of 120 kV. Attenuated total reflectance (ATR) infrared spectra were recorded on a Spectrum GX FT-IR System (Perkin Elmer; Norwalk, CT, USA), under accumulation of 8 scans using a ZnSe trough plate crystal. Dynamic light scattering (DLS) experiments were performed at 25 °C on a Malvern NanoZS (Malvern Instruments, Malvern UK) which uses a detection angle of 173°, and a 3 mW He-Ne laser operating at a wavelength of 633 nm. The hydrodynamic diameter and the polydispersity index (PDI) values were obtained using cumulants analysis. PDI values below 0.2 indicate a monodisperse suspension. The frequency dependence of the water ^{1}H relaxation, at 25 °C, was recorded over the frequency range 0.01–20 MHz using a Spinmaster FFC- 2000 Fast Field Cycling NMR Relaxometer (Stelar SRL, Mede, Italy). The system operated at a measurement frequency of 9.25 MHz for ^{1}H, with a 90° pulse of 7 μs. A re-conditioned Bruker WP80 electromagnet was used at 40 and 61 MHz. T_2 was measured using the CPMG pulse sequence. Total iron content was determined by ICP-AES using a Varian Liberty 220ICP. Suspensions were prepared for determination by acid dissolution. MRI images were recorded at 3T (120 MHz) using a gradient echo sequence with TE = 2.3 ms, TR 134 ms, flip angle 80^{o}, voxel size 0.45x0.45x3.00 mm.

Complexation of siRNA with MNP-*g*-PLL-*b*-(PPLG-*c*-Gal)):

siGENOME non-targeting siRNA #4 (5’ AUGAACGUAAUUG-CUAA 3’) was obtained from Dharmacon and used in for complexation with iron oxide nanoparticles. The siRNA/MNP-*g*-PLL-*b*-(PPLG-*c*-Gal) complexes were prepared freshly prior to use.

Varying volume of PLL-*b*-(PPLG-*c*-Gal) grafted magnetic nanoparticle solution of known iron content (ca.2 mM in DI water) (1, 2, 4, 6, 8, 10, 15, 20 µL) was used for complexation with fixed quantity of siRNA (1 µg) in tris HCl buffer (pH 7.4) (25 µL). The incubation was done at room temperature for 30 min.

Gel Retardation Assay:

Above prepared MNP-PLL-GP/siRNA complexes were mixed with loading dye (Promega G190A-Blue/orange 6x) and analysed by running 20% non denaturating polyacryl-amide gel in TBE buffer at 100 V for 1 h. Upon completion, the gel was stained using Gelstar nuclic acid gel stain for 30 min. Visual images were then obtained by UV transillumination (G. Box, Syngene, UK).

Lectin Binding Experiment:

(a) MNP-*g*-(PLL-*b*-(PPLG-*c*-Gal)): In a typical lectin binding experiment, to a 0.5 mL (ca.2 mM) suspension of glycosylated block co-polypeptide grafted magnetic nanoparticles in DI water, 100 µL (2 mg/mL) Lectin from Ricinus communis (castor bean) Agglutinin RCA_{120} was added resulting in instantaneous aggregation of nanoparticles. Addition of excess free galactose (5 mg) resuspended the nanoparticle to form homogeneous suspension. A control experiment was performed with addition of 100 µL (2 mg/mL) Canavalia ensiformis (jack bean) Concanavalin A to the nanoparticle suspension.

(b) Fluorescently tagged MNP-*g*-(PLL-*b*-(PPLG-*c*-Gal)): Above set of experiments was performed with fluorescently labelled MNP-*g*-(PLL-*b*-(PPLG-*c*-Gal)) nanoparticles by coupling fluorescein isothiocyanate (FITC) to amines groups of poly(lysine) shell. Magnetic nanoparticle suspension (2 mL, ca. 2 mM) was stirred with FITC solution in DMSO (5µL, 1mg/mL) in dark conditions at room temperature. Traces of unbound FITC were removed by dialysis prior to lectin binding experiment.

(c) Fluorescently tagged siRNA complexed MNP-*g*-(PLL-*b*-(PPLG-*c*-Gal)): Magnetic nanoparticle dispersion in DI water (250 µL, 2 mM,) was allowed to complex with fluorescently tagged siRNA (2 µg) for 30 mins at room temperature.) Lectin from Ricinus communis (castor bean) Agglutinin RCA_{120} (50 µL, 2 mg/mL) was added to the siRNA complexed nanoparticle suspension which resulted in instantaneous aggregation The nanoparticle suspension before and after addition of lectin was viewed and photographed in the presence of UV light.

Synthetic Procedures

Aminopropyltriethoxysilane functional Fe_3O_4 nanoparticles (MNP-APTS): Magnetite nanoparticles were synthesized using our previously reported method.13 In short, the mixture of Iron (III) acetylacetonate (2 g) and benzyl alcohol (20 mL) was refluxed (200 °C) in round bottom flask under nitrogen for 7 hrs. The resulting black brown nanoparticles were washed twice with ethanol using magnetic separator (Dynamag). APTES (50 µL) in chloroform (2 mL) was added to wet Fe_3O_4 nanoparticles and tumbled for an hour. The nanoparticles were precipitated in methanol to remove excess APTES and redispersed in chloroform.

Synthesis of N-carboxyanhydride of Fmoc-L-lysine (NCA-FLL): The NCA-FLL was synthesized using literature procedure reported by *Gijs et al*[20] with some modifications. In a 250 mL three necks round bottom flask N_ε-fluorenylmethoxycarbonyl-L-lysine (5.00 g, 13.6 mmol) and α-pinene (4.28 g, 31.4 mmol) was added to dry anhydrous ethyl acetate (60 mL) . The mixture was stirred under nitrogen atmosphere and heated to reflux. Triphosgene (2.72 g, 9.17 mmol) ethyl acetate (20 mL) was added drop wise to this mixture over 30 min and refluxed overnight until all solid disappears. This clear reaction mixture was reduced to 1/3 by evaporating ethyl acetate and immediate precipitation was seen after addition of 40 mL n-heptane. The mixture was heated to clear solution and allowed to cool slowly. The precipitated NCA was filtered, washed with n-heptane, dried

under vacuum to yield NCA (4.10 g, 76.6%) as a white powder and stored in fridge for further use.

^{1}H-NMR (400 MHz, $CDCl_3$, δ, ppm): 7.77 (d, 2H, ArH, J = 7.5 Hz), 7.59 (d, 2H, ArH, J = 7.5 Hz), 7.40 (t, 2H, ArH, J = 7.2), 7.31 (t, 2H, ArH, J = 7.2), 6.68 (s, 1H, NH), 4.85 (s, 1H, NH), 4.44 (t, 2H OCH_2CH, J = 6.0), 4.29 (t, 1H, CHC(O), J = 5.4 Hz), 4.21 (t, 1H, $CHCH_2O$, J = 6.5 Hz), 3.18 (m, 2H, CH_2NH), 1.96 (m, 2H,CH_2CH), 1.53 (m, 2H, CH_2), 1.42 (m, 2H, CH_2) ^{13}C-NMR (100 MHz): 169.9 (OC(O)CH), 153.8 (C(O)NH), 152.5 ((CO)NH), 143.8 (Ar), 141.3(Ar), 127.7 (Ar), 127.1 (Ar), 125.0 (Ar), 120.0 (Ar), 66.7 (CH_2O), 57.4 (CH), 47.2 (CH), 40.0 (CH_2), 30.8 (CH_2), 21.3 (CH_2).

Synthesis of N-carboxyanhydride of propargyl glutamate (NCA-PLG): The NCA-PLG was synthesized by our previously reported procedure.[13]

MNP-*g*-PLL: To the NCA-FLL (200 mg) in a Schlenk tube, 2 mL suspension of amino functionalised magnetic nanoparticles (MNP-APTS) in anhydrous chloroform was added under nitrogen atmosphere. The reaction mixture was stirred for 24 h at room temperature and completion of polymerization reaction was confirmed with ATR-IR spectroscopy. Poly(Fmoc-L-lysine) (PFLL) grafted magnetic nanoparticles were precipitated in excess diethyl ether and separated as dry product. To a suspension of above mentioned magnetic particles in anhydrous DMSO (3 mL), piperidine (1 mL) was added drop wise to deprotect poly(Lysine) (PLL) side chain amine groups. The suspension was stirred for another 2 hours followed by precipitation in anhydrous diethyl ether to get PLL grafted magnetic nanoparticles. These nanoparticles were then dispersed in water and the pH of the suspension was adjusted to acidic (~4-5) by adding 1M HCl. The suspension was then dialyzed against water to remove piperidinium salt traces and excess acid. The PLL grafted iron oxide nanoparticles suspension was then sized and stored in a fridge.

MNP-*g*-(PFLL-*s*-PPLG): The NCA-FLL (200 mg) and NCA-PLG (50 mg) were weighed in a clean dry Schlenk tube to which MNP-APTS suspension in $CHCl_3$ (2 mL) was added under nitrogen atmosphere. The reaction mixture was stirred at room temperature to which 1 mL anhydrous DMSO was added after initial 15 minutes to improve the dispersibility of newly forming MNP-polypeptide hybrids. The reaction was stirred for 24 h and an exhaustion of monomer feed was confirmed by ATR-IR. MNP-*g*-(PFLL-*s*-PPLG) hybrids were then obtained as a dry powder by precipitating in diethyl ether.

MNP-*g*-(PFLL-*b*-PPLG): In a clean dry Schlenk tube NCA-FLL (200 mg) was weighed to which MNP-APTS suspension in $CHCl_3$ (2 mL) was added under nitrogen atmosphere at 0 ^oC in thermostat and stirred for 24 hrs. An aliquot (0.2 mL) was taken out after confirming the complete exhaustion of monomer added by ATR-IR. In a sequential step, a solution of NCA-PLG (50 mg) in an anhydrous DMSO (1 mL) was added to Schlenk tube. The reaction mixture was stirred at 0 ^oC for another 24 hrs time by which the complete conversion of second monomer added to polypeptide occurred confirmed by ATR-IR. MNP-*g*-(PFLL-*b*-PPLG) hybrids were then recovered as a dry powder by precipitating in diethyl ether.

Glycosylation of block and statistical PFLL-*co*-(PPLG) grafted magnetic nanoparticles and subsequent Fmoc deprotection: Copper catalyzed Azide Alkyne Click (CuAAC) was used for glycosylation of alkyne moieties of polypeptide shell as we reported previously[13] with minor modifications. Exact procedure was followed for both block and statistical co-polypeptide grafted magnetic nanoparticles. In a Schlenk flask, to 5 mL suspension of PFLL-*b*-PPLG grafted magnetic nanoparticles (0.237 mmol alkyne, considering 100% conversion of monomer to polymer and 100% grafting of polymer on MNP surface) in an anhydrous DMSO, 1-azido-1-deoxy-B-Dgalactopyranoside (97 mg, 0.473 mmol, 2 equiv. to alkyne) and N-N diisopropylethylamine (21 µL, 0.12 mmol, 0.5 equiv to alkyne) were added. The suspension was degassed by purging dry nitrogen gas for 30 min. After addition of triphenylphosphine copper(I) bromide ($(PPh_3)_3CuBr$) (44 mg,

0.047 mmol, 0.2 equiv of alkynes) the reaction mixture was purged again with nitrogen for 30 min and left stirring for 48 h at room temperature. The glycosylated magnetic nanoparticles were then precipitated in anhydrous THF (50 mL). The dry nanoparticles were resupended in DMSO (5 mL) and reprecipitated in THF (50 mL) thrice to remove copper catalyst. To a catalyst free glycosylated magnetic particle dispersion in anhydrous DMSO (3 mL), piperidine (1 mL) was added dropwise and stirred for 2 hrs followed by precipitation in anhydrous diethyl ether. The final product poly(lysine)-co-glycopeptide grafted magnetic nanoparticles were suspended in water by adjusting the solution pH to acidic (~ 4-5) by addition of 1 M HCl solution. Pipiredinium salt, acid traces and excess sugar was removed by dialysis against DI water. Finally, the glycosylated co-polypeptide grafted MNPs were sized and stored in fridge for further use.

4.5 References

1. J. Funkhouser, *Curr. Drug Disc.*, 2002, **2**.

2. (a) Ryu, H., J.; Koo, H.; Sun, I.; Yuk, S., H.; Choi, K.; Kim, K.; Kwon, I., C.; *Adv. Drug Deliv. Rev.*, 2012, **64**, 1447. (b) Shim, M., S; Kwon, Y., J.; *Adv. Drug Deliv. Rev.*, 2012, **64**, 1046. (c) Koo, H.; Huh, M., S.; Sun, I.; Yuk, S., H.; Choi, K.; Kim, K.; Kwon, I., C.; *Acc. of Chem. Res.*, 2011, **44**, 1018.

3. G. Chen, H. Qiu, P. N. Prasad, and X. Chen, *Chem. Rev.*, 2014, **114**, 5161.

4. D. Ho , X. Sun and S. Sun, *Acc. Chem. Res.*, 2011, **44**, 875.

5. D. Yoo, J.-H. Lee, T.-H. Shin and J. Cheon, *Acc. Chem. Res.*, 2011, **44**, 863.

6. A. K. Gupta and M. Gupta, *Biomaterials*, 2005, **26**, 3995.

7. C. Corot and D. Warlin, Wiley Interdisciplinary Rev.: Nanomedicine and Nanobiotechnology, 2013, 5, 411.

8. J. Gallo, N. Kamaly, I. Lavdas, E. Stevens, Q.-D. Nguyen, M. Wylezinska-Arridge, E. O. Aboagye and N. J. Long, *Angew. Chem. Int. Ed.*, 2014, DOI: 10.1002/anie.201405442.

[9] U. I. Tromsdorf, O. T. Bruns, S. C. Salmen, U. Beisiegel and H. Weller, *Nano Lett.*, 2009, **9**, 4434.

10. T. Ninjbadgar and D. F. Brougham, *Adv. Funct. Mater*., 2011, **21**, 4769.

11. M. Monsigny, A.-C. Roche, P. Midoux, R. Mayer, *Adv. Drug Deliv. Rev.*, 1994, **14**, 1.

12. Gamblin, D. P.; Scanlan, E. M.; Davis, B. G., Glycoprotein Synthesis: An Update. *Chem.l Rev*., 2008, **109**, 131.

13. T. Borase, T. Ninjbadgar, A. Kapetanakis, S. Roche, R. O'Connor, C. Kersken, A. Heise and D. Brougham, *Angew. Chem. Int. Ed.*, 2013, **52**, 3164.

14. M. Byrne, D. Victory, A. Hibbitts, M. Lanigan, A. Heise and S-A. Cryan, *Biomater. Sci.*, 2013,**1**, 1223.

15. M. A. Quadir, M. Martin and P. T. Hammond *Chem. Mater.*, 2014, **26**, 461.

16. A. C. Engler , H. Lee , P. T. Hammond, *Angew. Chem. Int. Ed.*, 2009, **48**, 9334.

17. T. Borase, M. Iacono, S. I. Ali, P. D. Thornton, A. Heise, *Polym. Chem.*, 2012, **3**, 1267.

18. C. J. Meledandri, D. F. Brougham, *Analytical Methods*, 2012, **4**, 331.

19. J. Huang, G. Habraken, F. Audouin, A. Heise, *Macromolecules*, 2010, **43**, 6050.

20. G. J. M. Habraken, M. Peeters, C. H. J. T. Dietz, C. E. Koning and A. Heise, *Polym. Chem.*, 2010, **1**, 514.

Future Outlook

Synthetic polypeptides could be employed with organic/inorganic materials to create a new class of smart hybrid materials with improved biocompatibility and biodegradability. The bio-mimetic design of the synthetic polypeptides could potentially improve the bio-interaction ability of these hybrids. Especially, glycosylated synthetic polypeptides are of great importance for bio-interaction due to their specificity in recognition towards lectins. These glycosylated polypeptides hybrids could find advanced applications in drug delivery, implants, tissue engineering combined with imaging properties. Glycopeptide grafted iron oxide nanoparticles with excellent dispersibility are a good example of this. The surface grafted glycopeptides component not only improved aqueous dispersion properties of nanoparticles but also retained its recognition abilities towards specific lectins. Further studies could aim at the attachment of other clickable sugars or interaction facilitating moieties onto the polypeptide backbone to investigate specific cell attachment and internalization.

An increase in complexity of polypeptide component by polymerization of two or more amino acid NCA's could be of interest to obtain hybrids with multiple functionalities. The advantage of good control over the structure and polydispersities of grafted polypeptides by SI-NCA-ROP technique could be useful for compartmentalization of the polypeptide shell by grafting defined block co-polypeptides. These hybrids with defined polypeptide shell compartments might be interesting for loading cargos such as drugs, DNAs, siRNAs, imaging agents could find applications in advanced theranostics whereas, compartmentalization of catalysts and enzymes could open their applications as nanoreactors. A case study of poly(lysine)-b-glycopeptide grafted iron oxide nanoparticles as presented here is a first attempt towards grafting of defined polypeptide shell to create excellent water dispersible magnetic nanoparticles rendered with siRNA vector ability. In a further study, it is required to address the optimization of the glycopolypeptide shell thickness to provide efficient shielding of siRNA complexed with poly(lysine) inner shell to create monodisperse theranostic nanoparticles. It should also be possible to exploit the current system by using small nucleotides to complex with poly(lysine) inner shell to check effectiveness of glycopeptide shell and craft monodisperse nanoparticles. Detailed biological studies will shine light on the applicability of these hybrids in living systems.